Investigation of Pressure and Temperature Gradient in Four-Phase Flow in a Complex Horizontal Pipeline

by

©Mohamed Abdalla Odan, B.Sc., M.Sc.

A thesis submitted to

the School of Graduate Studies
In partial fulfillment of the requirements for the degree of

Doctor of Philosophy (Oil and Gas Engineering)

Faculty of Engineering and Applied Science

Memorial University of Newfoundland

June 2021

St. John's, Newfoundland, Canada

Dedicated to
Almighty Allah for His provision of blessings, guidance, and wisdom

Abstract

The oil and gas (O&G) industry uses multi-phase and multi-component pipeline flows to move product from one site to another or to different areas within the same site. In extreme environments, such as offshore or the Arctic, the development of four-phase flows in a complex pipeline can bring even more challenges to the project. Jumpers and bends need to be able to is to withstand pressure drops and hydrodynamic loads from internal multi-phase flows and the current, respectively.

The study outlines the development of an experiment to investigate of pressure and temperature gradients in four-phase flows in a complex pipeline. Due to the excessive temperatures and pressures of the oil transport pipeline system, the main pipes include shorter pipes (bends and jumpers) that are attached to the manifold at the pipeline. These shorter pipes are used to enable expandability and prevent system failure.

The present work examines the practicality of applying a system of four-phase, four-fluid flows for transporting a multi-phase flow (sand, water, gas, and oil) along a flow loop horizontal pipeline with many multiple bends and jumpers. This experimental set-up can be used for investigating a wide variety of multi-phase flow problems considered in the this research. As a means to precisely measure and predict the characteristics of thermo- and hydro-dynamic multi-component mixtures, models representing the multi-phase behavior and equilibrium phase are created and tested. Additionally, the study looks at heat transfer, mass, and momentum in both the flow and the pipeline walls, and offers equations to describe their interrelationships. Another focus of this research is to obtain a Computational Fluid Dynamics (CFD) investigation of multi-phase flow phenomena in order to characterize the impact of pressure gradients and flow regimes due to various types of phase flow techniques used in the petroleum industry and in horizontal pipelines.

The results of this thesis offer fundamental and practical guidance for the analysis and design of flow loop pipeline multi-phase flow systems and devices incorporating four-phase flows (sand, water, gas, and oil) through a flow loop pipeline. The novel results were obtained with carefully controlled flow loop pipeline and volume fractions, which show a significant impact on temperature and pressure drops. Dimensionless numbers in fluid mechanics and pressure drop results show good agreement with the experimental data.

Further, the experimental and modeling approach of this thesis makes a unique contribution to the O&G field and to the design of transport pipelines for processing four-phase flows that include bends and jumpers.

Keywords: Four-Phase Flow, Multi-Phase Flow, Horizontal Pipeline, Sand Transport, Flow Regimes, CFD.

Papers Published from this Research

The majority of the results and discussions presented in this thesis (please see google scholar) have been published in the following papers:

1. **Mohamed Odan**, "Investigation Four-Phase Multi-Component Flow Techniques in Horizontal and Sub-Sea Pipelines" (The International Pipeline Conference (IPC2020), September 28-October 02, 2020, Calgary, Canada.

2. **Mohamed Odan**, Faraj Ben Rajeb, Mohammed Azizur Rahman, Amer Aborig, Syed Imtiaz, Yan Zhang, Mohamed M. Awad, " Four-Phase Flow of Oil, Gas, Water, And Sand Mixtures in Pipelines" (39th International Conference on Ocean, Offshore & Arctic Engineering OMAE-2020), August 03-07, 2020, Fort Lauderdale, USA.
   https://asmedigitalcollection.asme.org/OMAE/proceedingsabstract/OMAE2020/84430/V011T11A077/1093210.

3. **Mohamed Odan**, Faraj Ben Rajeb, Mohammed Azizur Rahman, Amer Aborig, Syed Imtiaz, Yan Zhang, Mohamed M. Awad, " Experimental Investigation of Four-Phase Flow of Oil, Gas, Water, And Sand in Pipelines" (Proceedings of the ASME Fluids Engineering Division Summer Meeting FEDSM-2020), July 12-16, 2020, Rosen Shingle Creek Orlando, FL.

4. **Mohamed Odan**, Faraj Ben Rajeb, Mohammed Azizur Rahman, Amer Aborig, Syed Imtiaz, Yan Zhang, Mohamed M. Awad, " Examination and Analysis of Four-Phase Four-Fluid Flow Techniques in Offshore Pipelines" (38th International Conference on Ocean, Offshore & Arctic Engineering OMAE-2019), Scotland, UK, June 9-14, 2019.
   https://asmedigitalcollection.asme.org/OMAE/proceedingsabstract/OMAE2019/58806/V05AT04A036/1067761.

5. **Mohamed Odan**, Faraj Ben Rajeb, Mohammed Azizur Rahman, Amer Aborig, Syed Imtiaz, Yan Zhang, "Multi-phase Flow in a Subsea Hilly Terrain" (37th International Conference on Ocean, Offshore, and Arctic Engineering OMAE-2018), Madrid, Spain, June 17-22, 2018. https://asmedigitalcollection.asme.org/OMAE/proceedingsabstract/OMAE2018/51296/V008T11A009/275686.

6. **Mohamed Odan**, Faraj Ben Rajeb, Syed Hasnain Zaidi, Mohammed Azizur Rahman, Amer Aborig, Syed Imtiaz, Yan Zhang, "Experimental Investigation of Multi-phase Pressure and Temperature Loss Using High Pressure Flow Loop" (International Conference on Petroleum Engineering ICPE-2016), Dhaka, Bangladesh, December 2016.

7. **Mohamed Odan**, Faraj Ben Rajeb, Syed Hasnain Zaidi, Mohammed Azizur Rahman, Amer Aborig, Syed Imtiaz, Yan Zhang, "Experimental Investigation of Multi-phase Flow Effects on the Hydrate Formation Process in an Offshore Pipeline" (The First International Conference on Chemical, Petroleum, and Gas Engineering ICCPGE-2016), Alkhoms, Libya, December 2016.

Acknowledgement

First and foremost, I would like to express my deepest gratitude to my supervisor, Dr. Mohammad Azizur Rahman, my co-supervisors, Dr. Yan Zhang and Dr. Amer Abriq, and Dr. Syed Imtiaz of the supervisory committee for their continued support, guidance, and encouragement. I also wish to acknowledge the financial support provided. As well, I wish to acknowledge the care and patience of my supervisors and their generous provision of an excellent atmosphere to perform research. I thank them as well for allowing me to experience multi-phase flow in the field, for patiently correcting my writing, and for financially supporting my thesis.

I would also like to thank the Department of Engineering at Memorial University of Newfoundland for their financial support and their access to resources.

Additionally, I would like to thank all the people who helped me update the multi-phase flow experimental set-up. Particularly, I would like to thank Mr. Craig Mitchell for his encouragement. Special thanks goes to Mr. Matt Curtis, who was always willing to help and give suggestions.

Finally, I would like to thank my mother, my father, my wife, my children, my brothers and sisters, my friends, and my relatives for their love, prayers, and support.

Thank you all.

Mohamed A. Odan

Table of Contents

List of Tables

List of Figures

List of Symbols, Nomenclature or Abbreviations

Abbreviation	Description	Unit
D	inside diameter of pipe	m
A	cross-sectional area	m^2
L	actual length of pipe	m
Le	equivalent length due to pipe fittings	m
LT	total length of pipe	m
vsl	superficial liquid velocity	m/s
vsg	superficial gas velocity	m/s
vm	mixture velocity	m/s
Ql	liquid flow rate	L/min
Qg	gas flow rate	L/min
$\dot{m}l$	liquid mass flow rate	kg/s
$\dot{m}g$	gas mass flow rate	kg/s
$\dot{m}$	total mass flow rate	kg/s
G	total mass flow flux	$kg/m^2.s$
μl	liquid viscosity	cP
μg	gas viscosity	cP
μm	mixture viscosity	cP
μ_{NS}	no-slip viscosity	cP
η	kinematic viscosity	cP
ρl	liquid density	kg/m^3
ρg	gas density	kg/m^3
ρm	mixture density	kg/m^3

ρ_{NS}	no-slip density	kg/m^3
g	gravitational constant	kg.m/s^2
α_{L}	liquid volume fraction	dimensionless
αg	gas volume fraction	dimensionless
R_e	Reynold's Number	dimensionless
Re_{m}	Reynold's mixture number	dimensionless
f	friction factor	dimensionless
hf	head loss	m
ΔP	pressure drops	Pa
n	flow behavior index	dimensionless
Frm	Froude mixture number	dimensionless
We	Weber number	dimensionless
$\emptyset l$	liquid fraction	dimensionless
$\emptyset g$	gas fraction	dimensionless
x	wetness fraction	dimensionless
S	slip ratio	dimensionless
k/D	relative pipe roughness	dimensionless
β	volumetric quality	dimensionless
ε	Wall Roughness	dimensionless
Re	Reynold's Number	dimensionless
Re_{sL}	refers to the oil phase Reynolds number	dimensionless
Re_s	Reynolds number of solid particles	dimensionless
Pr_f	Prandtl number	dimensionless
Fr_L	Froude number of the liquid	dimensionless
f	friction factor	dimensionless

η	Joule-Thomson factor	dimensionless
$Q^{\cdot}$	heat transfer rate per unit volume	kW/m^3
s_k	specific enthalpy of phase K	kJ/kg
β	Angle β	+90° and −90°
S_{Ki}	surface tension from other phases	N/m
S_{Kw}	wall surface tension	N/m
$F_{K\mathrm{g}}$	gravity force	N
F_{Ki}	friction force in interaction with the other phases	N
F_{Kw}	friction force from the wall	N
F	Force	N
C_{PK}	heat capacity of phase K at constant pressure	J/K/mol
U	the overall heat transfer	W/(m^2°k)
K_s	thermal conductivity of sand particles	W/(m°k)
k	thermal conductivity of the pipe	W/(m°k)
K_f	fluid conduction coefficient	W/(m°k)
h_i	heat transfer coefficient for the inside pip	W/(m^2°k)
h_o	heat transfer coefficient for the outside pipe	W/(m^2°k)
τ	shear stress	Pa
τ_w	wall shear stress	Pa
τ_0	yield stress	Pa
γ	shear rate	sec^{-1}

Abbreviation	Description
ANSI	American National Standards Institute
AWG	American Wire Gauge Data
DAQ	Data Acquisition system
DN	Nominal Diameter (ISO 6708)
Fps	Frames per second
FS	Full Scale
GPM	Gallons per Minute
HP	Horsepower
MMC	McMaster-Carr
NI	National Instruments
NPS	Nominal Pipe Size
NPT	National Pipe Thread Taper
Psi	Pounds per square inch
Psia	Atmospheric pounds per square inch
Psig	Pounds per square inch gain
PVC	Polyvinylchloride
Rpm	Rotations per minute
SCFM	Standard cubic feet per minute
SS	Stainless steel
VDC	Volts Direct Current

Chapter 1

Introduction

1.1 Background

The use of multi-phase flow in the oil and gas (O&G) industry, such as liquid-gas, liquid-solid, and solid-liquid-gas three-phase flow, is steadily increasing. Flow travelling through pipelines makes it easier to transport required materials to their destinations. However, the overall performance of multi-phase flow is more complex in comparison to single-phase flow, because multi-phase flow faces more potential problems (e.g., corrosion, erosion, and slugging) in striving to achieve optimal results.

Multi-phase petroleum wells usually produce different configurations of oil and gas with the addition of water and sand particles, depending on the reservoir characteristics. An oil/water/gas/sand four-phase flow introduces many challenges with regard to understanding and analyzing its unpredictable and uncertain behavior, and the flow sometimes induces significant amplitude pressure gradients due to oscillating forces, particularly around well bends [1].

The O&G industry is currently interested in investigating the effect of oil-gas-water mixtures on the structure of pipelines, because a significant response would lead to potential fatigue damage, particularly when oil carries dense sand particles or if slug flow develops in the flowline. Moreover, oil sands reservoirs might develop chunks or slugs, which act as severe dynamic loads that can cause the pipe to vibrate at large magnitudes [1].

The chemical and physical interactions between phases, the nonlinearity of governing equations compared to multi-phase flows, and the large pressure gradient in flow characteristics with respect to process and operating conditions are the three main challenges encountered when studying multi-phase flow and designing corresponding equipment. Because this complexity presents a major challenge in the study of multi-phase flows, further study is required not only to achieve a greater understanding of the mechanisms

underlying the process, but also to analyze its unpredictable and unsteady behavior. Such behavior is particularly noticeable with regard to pressure gradients issues in particular on bends of pipeline jumpers [1]. Oil pumped to the surface from offshore reservoirs is typically comprised of a fluid mixture containing oil, gas and water, which is transported to onshore O&G processing sites via pipelines. Due to excessive temperatures and pressures of the oil transport pipeline system, the main pipelines include shorter pipelines (bends and jumpers) that are attached to the manifold at the well. These shorter pipes are used to enable expandability and prevent system failure. However, the functionality of bends and jumpers can be challenged by extreme internal flow hydro-dynamic loads and internal pressure. The heavy flow loads and immense pressure can cause major pressure gradients, leading to compromised safety levels and reduced system reliability [1].

Speaking for the Xodus Group in 2011, Rob Swindel noted that internal flow pressure gradient have caused nearly 22% of all failures in pipelines. This phenomenon, known in the industry as pressure gradient, results from interactions between the pipe and the flow, which leads to a trepanning of natural and fluid frequencies. While the primary cause for pressure gradients is high flow rates, little is known about the impact of two-phase flows on system pressure drops [1].

After the fluid mixture has been transported onshore, multi-phase flow separators can be used to separate the mixture. The separation of the fluid into its various elements essentially eliminates most pressure gradient issues in pipelines. However, such fluid separation is too costly to be carried out in offshore facilities. Further compounding matters, sand particles are often included in the mixture being transported to shore, which can restrict flow rates or even block the flow altogether. To resolve this dilemma, the sand can be flushed from the bends and jumpers by injecting a high-pressure flow, but this process can be expensive to employ over time, especially when the volume fraction of the sand is relatively high.

An alternative approach considers various system inputs and outputs as a means to gauge how well the fluid frequency matches the pipelines with bends and jumpers' natural frequencies. Based on an analysis of this data, flow rates, phase numbers and phase volume fractions can be adjusted to lessen the flow's impact

on bends and jumpers. To accommodate this approach, a standard guideline should be developed for O&G companies to determine the level of flow-induced pressure gradients occurring in horizontal pipeline. By assisting in the estimation of multi-phase flow impacts in pipeline systems that include bends and jumpers, a guideline standard could enable the O&G industry to better monitor pipeline structures and, thus achieve enhanced control over the production phase [1].

Understanding the physics of multi-phase flow as one of the most dominant flow regimes poses many challenges to researchers in the field of fluid dynamics, particularly, when production flow is always multi-phase. Pipeline engineers and operators must have a clear understanding of the multi-phase behaviour when transferring crude oil, associated gas, produced water, and solid particles from wellheads to processing facilities. Many researchers have simplified the treatment of complex flows by considering them as the flows of two or three different phases. A comprehensive two-phase liquid/gas model developed by Xiao et al. in 1990, a two-phase solid/liquid model developed by Doron and Barnea in 1993, and a three-phase liquid/liquid/gas model by Taitel et al. in 1995 are just a few examples of these approaches [2].

1.2 Statement of the Problem

Most offshore petroleum production projects in the oil and gas industry currently depend on the ability to transport the drilled product safely and efficiently to shore via multi-phase, multi-component pipelines. The present study examines the challenges, advantages, and disadvantages of using four-phase, four-fluid pipeline flow to transport four-phase multi-component substances (i.e., oil-water-sand-CO_2) in pipeline systems that include multiple bends and jumpers. Both phase-behavior and phase-equilibrium models are developed as a means to determine the thermo- and hydro-dynamic properties and other parameters of multi-component mixes. The current study also creates and applies a series of equations in order to investigate some critical factors affecting flow in pipelines, including mass, heat transfer, and momentum. Also of interest in this study is how temperatures and pressure gradients impact multi-phase flows occurring in horizontal pipeline systems with that have multiple bends and jumpers. The work will construct flow pattern and pressure drop models based on parameters specific to pipeline systems with numerous bends and jumpers. It is worth noting

that a phase can be defined as a state of matter (e.g., solid, liquid, gas), and that multi-phase flows are simply two or more of these phases flowing simultaneously. Moreover, flows described as two-phase may be, for instance, solid-liquid, solid-gas, liquid-gas, etc. From a practical perspective, research on multi-phase flows is important for its contribution to the O&G industry, as water or sand added to oil in a pipeline serves to reduce flow resistance and pressure gradient, thus creating a safer and more efficient way to transport drilled product to shore.

The fundamental objective of this thesis is the investigation of temperature and pressure gradients experimentally and theoretically in pipelines for four-phase (sand, water, gas and oil) flows. The scope of the experimental study has been limited to a handful of four-phase (sand, water, gas, and oil) flow conditions. Based on this, an experimental multi-phase flow loop was built that could be used to investigate multi-phase flow in two, three and four-phase pipeline flows under a variety of flow, operating, and bending conditions.

In this research, for the first time and to the best of our knowledge, a four-phase (liquid, liquid, solid and gas) flow mathematical model was developed to consider a stratified flow regime in a horizontal pipeline.

Prior to this work, there were no experimental data available for four-phase (liquid, liquid, solid and gas) flows in a horizontal pipeline with bends before. This research presents new predictive models in pipelines to describe four-phase (liquid, liquid, solid and gas) flows through a pipeline. The conservation equations of mass, momentum, and energy are used and simplified based on the flow conditions in the pipeline of interest in this research. The equations are solved numerically to determine the pressure, temperature, phase fractions, and velocity. The predictive models are validated against benchmark cases with mixture properties, with the comparisons exhibiting relatively good agreement.

1.3 Research Objectives and Contributions

The most important contributions of this research are as follows:

- This research presents a study of multi-phase flow and analysis for four-phase (sand, water, gas and oil) flow in a horizontal pipeline with multiple bends and jumpers.

- The study investigates temperature and pressure gradient experimentally and theoretically in horizontal pipelines for four-phase (sand, water, gas and oil) flows with numerous bends and jumpers.
- The work characterizes four-phase (sand, water, gas and oil) flow using the Data Acquisition (DAQ) system to collect data from different pressure transducer sensors, temperature thermocouple sensors, and flow transmitters installed in the flow loop pipeline.
- The research presents new experimental data on multi-phase analysis in a 20-mm-ID horizontal pipeline using (sand, water, gas and oil) four-phase flow.

Moreover, the study also aims to obtain a better understanding of measured pressure drops and to investigate temperature and pressure gradients in pipelines for four-phase flows. To accomplish this objective, we will analyze a four-phase multi-component flow system that features injections of internal multi-phase flow comprised of gas/oil, water/gas/oil, and sand/water/gas/oil.

The research objectives are outlined as follows:

- Establish a set-up that will enable us to investigate four-phase (sand, water, gas and oil) flow through a horizontal pipeline with many bends and jumpers.
- Conduct tests on the movement of four-phase four-fluid flow (sand, water, gas and oil) through a horizontal pipeline with many bends and jumpers.
- Conduct experimental measurements of pressure drops for three- and four-phase flows with different operating and hydrodynamic conditions and compare the outcomes with the experimental data of other researchers.
- Conduct an experimental measurements of flow regimes and development regime maps (similar to the Taitel and Duckler map) for three- and four-phase flows with different operating and hydrodynamic conditions and compare our outcomes with the experimental data of other researchers.
- Develop a mathematical model of four-phase (sand, water, gas and oil) flow for considering flow regimes in horizontal pipelines.

- Conduct a Computational Fluid Dynamics (CFD) model investigation of multi-phase flow in order to characterize the impact of pressure gradient and flow regime in short sections of horizontal pipelines.
- Use a CFD model of multi-phase flow through short sections of horizontal pipelines including bends to validate simulation results with existing experimental data.

Fluid flow through a pipeline that includes bends follows a fully non-linear or turbulent flow regime for a high flow rate. The experimental and CFD approaches of this thesis make a unique contribution to the O&G industry in the field of multi-phase flow in horizontal pipelines.

1.4 Lay Summary of the Research

The primary outcomes of this research project are presented below.

- The development of an experimental device that is able to characterize an experimental investigation of multi-phase fluid flow and to study the impact of four-phase fluid flow problems that occur in complex horizontal pipelines. This equipment can be used in other related research areas, such as hydrate formation and, multi-phase flow pipelines.
- This thesis presents a four-phase fluid flow problem that occurs in a complex horizontal pipeline.
- The research considers experimental and numerical approaches to study this problem in the context of the oil and gas (O&G) industry.
- The novel aspects of the study are published in seven articles in the proceedings of seven highly reputable prestigious international conferences.
- The results of the investigation of four-phase flow are organized in six chapters in the thesis.
- The experimental investigations of multi-phase fluid flow, in general, is limited by the availability of experimental techniques and apparatuses. In consideration of such limitations, the research conducts Computational Fluid Dynamics (CFD) simulations in order to extend the experimental results. The pathway to addressing some of the challenges of multi-phase flow is at the core of the overall contribution of the investigations of this thesis. In particular, CFD simulations help the relevant industry to improve traditional simulation tools.

- Primary experimental results towards the development of multi-phase flow are presented and published in the article of the International Conference on Petroleum Engineering ICPE-2016, Dhaka, Bangladesh, December 2016 and The First International Conference on Chemical, Petroleum, and Gas Engineering ICCPGE-2016), Alkhoms, Libya, December 2016.
- The experimental results including validation tests towards the development of the experimental facility are summarised and published in articles of the 37th International Conference on Ocean, Offshore, and Arctic Engineering OMAE-2018, Madrid, Spain, June 17-22, 2018 and the 38th International Conference on Ocean, Offshore & Arctic Engineering OMAE-2019, Scotland, UK, June 9-14, 2019.
- The results on the development of a CFD simulations model for multi-phase flow in horizontal pipelines using ANSYS fluent method are published in articles of Proceedings of the ASME Fluids Engineering Division Summer Meeting FEDSM-2020, July 12-16, 2020, Rosen Shingle Creek Orlando, FL, and the 39th International Conference on Ocean, Offshore & Arctic Engineering OMAE-2020, August 03-07, 2020, Fort Lauderdale, USA.
- The outcome of the research on experimental and CFD investigations of multi-phase flow phenomena to study to that impact the four-phase fluid flow problem occurring in a complex horizontal pipeline are published in articles of The International Pipeline Conference (IPC2020), September 28 – October 02, 2020, Calgary, Canada.

This thesis is written in traditional style, and the chapters are arranged as indicated blow.

1.5 Organization of the Thesis

This thesis is written in traditional style and contains six core chapters, which contain the following information:

Chapter 1 focuses on the introduction of research, the background and problem statement, the research gaps, the lay summary of the research, research objectives and contributions of investigations into pressure and temperature gradients in multi-phase flow in a complex horizontal pipeline with multiple bends and jumpers.

Chapter 2 presents a review of the literature of pressure and temperature gradients in four multi-phase flow in a complex horizontal pipeline with multiple bends and jumpers.

Chapter 3 describes the development of a four-phase multi-phase flow experimental facility including the methodology, specification of each component and selection procedure, experimental ranges, operating ranges including Reynolds number ranges, and safety analysis.

Chapter 4 focuses on the experimental investigation of pressure, temperature gradient and flow regime of four-phase (sand, water, gas, and oil) flow in a complex horizontal pipeline with multiple bends and jumpers.

Chapter 5 focuses on the development of a CFD model and simulation of multi-phase flow phenomena for four-phase (gas, liquid/, liquid and sand) flow in short sections of a complex horizontal pipeline.

Chapter 6 contains a summary of the thesis, and highlights the conclusions and contributions made by this research. In addition, recommendations for future research on this topic are suggested.

1.6 Co-Authorship Statement

I, Mohamed Odan, hold principal author status for all the chapters in this thesis. However, each manuscript is co-authored by my supervisor, Dr. Mohammad Azizur Rahman, my co-supervisors, Dr. Yan Zhang, Dr. Amer Abriq and supervisory committee, Dr. Syed Imtiaz, who have directed me towards the completion of this work as follows. I am the principal author and carried out the experiments. I drafted the thesis, and the co-authors assisted me in formulating research goals and experimental techniques, as well as reviewing and revising the manuscripts.

Chapter 2

Literature Review

2.1 Multi-Phase Flow

The majority of the published literature related to internal multi-phase flow centers on two-phase flow. The choice to focus on this type of flow (and typically to further confine the research to water and gas two-phase flow) is based not only on water and gas being the most common configuration for analysis, but also on it being easiest in terms of determining parameters like superficial velocity and flow patterns. In general, parameters can be based on factors such as pressure amplitude, induced forces, and natural frequency. However, it is also crucial to consider slug flow when determining parameters, as pipes tend to develop pressure gradients from these flows, which can then cause localized issues or problems across the entire system.

The pipeline sections most prone to flow- induced pressure gradient issues are jumpers and bends. Pontaza and Menon (2011) looked at flow-induced pressure gradients occurring in underwater M-shaped well jumpers. Their research aimed to determine fatigue life through numerically simulating a jumper's transient internal two-phase flow [2]. Flow fluctuations can cause pressure gradients of varying degrees, depending on how close the pipe's natural frequency is to the slug frequency. Riverin, de Langre, and Pettigrew (2006) discovered that pressure drops nearly always occur when multi-phase flows – especially slug flows – pass through bends [3].

A few years after their above-mentioned work, Pontaza and Menon (2013) created a process for investigating the fatigue life and flow- induced pressure gradient response in a well jumper that featured impact tees and short radius bends. In their recent study, the researchers carried out several different experiments, including developing a numerical simulation for the jumper's unsteady flow, estimating the jumper's fatigue life by utilizing a single-slope S-N curve, and determining flow-induced impacts and

spectral forces. Overall, the researchers discovered that the jumper spectrum that had tees had a much broader frequency range compared to the jumper spectrum that had short radius bends.

The stress cycle response in this research showed that although the two well jumper configurations had nearly the same stress ranges, they differed in their respective energy spectral frequencies. Flow-induced force spectra results indicated that the well jumper that had short radius bends showed a more significant structural response signal for lower frequencies, whereas the jumper that had impact tees showed higher frequency excitation. In fact, there was an increase by a factor of two in the fatigue life for the well jumper that had impact tees. The proposed study will employ a method that follows on Pontaza and Menon's (2013) research approach [4].

How tees and bends affect fluctuating force amplitude in various structures was also examined by Riverin et al. (2006). The researchers looked at variations in force magnitude according to factors such as geometry, superficial velocity, phase number, and others. In their study, they formulated force magnitude in accordance with localized pressure gradients in a flow's void fractions. The rms force value was experimented on through alternating two phases along with related spectral force density. The set-up comprised a dual-configuration PVC tube test section air-water loop to measure superficial velocity and air void fraction. The researchers discovered that forces at tees and bends are nearly the same in certain flow velocities and void fractions for equivalent bend forces. Specifically, flow-induced forces at 50% and 75% (void fraction) were found to be nearly the same despite having different magnitudes [3].

The present study models flow regimes using liquid and gas slugs to correspond to the force tee or bend to void fractions. Flow velocity and the density fraction inside the band (as well as inlets and outlets) determine the flow pattern. By applying a momentum equation, we found that the slugs' estimated forces appear to agree with Tay and Thorpe's (2004) experiments with horizontal pipes. However, determining vertical flow momentum balance (e.g., a tee configuration) can be highly complicated, as the phase dynamics are more variable compared to horizontal flows.

Riverin and Pettigrew (2007) conducted experiments using four U-shaped piping elements to determine the extent of dynamic reaction force at elbow pipeline sections and in pressure gradients. The pressure

gradients response showed that periodic fluctuating pressures were the same as the pipe's pressure gradient modes, and that the forces caused some resonance. Furthermore, the researchers found a narrow-random response frequency from the excitation forces, with the spectra revealing a frequency which increased as the fluid velocity increased in the void fraction, with a maximum force achieved at a void fraction of around 50% to 60%. In addition, the researchers noted that the U-shaped geometry, which featured a radius of curvature at the elbows, did little to impact the excitation forces [5]. Using bubble and droplet passage frequency for correlation force spectra, the researchers determined that, at low velocities, peak frequency was the same as the force spectra's predominant frequency, indicating that larger bubbles/droplets could potentially be the elbows' excitation force source.

Analysis of multi-phase flow in pipelines can be conducted using computational fluid dynamics (CFD), which is able to solve the interface between phases using strategies like the level set method and volume of fluid. Using CFD, Ramdin and Henkes (2011) carried out a numerical study that simulated two-phase flow configurations (e.g., Taylor and Benjamin bubbles). The analysis was modeled by employing a VOF multi-phase strategy and validating the results using CFD. Taylor bubbles, which typically rise in a liquid flowing up vertical pipes, contrast with Benjamin bubbles, which typically occur in stagnant liquid flowing along horizontal pipes. Both Taylor and Benjamin bubbles can assume slug flow patterns in gas or oil that is being moved through pipes [6].

In the Ramdin and Henkes (2011) experiments using Benjamin bubbles, there was strong agreement with analytical outcomes of bubble velocity if surface tension and viscosity impacts were neglected. Concerning viscosity, bubble velocity reduces in accordance with the Reynolds number when moving through a pipe and with rising surface tension. Concerning Taylor bubbles, no agreement could be found using CFD if surface tension and viscosity were neglected. Instead, there was a reduction in bubble velocity in accordance with the Reynolds number as well as the Eötvös. This outcome agrees with both the Wallis correlation and experimental results. Furthermore, unlike Benjamin bubbles, Taylor bubble velocity through the pipeline was constant if viscosity was considered. From this, we can see that viscosity and surface tension can be considered key parameters for inclusion in CFD simulations, as the values of these parameters can

have a significant impact on interactions between phases as well as the creation of slug flow regimes in flows [6].

In the O&G industry, three-phase flow patterns in pipelines can be defined either by their gas-liquid relationship or their liquid-liquid relationship [7]. Using this definition, Keskin, Zhang, and Sarica (2007) categorized twelve flow patterns for three-phase (gas-oil-water) flows in horizontal pipes. The flow patterns in large part determined pipeline erosion as well as holdups and pressure fluctuations. Keskin et al.'s (2007) literature review shows that a few research studies categorized flow patterns according to a gas-liquid relationship, a liquid-liquid relationship, or even a liquid-wall relationship, and that some studies combined two-phase flow patterns when defining three-phase flow patterns. Working from this knowledge base, Keskin et al.'s (2007) carried out tests of water, mineral oil and air (gas) moving in a horizontal pipe. The researchers further refined their tests using a variety of superficial velocities as well as water fractions. For superficial velocities, the water, oil and gas ranged between 0.01 m/s and 1.0 m/s, 0.02 m/s and 1.5 m/s, and 0.1 m/s and 7.0 m/s, respectively. The water portion, by percentage, was 20, 40, 50, 60, and 80 [8].

In these experiments, the categorization includes two specified terms. The first term designated a flow pattern of gas-liquid, while the second term designated a flow pattern of oil-water. In the study, the following flow patterns of gas-oil-water had been identified by the researchers (arranged here alphabetically): annular-oil continuous (AN-OC), annular-water continuous (AN-WC), dispersed bubble-oil continuous (DB-OC), dispersed bubble-water continuous (DB-WC), intermittent-dual continuous (IN-DC), intermittent-oil continuous (IN-OC), intermittent-stratified (IN-ST), intermittent-water continuous (IN-WC), stratified-stratified (ST-ST), stratified-dual continuous (ST-DC), stratified-oil continuous (ST-OC), stratified-water continuous (ST-WC). It is worth noting that, in these experiments, the formation of dispersed and annular bubble flows did not occur.

In O&G underwater pipelines, it is not uncommon for hilly portions of the line to accumulate liquid phases near low sections in a phenomenon called terrain slugging. Slugging might also occur along horizontal sections of the pipeline as a result of wavy flow from gas-liquid interfaces. This latter manifestation of slug flows was recorded in a University of Tulsa experiment that aimed to show how three-phase slug flow moves

in curved and horizontal M-shaped jumper portions. The experiment examined gas-oil-water flow through a pipeline situated in hilly terrain that featured downward- and upward-inclined portions as well as horizontal stretches. The study aimed to determine the behavior of slug flow when moving through differently angled portions of the pipeline, and also to better gauge the impact of liquid velocity, gas velocity and water proportion on flow patterns. In the experiment, the researchers used a transparent pipe (50.8 mm inner diameter) that featured horizontal and inclined sections connected via a U-shaped PVC bend. Among other items, the pipe was equipped with valves and sensors for measuring temperature, pressure, total liquid holdup, phase fraction distribution, etc. Cameras placed along the length of the pipeline enabled the researchers to visualize the three-phase flow pattern.

The flow patterns revealed intermittent (IN) flow of gas-liquid for every test in the pipeline's horizontal portion. Additionally, in sections which featured low flow rates, intermittent-stratified (IN-ST) flows of segregated oil and water phases were noted in every percentage of water proportion [9]. The researchers also found that at higher rates of flow, there was a mixture of the water and the oil, along with a dispersion of both water-in-oil and oil-in-water. As well, a fully separate layer of water was formed over the dispersed phases of water and oil, which is a flow pattern called "intermittent-water-in-oil and water" (IN-W/O&W) when oil is continuous, or "intermittent-oil-in-water and water" (IN-O/W&W) when water is continuous. Upon the slug's development, and depending on the proportion of the water cut, an annular thin film of oil or water forms. This fully separated layer of liquid film disappears during higher rates of flow if the water and oil form a homogeneous mixture. In the Tulsa experiments, the researchers noted that the downstream horizontal three-phase flow appeared to have a more mixed consistency than the upstream horizontal water-oil flow. They assumed from this that the U-shaped portion of their experimental pipe helped the water and oil phases mix prior to moving to the level portion of the pipe [9].

The researchers also looked at pressure changes along the stretch of the pipe. They found that the inclined pipe's lower area had maximum pressure. This is also the area where slugs are first formed. Otherwise, in other portions of the experimental pipe, the frequency and length of the slugs remained consistent during rates of low flow. Rates of moderate or high flow, however, showed marked differences in

slug frequency and length for water cuts of 20% to 80%.

After being pumped out of an undersea reservoir, sand enters the multi-phase flow transport pipeline system. It is crucial at this stage to control the impact of sand on the transport and production processes, as sand can have a major negative impact on the pipeline structural integrity by causing corrosion, pressure build-ups, and deleterious flow patterns. A chief concern during the transport of multi-phase flows is the accumulation of sand particles along pipe bottoms and bends. Such accumulation can affect the continuous flow's minimum critical velocity as well as other flow patterns. Despite the importance of managing the amount of sand that enters a pipeline from the reservoir source, very few studies have investigated this issue in relation to multi-phase flows. In one study, Al-lababidi, Yan, and Yeung (2012) performed a series of tests on sand in the transport of oil and gas, analyzing the sand's deposition behaviors when flowing as part of a mixture through inclined and horizontal pipe systems. The researchers aimed to find out the minimum velocity that sand had to move through a pipe as part of a multi-phase flow to avoid the formation of sand dunes (accumulation of sand) within the structure of pipelines [10].

In the tests, the researchers used six types of sand concentrations. The sand particles measured around 0.2 mm in diameter, while the pipe had an inner diameter of 0.05 m. The researchers found the minimum transport condition (MTC) of the sand in both the inclined (+5°) and horizontal pipeline to be nearly the same as the MTC for the water flow test. In the air-water tests, the results showed that horizontal pipeline MTC manifested as hydrodynamic and stratified wavy slug flow patterns, whereas in the inclined pipes, the MTC resembled the terrain slug flow pattern. A terrain slug flow regime mostly manifests in hilly portions of the pipeline, where the constant and relatively swift movement of the flow prevents sand deposition. The researchers concluded that all these factors should be taken into consideration during the pipeline design process if issues concerning erosion and harmful flow patterns are to be avoided.

For oil-gas-sand multi-phase flows, one of the most worrisome conditions is sand holdup, as it can negatively impact and disrupt pressure drops, mass flux, and flow patterns. The majority of these and other parameters are strongly affected by solid and liquid features like liquid or gas superficial velocity and sand particle weight. Bello, Reinicke and Teodoriu (2005) conducted experiments to investigate sand loading and

phase velocity, measuring sand holdup (particle size ~ 0.6 mm) and static/dynamic pressure distribution for a three-phase water-air-sand slug flow [11]. The researchers discovered that the pipe's axial distribution (i.e., from the bottom to the top) of the sand holdup revealed non-linear characteristics, with the highest values near the walls. The researchers also noted that, for gas superficial velocities of 0.505 m/s and 0.606 m/s, the values peaked near the center. They concluded that sand particle distribution must rely on the vortex motion of the slug caused by sand particles colliding with gas bubbles. Hence, the sand holdup was reduced when the superficial gas velocity was increased. Another study concluded, however, that sediments can cause pipeline erosion with water volume fractions at 10% or higher [12].

2.2 Conservation Equations in Multi-Phase Flow

Multi-Phase flows adhere to three main conservation principles, but as each principle applies thrice in every phase, we have seven equations for oil-gas-water flows. This format does not take into account simplifications or correlations which may be made or added to better explain any interactions occurring between a pipe's wall and the phases. So, for instance, every phase is likely to undergo alterations as it travels through the pipeline. These alterations are caused by transient flow patterns arising from the interference of bubbles, droplets, sand particles, slugs, etc., with the flow.

Conservation (or Naiver-Stokes) equations take into account terms related to diffusion and convection. Diffusion terms explain interactions among fluid particles caused by a flow's turbulent kinetic energy, whereas convection terms delineate a fluid particle's organized motion, including the properties transfer of the particles (National Aeronautics and Space Administration, 2008) [13].

2.2.1 Continuity Equation in Multi-Phase Flow

The continuity equation multi-phase flow for a control volume is expressed as follows [14]:

$$\frac{d}{dt}(\alpha_K \rho_K) + \frac{1}{A}\frac{d}{d_x}(A\alpha_K \rho_K v_K) = \Gamma_K \tag{2.1}$$

The sum of the volume fraction of all phases in cross-section should be equal to one.

$$\sum_{K=1}^{N} \alpha_K = 1 \tag{2.2}$$

$$\alpha_g + \alpha_O + \alpha_w + \alpha_s = 1 \quad (2.3)$$

$$\sum_{K=1}^{N} \Gamma_K = 0 \quad (2.4)$$

where v is velocity, α is the volume fraction, ρ is density, A is the pipe's cross-sectional area, and Γ_K is the sum of mass transfer rates from the wall and other phases to phase K. The subscript K in the above equation implies gas (g), water (w), oil (o), and solid particles (s).

Assuming a steady-state flow and constant pipe cross-sectional area with no mass transfer between phases, the continuity equation reduces to:

$$\frac{d}{dx}(\alpha_K \rho_K v_K) = 0 \quad (2.5)$$

2.2.2 Conservation of Mass

According to the general principle of mass conservation, a system's mass is conserved over time, and its quantity does not change until mass has either been removed or added. This principle can be applied to the multiple phases, giving [14]:

$$\frac{\partial}{\partial t}(\alpha_k \rho_k) + \frac{\partial}{\partial x}(\alpha_k \rho_k \upsilon_k) = \Gamma_{ki} + \Gamma_{kw} \quad (2.6)$$

where the first term indicates accumulated mass in the pipe's interior, the second term denotes total mass flow in the pipe, the third term indicates mass flow out of other phases, and the fourth term refers to mass flow out of other external sources. In the present work, the final term equals zero, as none of the flow passes through a pipe wall and out the other side.

2.2.3 Conservation of Momentum

Multi-Phase flow adheres to Newton's second law, in that friction forces, gravity and pressure comprise the primary forces being exerted on phases. Other forces also should be included in this law to represent interactions that are phase-to-phase, as these forces cause alternations in pipeline flow patterns. Equation (2.7) below shows that the sum of the forces exerted among all phases equates to zero [14]:

$$\sum_{k=1}^{N} R_{ki} + S_{ki} + \upsilon_k \Gamma_{ki} = 0 \quad (2.7)$$

where R_{ki} indicates friction force coming from the other phases, S_{ki} represents surface tension force coming from the other phases, and $\upsilon_k \Gamma_{ki}$ denotes momentum exchange or mass transfer [14].

2.2.3.1 Surface Tension

A key force active in every phase is surface tension. This type of tension is derived from intermolecular force drawing molecules together. Surface tension helps determine flow patterns because any change in tension could potentially point to momentum transfer occurring among the phases. Equation (2.8) expresses forces acting in the pipe's axial direction [14]:

$$\frac{1}{Adx}\sum F_K = F_{Kpg} + F_{Kg} + R_{Ki} + R_{KW} + S_{Ki} + S_{KW} \tag{2.8}$$

where force (the first term) is caused by the pipe's pressure gradient, the second term denotes gravity force, the third and fourth terms indicate the friction forces, and the fifth and sixth terms represent forces caused by surface tension. The sum of these forces is expected to vary during the change-over to three phases from two.

2.2.3.2 Pressure Correction

Pressure correction is important for anticipating the change-over between stratified and slug flows. The term is used to describe pressure differences which can occur between phases and is caused by different elevations in relation to the pipe bottom. Pressure correction plays a major role in forming wavy flow. It is worth noting that numerical problems can arise if the pressure correction term is not taken into account and the pressure is assumed as being the same across all phases. As presented later in this work, analytical equations can be used to describe the pressure for individual phases.

2.2.4 Conservation of Energy

As with momentum and mass laws of conservation, energy is also conserved over time. Furthermore, although it cannot be either created or destroyed, energy is able to alter forms. Heat from the outside can be added or removed from the system. The present study ignores external energy sources, but internal and external energy interacting with the phases would be expressed as [14]:

$$\frac{\partial}{\partial t}(\alpha_k E_k) = -\frac{\partial}{\partial x}[\alpha_k \upsilon_k (E_k + P_k)] + q_{ki} + q_{kw} + w_{ki} + w_{kw} + \Gamma_{ki} h_{ki} + \Gamma_{kw} h_{kw} \tag{2.9}$$

where the first term indicates internal energy, q denotes specific heat, w represents specific work, r shows the specific mass flow term, and h refers to specific enthalpy. Sub-index I denotes energy moving to phase k from other phases, while w stipulates energy moving to phase k from outside.

Assuming that the phases have equal temperature, the energy equation is stated as [15]:

$$\sum_k(\alpha_k \rho_k C_{PK}) \frac{\partial T}{\partial t} + \sum_k(\alpha_k \rho_k \nu_k C_{PK}) \frac{\partial T}{\partial x} = \sum_k(\alpha_k \rho_k \eta_N C_{PK}) \frac{\partial p}{\partial t} + \sum_k(\alpha_k \rho_k \nu_k \eta_k C_{PK}) \frac{\partial p}{\partial x} +$$

$$\sum_k(\alpha_k \rho_k \frac{\partial}{\partial t}(\frac{p}{\rho_k})) + \sum_k(\alpha_k \rho_k \nu_k \frac{\partial}{\partial x}(\frac{p}{\rho_k})) - ((\Gamma_k(s_k - \frac{p}{\rho_k})) + Q^{\cdot} \quad (2.10)$$

where C_{PK} is the heat capacity of phase k at constant pressure, T is fluid temperature, η is Joule-Thomson factor, and s_k is specific enthalpy of phase k. For a steady-state flow with no mass transfer between phases, the energy equation is reduced to:

$$\sum_k(\alpha_k \rho_k \nu_k C_{PK}) \frac{\partial T}{\partial x} = \sum_k(\alpha_k \rho_k \nu_k \eta_k C_{PK}) \frac{\partial p}{\partial x} + \sum_k(\alpha_k \rho_k \nu_k \frac{\partial}{\partial x}(\frac{p}{\rho_k})) P \frac{\partial}{\partial x}\sum_k(\alpha_k \nu_k) - \frac{p}{\rho_k})) +$$

$$Q^{\cdot} \quad (2.11)$$

The last term in the energy equation, $Q^{\cdot}$, is the heat transfer rate per unit volume added to the fluid, which is obtained as follows:

$$Q^{\cdot} = 2U \frac{r_o}{r_i^2}(T_o - T_i) \quad (2.12)$$

where r_i is the inside radius, r_o is the outside radius, and U is the overall heat transfer coefficient. T_o and T_i represent the surrounding temperature and the average fluid temperature inside the pipe, respectively. The overall heat transfer coefficient can be calculated by [16]:

$$\frac{1}{U} = \frac{1}{h_i} + \frac{r_i}{K} \ln\frac{r_i}{r_o} + \frac{r_i}{h_o r_o} \quad (2.13)$$

where k represents the thermal conductivity of the pipe, and h_i and h_o are the convective heat transfer coefficient for the inside and outside of pipe, respectively. Depending on the fluid Reynolds number, h_i and h_o can be estimated for laminar or turbulent flows. Bergman et al. suggest that for laminar flow ($Re_f < 2300$) in a pipe with constant surface temperature [16]:

$$h = 3.66 \frac{K_f}{D} \quad (2.14)$$

where K_f is the fluid conduction coefficient and should be evaluated at mean temperature. Gnielinski suggests the following correlation for turbulent flow [17]:

$$h = \frac{K_f}{D} \frac{(f/8)(Re_f - 1000)Pr_f}{1.07 + 12.7\left(\frac{f}{8}\right)^{1/2}(Pr_f^{2/3} - 1)} \tag{2.15}$$

where f is the friction factor stated previously. Gnielinski's correlation is valid under the following limitations:

$$2300 \leq Re_f \leq 5 \times 10^6 \tag{2.16}$$

$$0.5 \leq Pr_f \leq 2000 \tag{2.17}$$

To find the convection heat transfer coefficient for solid sphere sand particles, Whitaker recommends a correlation of the form [18]:

$$h = \frac{K_S}{D_S} [2 + (0.4Re_s^{1/2} + 0.06Re_s^{2/3}) Pr_f^{0.4} (\frac{\mu_f}{\mu_{fs}})] \tag{2.18}$$

where K_s is thermal conductivity of sand particles, Re_s is the Reynolds number of solid particles, and Pr_f is the continuous phase (gas phase) Prandtl number. Here, μ_f and μ_{fs} represent the dynamic viscosity of the gas phase at the fluid temperature and wall temperature, respectively. The fluid convection coefficient is estimated based on a volume averaging method, using each phase convective coefficient.

2.2.5 Conservation Equations in Solid Mechanics

Solid mechanics is a branch of physics which investigates the features of solid materials when they are in some way impacted by external loads.

2.2.5.1 Elasticity Equations

In continuum mechanics, a deformable solid with elastic qualities adheres to the conservation law whereby the sum of the forces equates to zero. The forces distribute the stress across a surface region. In cases of sizeable forces, a material might expand beyond the elastic region, ultimately failing through fracture. As stress differs in accordance with the area where the force is applied, it is useful to discretize elastic masses into smaller masses to avoid stress incidents. Figure 2.1 below illustrates normal stress and shear stress.

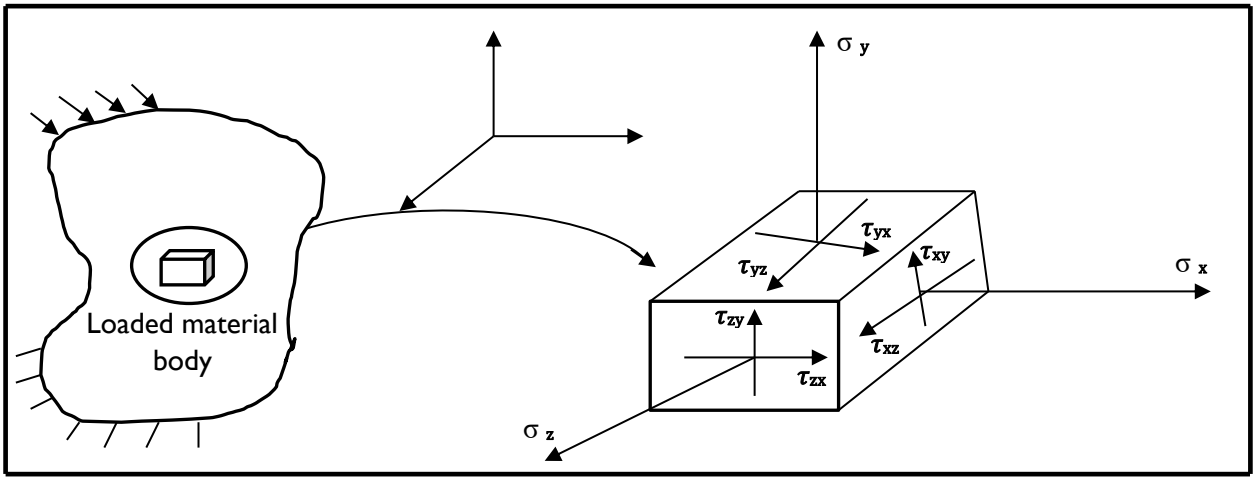

Figure 2.1 Stress Vectors in a Hexahedral Element [19].

Summing all forces in the x, y and z directions of the cube, the following equations can be written if we employ Newton's first law of motion [19]:

$$\frac{\partial}{\partial x}\sigma_x + \frac{\partial}{\partial y}\tau_{xy} + \frac{\partial}{\partial z}\tau_{xz} + X_b = 0 \tag{2.19}$$

$$\frac{\partial}{\partial x}\tau_{xy} + \frac{\partial}{\partial y}\sigma_y + \frac{\partial}{\partial z}\tau_{yz} + Y_b = 0 \tag{2.20}$$

$$\frac{\partial}{\partial x}\tau_{xz} + \frac{\partial}{\partial y}\tau_{yz} + \frac{\partial}{\partial z}\sigma_z + Z_b = 0 \tag{2.21}$$

where σ indicates normal stress, τ denotes shear stress, and X_b, Y_b, Z_b represent body forces as measured per unit volume. Here, the sole body force being exerted upon the system is gravity. As can be seen in the figure, nine stress components are acting on the infinitesimal cube [19].

In the above, the physics problems incorporate the Finite Element Method (FEM), where the domain structure has been demarcated as infinitesimal elements in order to solve Equations (2.19) to (2.21) for each element. In these instances, the greater the number of elements, the more accurate the solutions. On the other hand, if we adopt this approach (using a large number of elements), the cpu will have to solve a large number of partial differential equations in order to find solutions, which would require both intensive computational

effort and a lot of time. Given this dilemma and the desire to find solutions quickly and accurately, a balance is needed to overcome the dual burdens of excessive computation time and excessive elements.

2.3 Multi-Phase Flow Regimes and Patterns

Production liquids flowing out of a well or reservoir can be a mixture of gas, oil and water, creating a 'multi-phase' or 'three-phase' flow. Such flows can be prone to developing slugs. Moreover, when the sand amount exceeds the minimum safety volume fraction, the sand can potentially accumulate at the pipe bottom, slowing the flow or creating a blockage. To maintain a continuous flow of particles, a minimum fluid velocity mixture can be used in a pipe [20].

The three main parameters that characterize a multi-phase flow are: 1) volume fraction, 2) phase number, and 3) phase velocity. The next section in this paper defines flow patterns for horizontal pipeline and also compares and contrasts the characteristics of liquid-solid, two-phase and three-phase flows. Three-phase flows can occasionally serve as two-phase flows, depending on circumstances, as mentioned below [16].

2.3.1 Two-Phase Flow Pattern Map

Maps of flow regimes can be used for identifying and categorizing flow patterns both for vertical and horizontal pipes. The maps categorize flow patterns according to each phase's superficial velocity. The patterns undergo changes depending on parameters such as surface tension, pipe diameter, pipe inclinations, and fluid phases. Identifying which flow regimes or patterns lead to instabilities or fatigue issues in the pipeline is important, as such identification can assist engineers in controlling flow conditions to avoid the creation of slug flows and other undesirable and damaging flow patterns [14].

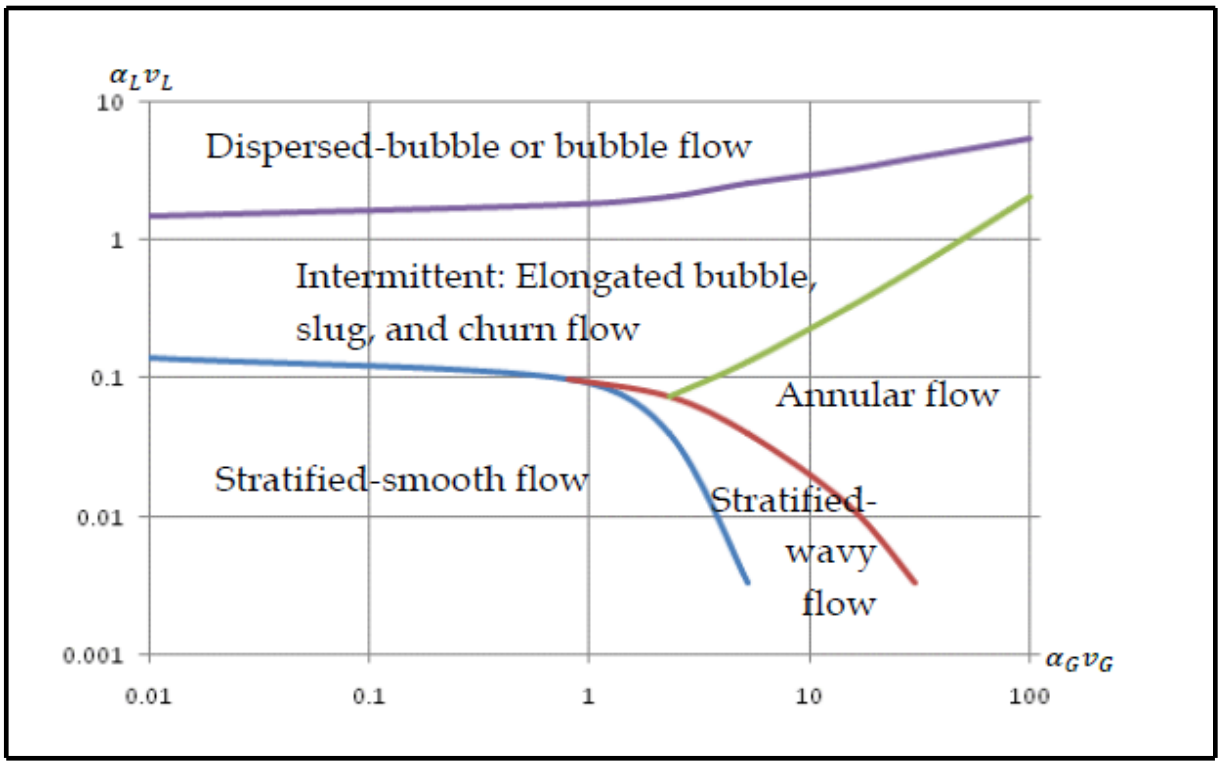

Figure 2.2 General Flow Pattern of Two-Phase Flow [14].

2.3.1.1 Horizontal Pipeline Flow Patterns

Generally speaking, the majority of oil pipelines around the world are inclined/horizontal pipelines with minimum two-phase forming flow patterns. In multi-phase gas-liquid flows, there are five possible flow patterns [14]. These patterns are illustrated in Figure 2.3 below:

- Annular flow: If gas superficial velocity is relatively high in comparison with the liquid, the gas migrates to the pipe center and is enveloped in a thin layer of fluid at the pipe wall. In this regime, some droplets move through the pipe-center (see Figure 2.3 (e)).
- Dispersed bubble flow: When superficial velocity is comparatively high, this flow pattern is likely to form and is distinguished by bubbles throughout the pipe length as well as larger bubbles near the top (see Figure 2.3 (a)).
- Slug flow: This flow pattern features long discontinuous gas bubbles interspersed with liquid pieces. Slug flows typically cause pipe blockage (see Figure 2.3 (d)).

- Stratified flow: This pattern is the most common of the five different flows and features a fairly low liquid and gas superficial velocity. In most cases of stratified flow, the gas hovers over the fluid (the latter of which usually is denser) and an interface divides the two (see Figure 2.3 (b)).
- Wavy flow: In this flow type, gas superficial velocity rises, resulting in higher surface tension and the formation of waves near the interface boundary (see Figure 2.3 (c)).

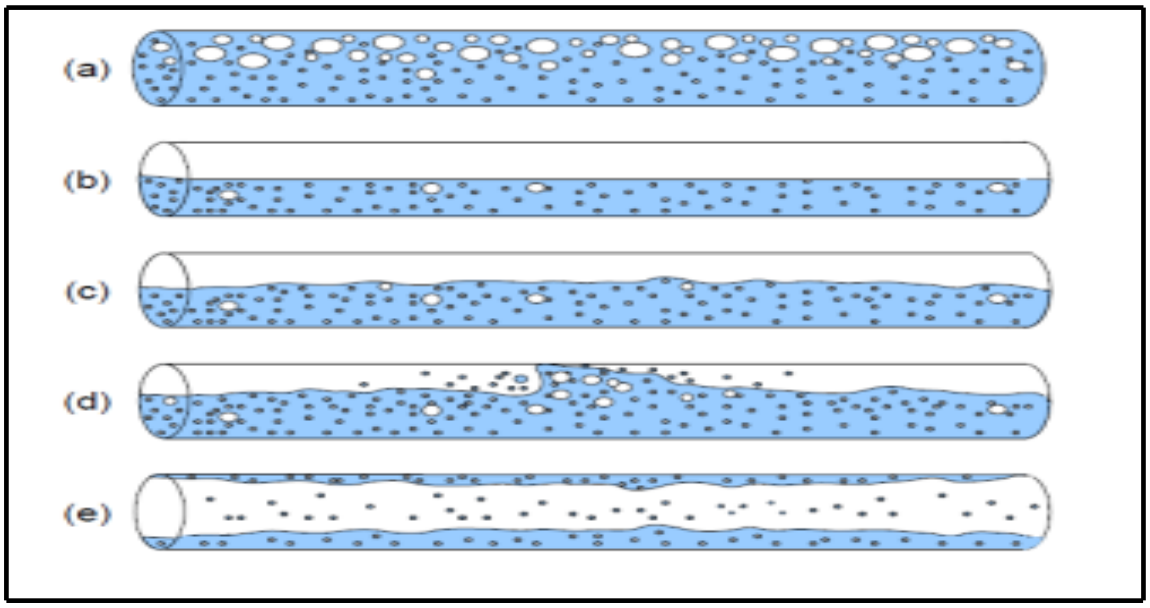

Figure 2.3 Flow Patterns Occurring in Horizontal Pipeline [14].

2.3.1.2 Volume Fraction

In the O&G industry, the ratio of the volume of gas coming out of the well at room temperature to the volume of oil produced at the same environmental conditions is reported as the GOR or gas-oil ratio. This is usually measured in cubic feet of gas per barrel unit. The volume fraction or area fraction of a phase is the cross-section occupied by this particular phase. The sum of the volume fraction of all phases in the cross-section should be equal to one. This is used in conjunction with the velocity of the phases [17].

2.3.1.3 Superficial Velocity

The area fraction of a phase is expected to change over space and time, so the average velocity of the flow varies depending on the volume fraction of each phase and its respective velocity. In this case, the average velocity of each phase is defined at its part of the cross-section as [14]:

$$\upsilon_{SG} = \alpha_G \, \upsilon_G = \frac{Q_G}{A} \tag{2.22}$$

The volumetric flow rate Q_G at the whole cross-section area A determines the superficial velocity of the phase. This tends to be lower than the average velocity of the flow.

In oil pipelines, two-phase flow is made up of a gas and oil mixture. Because multi-phase flow should be able to solve every conservation equation, simplifying two-phase models as a means to get rid of pressures and forces which exert relatively minor influence over the flow is the generally preferred approach. In this section, we first present a stratified flow model which has been simplified based on assumptions of gas-oil flow estimates. The model also accounts for pressure corrections. Next, we discuss the Taitel and Duckler model, which illustrates transition relationships of different flow regimes. Finally, in this section, we introduce a simplified model for a slug flow to calculate slug length and frequency.

2.3.1.4 Pressure Difference in Stratified Flow

If the cross-section pressure were found to be equal, surface waves could not be formed near the surface of the interface. As a result, numerical problems would likely occur in the system.

Therefore, in finding pressure differences near cross-sections, we need to assume the following:

- The speed of the phase flow is quite low, resulting in a stratified flow.
- The liquid is unable to dissolve the gas.
- The fluids are unable to move beyond the wall of the pipe.
- The flow is described as isothermal.

In accounting for any differences in average speed between the phases, we can use the Bernoulli-effect as a reference point. The calculation has been correlated against pressure differences occurring for the cross-section's various heights. Figure 2.4 illustrates how the surface of the interface can be used for a reference to determine any pressure differences that may exist between the phases. By applying this method, we can formulate the pressure difference as shown below [14]:

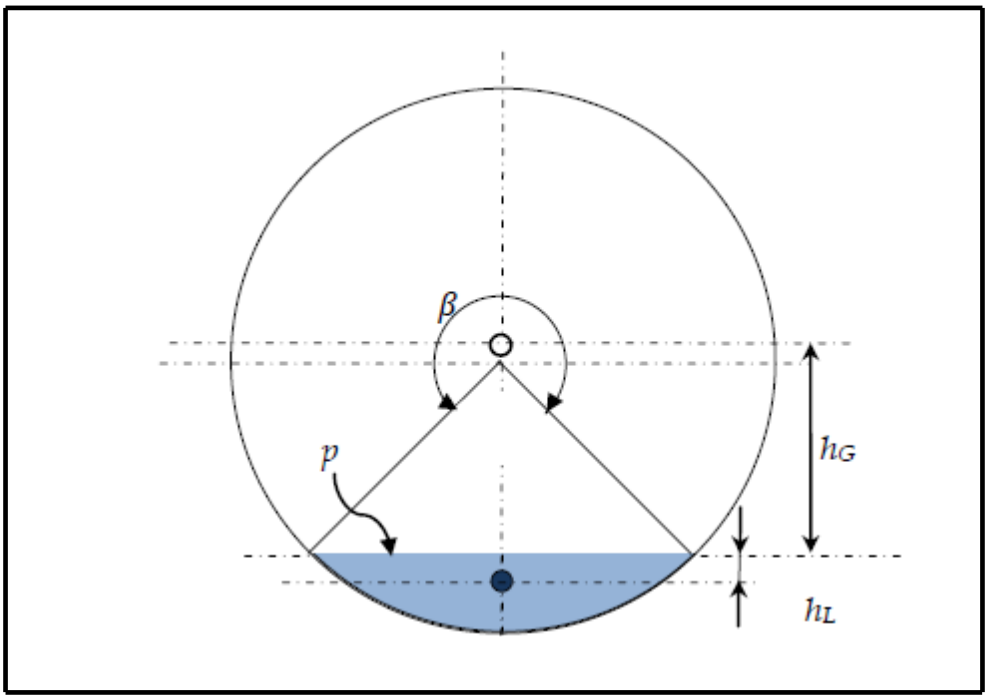

Figure 2.4 Stratified Flow Diagram for Pressure Difference at Cross-Section [14].

$$\Delta P_G = P_G - P = \rho_G g P h_G \tag{2.23}$$

$$\Delta P_L = P_L - P = \rho_L g P h_G \tag{2.24}$$

where P_G and P_L denote pressures occurring at the gas and liquid centers of gravity, respectively, ρ_G refers to gas density; and ρ_L expresses liquid density. At the center of gravity, the static pressure for every phase the represents surface interface distance, as written in Equations (2.25) and (2.26):

$$h_L = [-\frac{1}{2}\cos(\pi-\frac{\beta}{2}) + \frac{1}{3\pi\alpha_L}(\sin(\pi-\frac{\beta}{2}))^3]\, d\cos\Theta \quad (2.25)$$

$$h_G = [\frac{1}{2}\cos(\pi-\frac{\beta}{2}) + \frac{1}{3\pi\alpha_G}(\sin(\pi-\frac{\beta}{2}))^3]\, d\cos\Theta \quad (2.26)$$

These Equations can be considered valid if the pipe has a mostly horizontal inclination angle Θ that can create waves via gravity. In Biberg, an approximation for angle β can be applied as a function for the liquid fraction α_L, giving an accuracy of ± 0.002 rad, as written in Equation (2.27) [14]:

$$\beta = 2\pi - 2\{\pi\alpha_L + (\frac{3\pi}{2})^{1/3}[1-2\alpha_L + \alpha_L^{1/3} - (1-\alpha_L)^{1/3}]\} \quad (2.27)$$

2.3.1.5 Slug Flow

Slug flow describes problematic intermittent flows of liquid slugs and elongated (Taylor) bubbles.

Figure 2.4 illustrates how these bubbles move to upper sections of horizontal pipes. Slug flow can cause serious issues in pipeline flows, such as corrosion, flooding, and major pressure fluctuations. This work will look at three different types of slugs:

- Terrain slugs: Long liquid slugs that accumulate around low portions of a pipe. These are caused by different angle inclinations and can persist for several hours.
- Hydrodynamic slugs: Short slugs which result from surface interface instability. Specifically, if the gas hydrodynamic force is greater than the interface surface tension, the liquid pools near the uppermost portion of the pipe.
- Operational-induced slugs: Liquid slugs that accumulate near low points along the pipeline and emerge from the pipe as a slug, typically during pigging operations in a system shut-down.

To determine average slug frequency and length, Zabaras developed a correlation for slug frequency (f_s) in relation to pipe diameter (between 0.0254 m and 0.20 m) as well as angle of elevation (between 0° and 11°), as expressed in Equation (2.28) [14]:

$$f_s = 0.0226(\frac{\alpha_l \upsilon_l}{gd})[\frac{64.8}{\alpha_G\upsilon_G+\alpha_L\upsilon_L} + 3.28\ (\alpha_G\upsilon_G + \alpha_L\upsilon_L)]^{1.2}[0.836 + 2.75(\sin\Theta)^{0.25}] \quad (2.28)$$

In this formulation, α_G and α_L indicate volume fractions that have been averaged for the entire slug. Hence, the frequency of the slug has been made contingent on the length of the slug. In Equation (2.29), slug length has been estimated according to Scott's empirical relationship, which considers slug length to be a function of diameter d, as follows [14]:

$$L_S = \max \{30d, \exp \{-26.8 + 28.5[\ln \frac{d}{0.0254})]^{0.1}\}\} \quad (2.29)$$

In another calculation, as shown in Equation (2.30), slug frequency is correlated to pipe length as determined at the inlet. This curve-fitting approach, which has shown fair agreement with data from both field and lab tests, is given below:

$$f_s = \frac{0.47(\alpha_l v_l)^{0.75}}{d^{1.2} {l_{in}}^{0.55}} \quad (2.30)$$

The empirical formulations currently applied for predicting slug length and frequency do not provide a general correlation for predicting overall slug behavior. However, CFD simulations can provide reasonably good predictions for modeling fluid dynamic problems.

2.3.2 Three-Phase Flow Pattern Map

In pipelines, the flow of gas and oil is typically accompanied by water. Although two- and three-phase flows are calculated using the same conservation equations, three-phase flows present with more complex and varied flow patterns beyond liquid-liquid and liquid-gas flows.

Figure 2.5 depicts a map of three-phase flow regimes according to velocity and volume fraction for each phase. The different patterns illustrate the dispersion of different fluid types, showing how slug and stratified flows are transported across horizontal and inclined pipeline systems. The following sections provide further details on these types of flows.

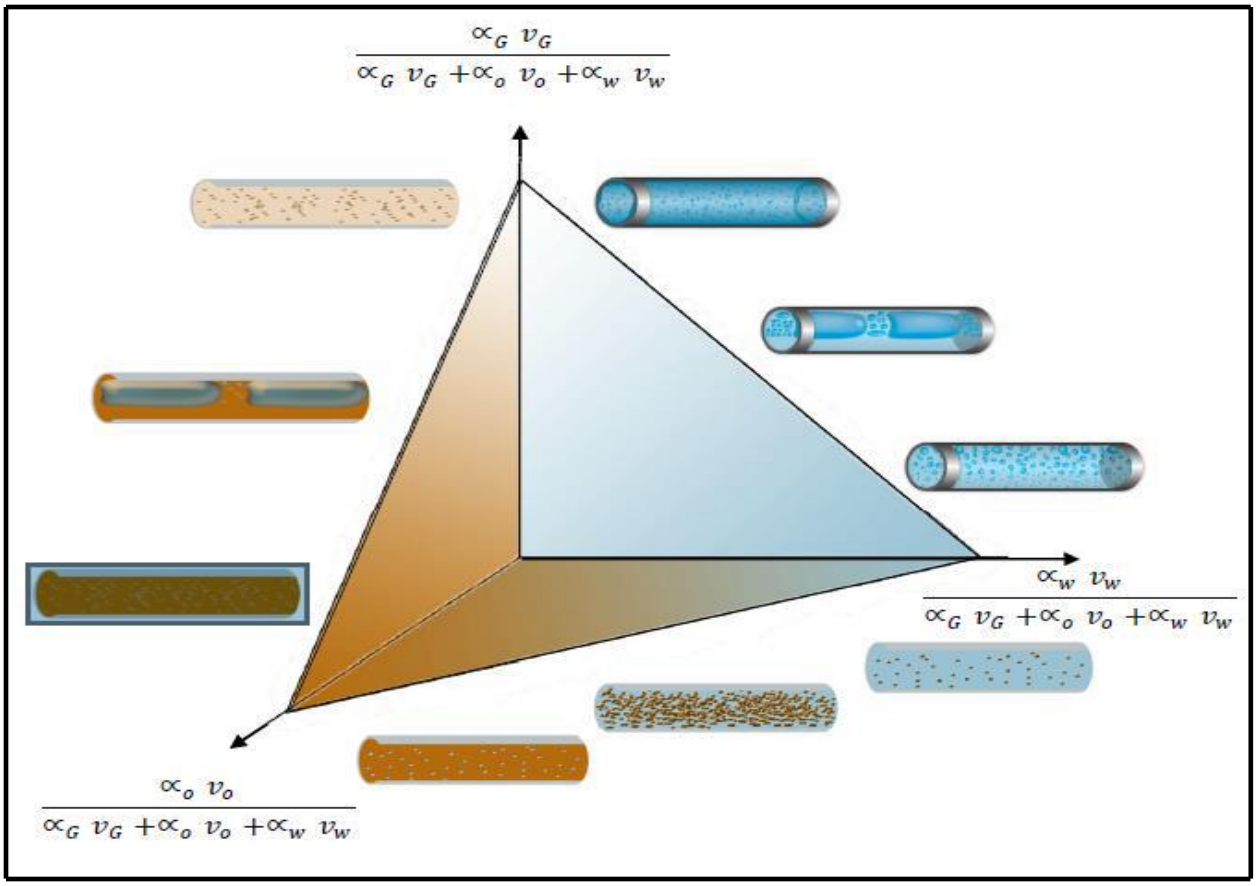

Figure 2.5 Three-Phase Flow Pattern Map Used for Horizontal Pipeline [14].

2.3.2.1 Gas-Oil-Water Stratified Flow

In three-phase flows, the forces of surface tension and friction must be considered, just as they are for two-phase flows. Similarly, the pressure correction term also must be taken into consideration.

Figure 2.6 illustrates how pressure can be determined near the gas and denser liquid boundary. In this case, the gas pressure correction term used in two-phase liquid-gas flows can be applied as follows:

$$\Delta P_G = P_G - P = \rho_G g h_G \tag{2.31}$$

To calculate liquid correction terms, we can take as our reference the center of gravity for individual liquid phases in order to determine pressure correction terms for oil and water:

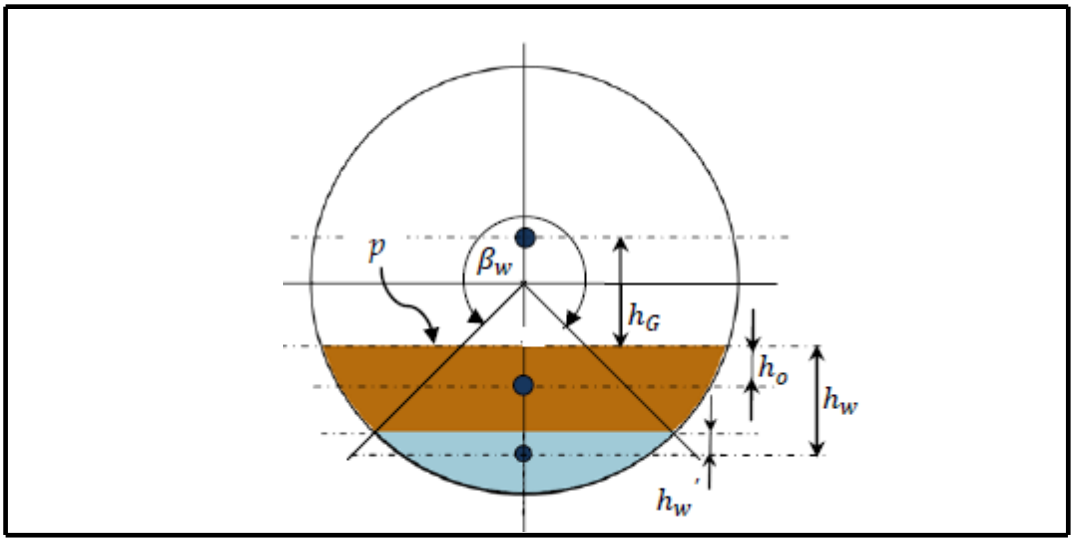

Figure 2.6 Three-Phase (Gas-Oil-Water) Stratified Flow Configuration with Center of Gravity Points [14].

$$\Delta P_O = P_O - P = \rho_O g h_O \tag{2.32}$$

$$\Delta P_W = P_W - P = \Delta P_O + \rho_W g h_W \tag{2.33}$$

where h_o denotes distance from the gas-oil interface to the oil's center of gravity, and h_w indicates distance from the gas-oil interface to the water's center of gravity. Further, by applying Petalas and Aziz's (1998) empirical equation, we can formulate the interfacial frictions if we neglect the impacts of velocity profile, turbulence, and wall friction, as expressed in Equation (2.34) below [14]:

$$F_{GL} = (0.004 + 0.5 \times 10^{-6}\ Re_{sL}) Fr_L^{1.335}\ \frac{\rho_L d g}{\rho_G \upsilon_G^2} \tag{2.34}$$

where Re_{SL} refers to the oil phase Reynolds number, and Fr_L indicates the Froude number of the liquid, which in this formulation depends on the velocity and density of each phase as well as pipe diameter d and gravity g. In Equation (2.35), the Froude number has been applied to describe how liquid velocity v_L is impacted by gravity effects [14]:

$$Fr_L = \frac{\upsilon_L}{\sqrt{g h_L}} \tag{2.35}$$

It is worth noting that this Equation system has not yet been examined to determine whether or not it is hyperbolic. If it is, numerical problems may arise, resulting in a crash of the simulations. Perturbation methods or eigenvalue analysis would be useful for determining these equations' hypertonicity.

2.3.2.2 Gas-Oil-Water Slug Flow

Three-Phase flows can be treated in two main ways:

- For liquid phases, such as oil-water, flows can be considered as single-phase flows if the liquids are mixed. In cases where the flow is combined with gas, it should be considered a two-phase flow and treated accordingly.
- Liquid phases are separated as two individual layers, where the liquid which is denser (in this case, the oil) is positioned at the top, as shown in Figure 2.7.

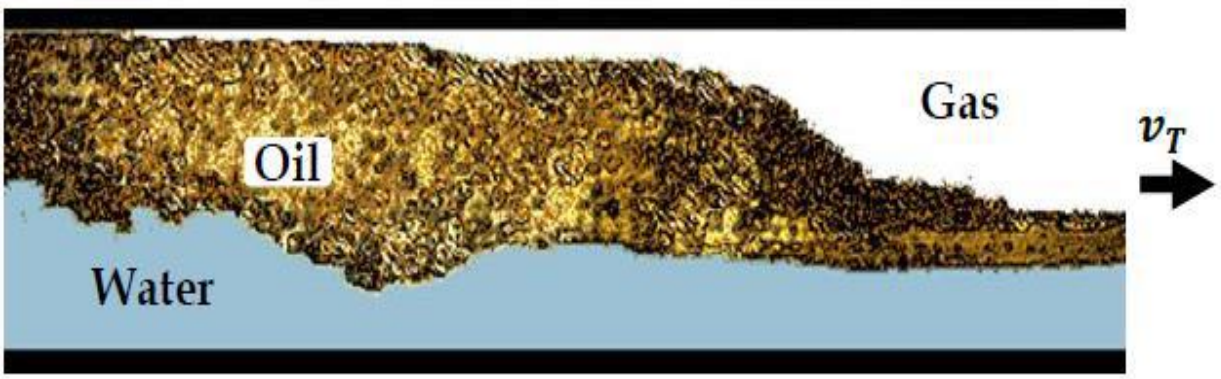

Figure 2.7 Horizontal Three-Phase (Gas-Water-Oil) Flow Showing Slug Behavior [14].

Slugs typically exhibit unstable dynamic behavior characterized by random superficial velocities and frequencies that change according to different geographical situations and other factors. Consequently, solving mass and momentum differential equations for slugs can be very challenging. If we assume a steady-state stratified flow without any liquid entrainment in the gas, we can use the following formulation:

$$(1-\alpha_{WGS})\,(1-\alpha_{os})\,(\upsilon_T-\upsilon_{os}) = \alpha_{oT}(\upsilon_T-\upsilon_{oT}) \tag{2.36}$$

where the first term indicates the oil slug fraction (with bubbles), the second term denotes the oil-water slug fraction of water (without bubbles), and the third term represents velocity differences between the slug's oil fraction and the Taylor gas bubbles.

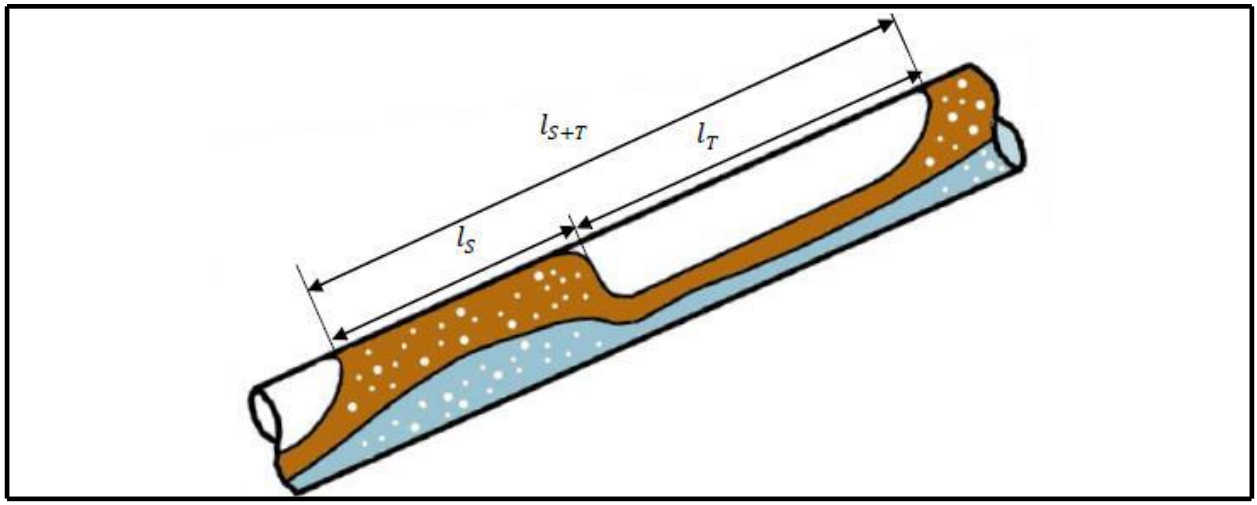

Figure 2.8 Slug Flow Configuration with Gas Entrainment in Oil and Water Layers [14].

In order to develop a formula which can readily be compared with numerical or experimental solutions, we can consider the mixture as a steady-state flow. In this case, velocity can be expressed as in Equation (2.37):

$$\upsilon_M = \alpha_G \upsilon_G + \alpha_O \upsilon_O + \alpha_w \upsilon_w \tag{2.37}$$

$$\upsilon_M = \upsilon_{SG} + \upsilon_{SO} + \upsilon_{SW} \tag{2.38}$$

Furthermore, when slug and Taylor bubbles are formed, their mixture velocity can be expressed by applying Equations (2.39) and (2.40), respectively, as closure relationships [14]:

$$\upsilon_M = (1- \alpha_{WGS})\upsilon_{OS} + \alpha_{WGS}\, \upsilon_{WS} \tag{2.39}$$

$$\upsilon_M = \alpha_{OT}\upsilon_{OT} + \alpha_{WT}\upsilon_{WT} + (1- \alpha_{OT}- \alpha_{WT})\, \upsilon_{GT} \tag{2.40}$$

Should fatigue damage take place, volume fraction helps determine both the amount and the rate of flow for each slug phase. In the flow's slug portion, the gas, oil, water and oil average can be formulated as in Equations (2.41), (2.42) and (2.43):

$$\alpha_O \upsilon_O = \frac{l_s}{l_{s+T}} (1- \alpha_{WGS})(1 - \alpha_{OS})\, \upsilon_{OS} + \frac{l_s}{l_{s+T}} \alpha_{OT}\upsilon_{OT} \tag{2.41}$$

$$\alpha_W \upsilon_W = \frac{l_s}{l_{s+T}}\, \alpha_{WGS}(1 - \alpha_{WS})\, \upsilon_{WS} + \frac{l_s}{l_{s+T}} \alpha_{WT}\upsilon_{WT} \tag{2.42}$$

$$\alpha_G \upsilon_G = \frac{l_s}{l_{s+T}}\, [(1 - \alpha_{WGS})\alpha_{OS}\upsilon_{OS} + \alpha_{WGS}\alpha_{WS}\upsilon_{WS}] + \frac{l_s}{l_{s+T}}\, (1 - \alpha_{OT} - \alpha_{WT})\upsilon_{GT} \tag{2.43}$$

In Figure 2.8, l_{s+T} indicates total slug length. Steady-state momentum equations are used for representing water behavior and Taylor bubbles in a slug flow. The expressions include, among other factors, velocity, shear stress between phases, and slug length phase mass.

The mixture (average) velocity in a mixture of N phases is defined as:

$$\upsilon_M = \sum_{K=1}^{N} \alpha_K \upsilon_K \ = \alpha_G \upsilon_G + \alpha_O \upsilon_O + \alpha_w \upsilon_w \quad (2.44)$$

where α is the volume frication, υ is the superficial velocity and the subscript k represents gas (g), oil (o), and water (w) [14]. We sometimes make use of the mixture (average) density, which is defined as:

$$\rho_M = \sum_{K=1}^{N} \alpha_K \rho_K \ = \ \alpha_G \rho_G + \alpha_O \rho_O + \alpha_w \rho_w \quad (2.45)$$

Other mixture properties or quantities can be defined in a similar fashion.

2.3.2.3 Liquid-Solid-Gas Flow Regimes

In the transport of oil and gas from subsea reservoirs to onshore production sites, the presence of sand in the flow can lead to pipeline erosion as well as issues with stability, blockage, and structural integrity. These sand-related problems can be avoided or at least mitigated by preventing the accumulation of sand and preventing sand from entering the pipeline through the use of downhole sand exclusion systems. In such an exclusion system, however, added pressure drops may occur. Therefore, adopting measures against sand accumulation can be useful if flow conditions are able to be adequately controlled.

Two main factors which should be taken into account when devising approaches to combat sand build-up are particle size and volume fraction. In most instances of crude oil production, the sand production typically remains less than 0.05 mm [14], while sand particle diameter is typically 1 mm or less [17]. Particles are categorized according to the following size features [18]:

very fine (0.05 - 0.1 mm), fine (0.1 - 0.25 mm), medium (0.25 - 0.5 mm), coarse (0.5 - 1 mm), and very coarse (1 - 2 mm) [18].

In pipelines, stratified flow enables sand particles to accumulate near the bottom portions of a pipe, especially at bends. When this occurs, it increases pressure losses, which then leads to blockage and lost production time. The specifications of solid particles used in different experiments has been summarized in Table 2.1.

Table 2.1 Specifications of Solid Particles Used in Different Experiments.

Author (Year)	Phases	Pressure	Solid Parameters				
			Type	Diameter	Reynolds Number	Density	Avg. Density
Gul et al. (2017)	liquid-gas-solid	-	Industrial sands	2.75 mm	-	2762 kg/m^3	2600 kg/m^3
Al-lababidi et al. (2012)	Water-gas -sand		Sand	0.2 mm	-	2650 kg/m^3	
Oudeman et al. (1993)	Air-water-sand	above atm.	Sand grain	0.15 -0.30 and 0.69 mm	-	-	
Kelessidis (2007)	liquid-gas-solid	atm.	Glass beads	2 mm	-	2590 kg/m^3	
Shadizadeh et al. (2012)	liquid-gas-solid	-	Sandstone + limestone	3.23, 2.03 and 1.02mm	-	2400 kg/m^3	
Duan et al. (2006)	liquid-gas-solid	-	Rock cuttings	0.45, 1.4 and 3.3 mm	-	-	
Han et al. (2010)	liquid-gas-solid	-	Sand particles	1 mm	-	2550 kg/m^3	
Ju Kim et al. (2008)	liquid-gas-solid	-	Sand particles	1 mm	-	2550 kg/m^3	
Osho et al. (2012)	Water-gas-sand	-	Sand	0.27 mm	-	2650 kg/m^3	
Bello et al. (2005)	Water-gas-sand	atm.	Sand	0.6 – 0.8 mm	84.00	2600 kg/m^3	
Avila et al. (2008)	liquid-gas-solid	-	Commercial gravel	2.77 mm	-	2300 kg/m^3	
Zhou et al. (2004)	liquid-gas-solid	185-500 psi	Cuttings	-	-	2610 kg/m^3	
Naganawa et al. (2002)	liquid-gas-solid	-	Cuttings	3.66 mm	-	2400 kg/m^3	
Walker et al. (2000)	liquid-gas-solid	-	Sand	0.15 – 7 mm	-	2600 – 2710 kg/m^3	
Adari et al. (2000)	liquid-gas-solid	-	Sandstone cuttings	3.175 mm	-	2560 kg/m^3	

For three-phase (solid-liquid-gas) flows, four flow types (plug, slug, stratified and annular) are possible in horizontal pipes. The four different flow types are presented in Figure 2.9:

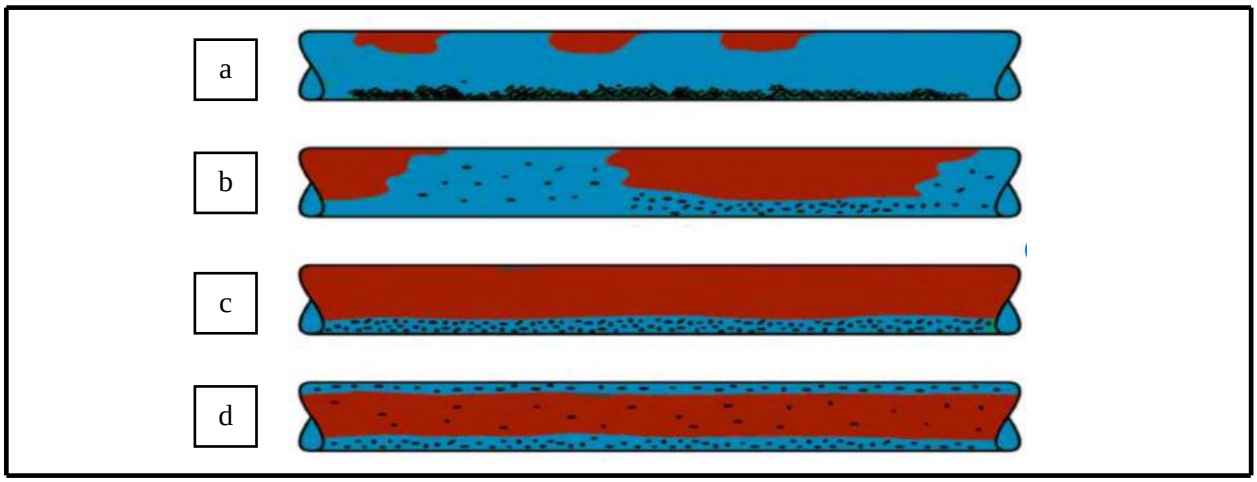

Figure 2.9 Three-Phase (Solid-Liquid-Gas) Flow Regimes for Multi-phase Flow in Horizontal Pipeline (adapted from Multi-Phase Design Handbook, 2005).

- Plug flow: Normal flow of gas that features bubbles near the annulus top. This flow type has only a minor impact on solids (Figure 2.9 (a)).
- Slug flow: As the gas flow rate increases, plug sizes also increase. These changes result in a slug flow pattern (Figure 2.9 (b)).
- Stratified flow: In this flow type, a liquid-gas interface develops that features liquid flowing near the annulus bottom (Figure 2.9 (c)).
- Annular flow: In this flow, solid particles are moved along with the liquid film (Figure 2.9 (d)).

2.3.2.4 Pressure Build-Up of Particles

When sand begins to accumulate along stretches of a pipeline, there is a subsequent increase in pressure and friction loss. The extent of these losses is determined by the flow's mixture velocity. For this reason, it is important not only to anticipate but to try to prevent solids from disrupting production in the field and onshore. When there is no sand in the pipe, friction loss will increase quadratically according to the speed at

which the mixture is transporting through the pipe. However, if sand is added to the mixture, the friction loss increases much faster and there is a concurrent pressure drops. Figure 2.10 depicts this process.

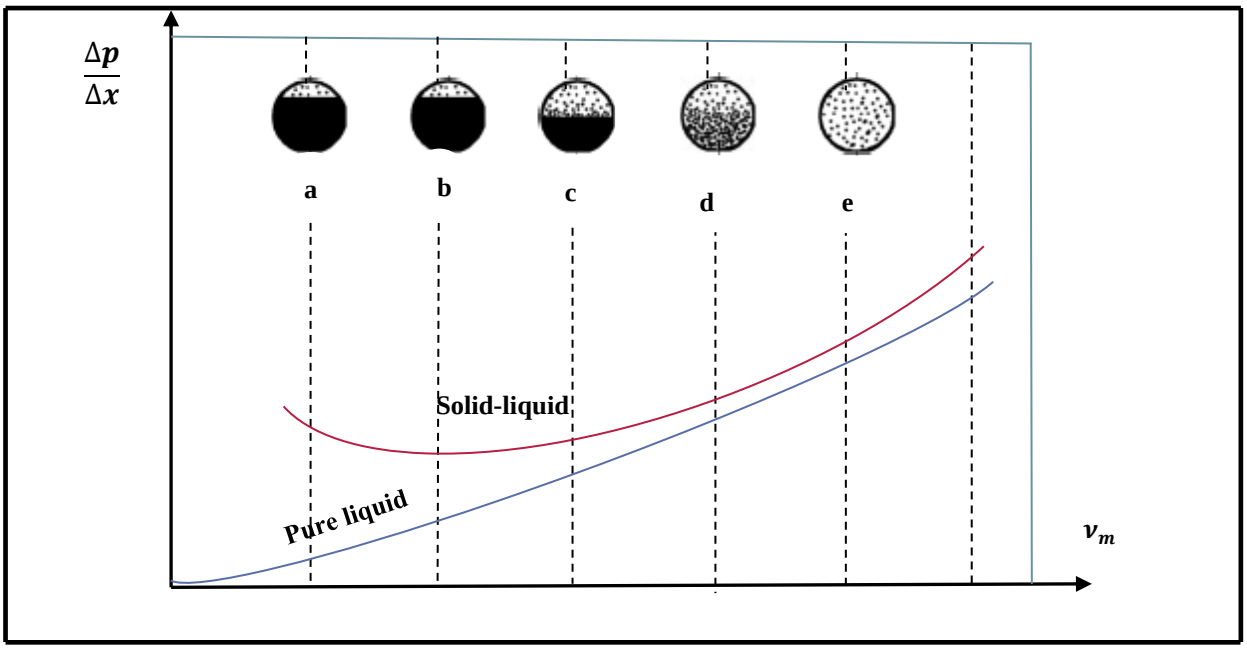

Figure 2.10 Friction Loss as a Function of the Mixture Velocity When Sand Particles Flow in the Pipeline (Adapted from Bratland, 2010).

As can be seen in Figure 2.10, the solid-liquid curve illustrates how reductions in flow velocity lead to reductions in pressure drops. It is worth noting that even though sand might accumulate along lower portions of a pipeline, the rest of the mixture can continue being transported. In this instance, however, the continued reduction in the mixture velocity will likely cause a further build-up of sand, leading to yet another increase in pressure drops. To avoid this process, the key is to maintain a constant and balanced velocity to avoid large pressure drops or blockage.

2.3.2.5 Minimum Required Velocity

A mixture's velocity is the foremost parameter that impacts sand build-up in a pipeline. Accordingly, the mixture should maintain a minimum required velocity to ensure that the sand particles continue to move along with the rest of the flow and do note accumulate in any portion of the line. To devise a minimum velocity formula, we assume the following:

1. The pipeline is horizontal and has few to no inclinations.
2. Compared to the liquid flow in the pipe, the sand's volume fraction is quite low.
3. All the sand particles in the pipeline have a similar diameter and are spherical in shape.

Figure 2.11 shows both the gravity force and the static forces existing between the particles. Using these parameters, we can apply the critical velocity expression in Equation (2.46) to move the sand through the pipe [14]:

$$\upsilon_L^* = \sqrt{\frac{16(\rho_S - \rho_L)}{3f\rho_L} gds\left[\frac{\text{Sin}\left(\Theta+\frac{\pi}{6}\right)+\mu_{fs}\,\text{COS}\left(\Theta+\frac{\pi}{6}\right)}{\text{COS}\left(\frac{\pi}{6}\right)-\mu_{fs}\,\text{Sin}\left(\frac{\pi}{6}\right)}\right]} \tag{2.46}$$

where ρ_S denotes solid particle density, ρ_L expresses liquid density, f refers to flow friction, g indicates gravity, ds stands for solid particle diameter, Θ represents the pipe's inclination, and μ_{fs} indicates the friction coefficient among grains. Furthermore, if we assume that the sand particles move in a rolling motion instead of a sliding one, we can add $\mu_{fs} = 0$. On the other hand, if we attribute a high degree of smoothness to the pipe wall, the sand particles might slide by the wall, in which case the angle $\frac{\pi}{6}$ must be altered to 0 and the Equation be written as [14]:

$$\upsilon_L^* = \sqrt{\frac{16(\rho_S - \rho_L)}{3f\rho_L} gds[\text{Sin}\,\Theta + \mu_{fs}\,\text{COS}\Theta]} \tag{2.47}$$

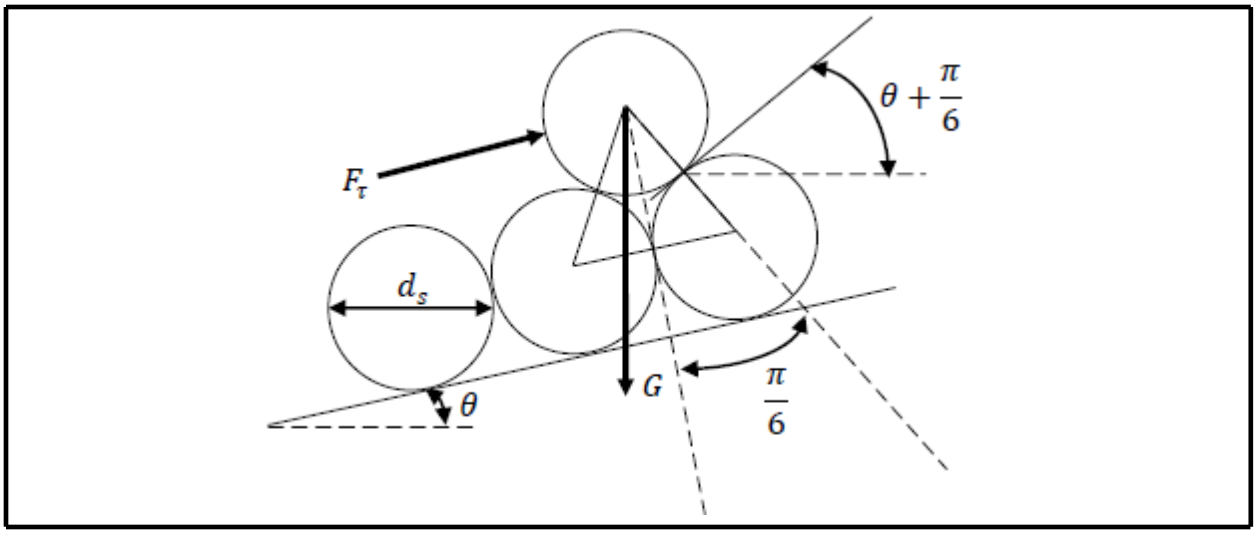

Figure 2.11 Free Body Diagram of Static Forces on a Sand Particle (in Case of Vertical Pipes, the Sand Particles are Treated as Bubbles or Droplets Distributed Across the Pipe's Cross-Section) [14].

Table 2.2 Summary of Previous Studies of Multi-Phase Flow in Pipelines

Summary of Previous Studies of Multi-Phase Flow in Pipelines												
Author (Year)	**Phases**	**Experimental Measurement Technique**	**Pipe Diameter**	**Liquid Flow rate**	**Flow Velocity**	**Gas velocity**	**Pressure**	**Incline (degree)**	**Solid Parameters**			
									Type	**Diameter**	**Reynolds Number**	**Density**
Gul et al. (2017)	liquid-gas-solid	Visualization and Computational Analysis	2.91-in. & 1.85-in.	30 –100 gpm or 136 –455 lpm	4 - 13 m/s	-	-	0^0 (horizontal)	Industrial sands	2.75 mm	-	2762 kg/m^3
Al-lababidi et al. (2012)	Water-gas-sand	Visualization and Computational Analysis	0.05m (1.97-in.) (inner dia.)	-	0.1 – 1 m/s	-	-	0 and + 5^0	Sand	0.2 mm	-	2650 kg/m^3
Osho et al. (2012)	Water-gas-sand	Visual observation	-	-	-	-	-	0^0 (horizontal)	Sand	0.27 mm	-	2650 kg/m^3
Shadizadeh et al. (2012)	liquid-gas-solid	Visual observation	-	-	-	-	-	0^0 (horizontal)	Sandstone + limestone	3.23, 2.03 and 1.02 mm	-	2400 kg/m^3
Han et al. (2010)	liquid-gas-solid	Visual observation	-	-	-	-	-	0^0 (horizontal)	Sand particles	1 mm	-	2550 kg/m^3
Ju Kim et al. (2008)	liquid-gas-solid	Visual observation	-	-	-	-	-	0^0 (horizontal)	Sand particles	1 mm	-	2550 kg/m^3
Young (2008)	liquid-gas-solid	Visualization and numerical Analysis	30 mm and 44 mm	8.5 lpm	0.2-2 m/s	-	-	30 from vertical	Sand	10 mm	-	2.55 g/cm^3
Avila et al. (2008)	liquid-gas-solid	Qualitative Analysis	8-in. & 4.5-in.	757-1893 lpm	-	-	-	30, 45 and 60 (from vertical)	Commercial gravel	2.77 mm	-	2300 kg/m^3
Kelessidis (2007)	liquid-gas-solid	Visual observation	-	-	-	-	atm.	0^0 (horizontal)	Glass beads	2 mm	-	2590 kg/m^3
Cont…												

Duan et al. (2006)	liquid-gas-solid	Visual observation	-	-	-	-	-	0^0 (horizontal)	Rock cuttings	0.45, 1.4 and 3.3 mm	-	-
Bello et al. (2005)	Water-gas-sand	Visual observation	-	-	-	-	atm.	0^0 (horizontal)	Sand	0.6 – 0.8 mm	84.00	2600 kg/m^3
Zhou et al. (2004)	liquid-gas-solid	Visualization and Computational Analysis	6-in. & 3.5-in	302-568 lpm	1.6 – 3 m/s	-	185-500 psi	0^0 (horizontal)	Cuttings	-	-	2610 kg/m^3
Naganawa et al. (2002)	liquid-gas-solid	Visualization and Computational Analysis	5-in. & 2-in	15-70 m^3/h or 250-1167 lpm	0.4-1.85 m/s	-	-	$30 – 90^0$ (with 15^0 interval)	Cuttings	3.66 mm	-	2400 kg/m^3
Walker et al. (2000)	liquid-gas-solid	Fluid Rheology Analysis	5-in. and 2- 3/8 in.	-	-	-	-	$15 – 90^0$ (with 15^0 interval)	Sand	0.15–7 mm	-	2600 – 2710 kg/m^3
Adari et al. (2000)	liquid-gas-solid	Fluid Rheology and Computational Analysis	8-in. & 4.5-in	757-1514 lpm	-	-	-	87^o and 90^o	Sandstone cuttings	3.175 mm	-	2560 kg/m^3
Oudeman et al. (1993)	Air-water-sand	Visual observation	0.07 m	-	0.1-1.2 m/s	-	above atm.	0^0 (horizontal)	Sand grain	0.15 -0.30 and 0.69 mm	-	-

The research reviewed and summarized in this chapter presents work previously conducted on multi-phase flows for two- and three-phase flow pipeline systems. The summary provides a foundation for the observations made in the present work.

This research has direct application for the study of critical conditions required to investigate temperature and pressure gradients experimentally and theoretically in pipelines for four-phase (sand/water/gas/oil) flow.

The experimental analyses performed by the researchers indicate that spherical sand particles are preferred for the solid phase of slurry flow. This is because the spherical glass beads offer the desired sand property, which can perfectly simulate the properties of sand. Moreover, the glass beads are uniform in diameter and density, thus satisfying the very sensitive parameters in these experiments.

The comprehensive literature review has been summarized in Table 2.2.

Many multi-phase flow loop pipeline experiments published in the literature were investigated for experiments similar to those in our present study. They were collected to investigate the phenomena of multi-phase flow through a horizontal pipeline. An overview of the studies' findings reveals that different parameters have the potential to play a significant role in the outcomes of multi-phase flow. The major controlled variables in the present study are fluid flow rate, pressure drop, volume fraction, and input solid concentration. The experimental conditions are summarized in the table above.

The experiments have been simulated in a multi-phase flow loop pipeline in a lab at Memorial University of Newfoundland, Canada, for four-phase flow conditions (water, oil, gas and solid).

The multi-phase flow system must contain the slurry, which is a mixture of solid particles and liquid, especially water. Whether a Newtonian or non-Newtonian flow, the slurry must contain certain amounts of solid particles. Generally, a sand-based solid, like glass beads and sandstone, is used as solid phase. However, limestone, commercial gravel, and sand grain have also been used in the experimental analyses.

2.4 Rheological Model

The major rheological models are the Newtonian, Bingham, Power Law, and Herschel Bulkley models. The shear stress versus shear rate data is plotted for determining which rheological model is the best fit for the behavior of the fluid system.

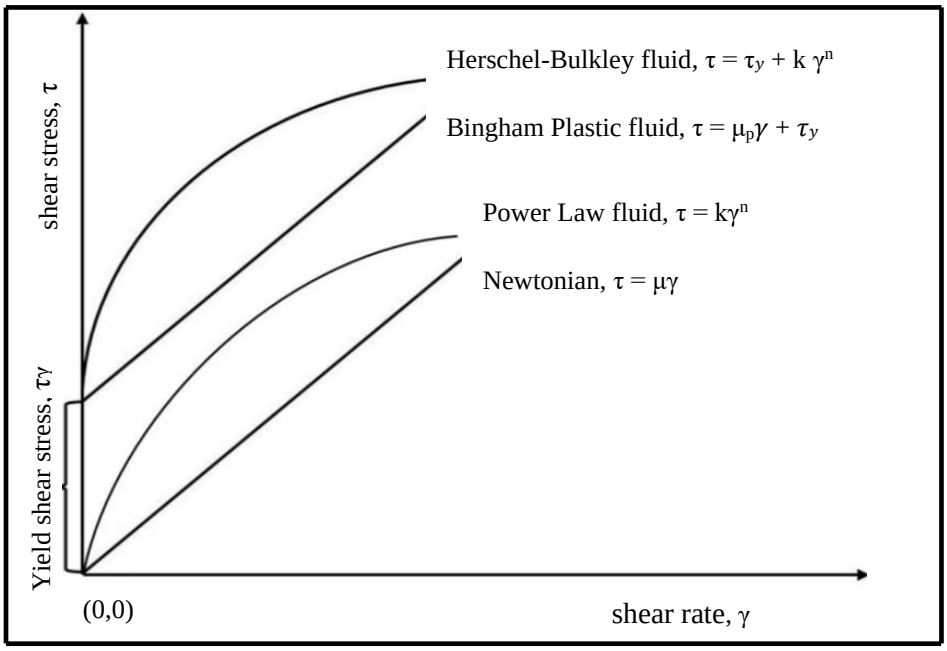

Figure 2.12 Schematic Comparison of the Four Rheological Models [20].

2.4.1 Newtonian Model

Newtonian fluid has a linear relationship between shear stress (τ) and shear rate (γ) according to:

$$\tau = \mu\gamma \tag{2.48}$$

where: τ = shear stress, lb/100ft^2 or Pa,

μ = viscosity, cp or mPa.s,

γ = shear rate, s^{-1}

Here, the shear stresses can be estimated as a function of viscosity and calculated by the following equations:

$$\mu = \theta_{300} \tag{2.49}$$

Shear stress can be calculated by:

$$\tau = \frac{\mu}{478.8}\gamma \tag{2.50}$$

where: Θ_{300} = dial reading of viscometer at 300 rpm; and 1 lb/100ft^2 = 478.8 cp.

2.4.2 Bingham Plastic Model

The Bingham plastic model describes time independent fluids. It is a two-parameter rheological model that is commonly used in the drilling industry. For Bingham plastic fluids, initial stress is required to initiate the flow. The modeled shear stresses can be calculated by the following equations:

$$\tau = \mu_p\gamma + \tau_y \tag{2.51}$$

$$\mu_p = \theta_{600} - \theta_{300} \tag{2.52}$$

$$\tau_y = \theta_{300} - \mu_p \tag{2.53}$$

where: μ_p = plastic viscosity, cp; τ_y = yield point, lbs/100ft^2.

2.4.3 Power Law Model

The Power Law model describes the flow behavior of pseudo-plastic fluid and is a two-parameter rheological model. Here, the viscosity of the Power Law fluid decreases with increasing shear rate. No initial stress is required for initiating the flow. The Power Law relationship is defined as:

$$\tau = k\gamma^n \tag{2.54}$$

where n is the flow behavior index and K is the consistence index.

$$n = 3.32 \log\left(\frac{\theta 600}{\theta 300}\right) \tag{2.55}$$

$$K = \frac{510\times\theta 300}{511^n} \text{ dyne sec}^n/100\ cm^2 \tag{2.56}$$

2.4.4 Herschel Bulkley Model

The Herschel Bulkley model is a Power Law model, that accommodates the existence of a yield point. It is a three-parameter rheological model. Herschel-Bulkley model parameters are calculated as below:

$$\tau = \tau_y + k\,\gamma^n \tag{2.57}$$

$$\tau_y = 2\theta_3 - \theta_6 \tag{2.58}$$

The parameter τ_0 is the actual yield point of fluid, which indicates the lowest shear stress that propels the fluid to flow. It is not an extrapolated value, so it means something completely different than the Bingham yield point τ_y. The value of τ_0 is related to the type and concentration of the polymer agents; the solid content also affects it. The shear stresses can be calculated by the following Equations:

$$n = 3.32 \log \left(\frac{\theta 600 - \tau 0}{\theta 300 - \tau 0}\right) \tag{2.59}$$

$$K = (\theta_{300} - \tau_0)\, 511^n \tag{2.60}$$

2.5 Four-Phase Flow Definitions and Terminology

2.5.1 Volume Fraction (α)

The volume fraction or area fraction of a phase is the cross-section occupied by this particular phase. The sum of the volume fraction of all phases in cross-section should be equal to one. This is used in conjunction with the velocity of the phases [14].

$$\alpha_k = \frac{\text{Volumetric flow rate of phase K}}{\text{total of flow rate}} \tag{2.61}$$

The sum of volumetric fractions for all phases are expressed as follows:

$$\sum_{K=1}^{N} \alpha_K = 0 \tag{2.62}$$

$$\alpha_g + \alpha_O + \alpha_w + \alpha_s = 1 \tag{2.63}$$

To develop a formula that which can readily be compared with numerical or experimental solutions, we can consider the mixture as a steady-state flow [14].

Volumetric fraction of gas (α_g):

$$\alpha_g = \frac{Q_g}{Q_{total}} \tag{2.64}$$

Volumetric fraction of oil (α_O):

$$\alpha_O = \frac{Q_O}{Q_{total}} \tag{2.65}$$

Volumetric fraction of water (α_W):

$$\alpha_W = \frac{Q_w}{Q_{total}} \tag{2.66}$$

Solid fraction (α_S):

$$\alpha_S = \frac{Q_S}{Q_{total}} \tag{2.67}$$

Q_g, Q_O, Q_w and Q_s represent the volumetric flow rate of gas, oil, water, and solid phases, respectively while α_g, α_O, α_w and α_s dente the in-situ volumetric fractions for each of the phases, respectively.

2.5.2 Velocity of Mixture (υ_m)

In this case, the velocity of the mixture can be expressed as in Equation (2.68):

$$\upsilon_m = \sum_{K=1}^{N} \alpha_K \upsilon_K \tag{2.68}$$

The subscript K in the above equation implies gas (g), water (*w*), oil (o), and solid particles (s).

2.5.3 Superficial Velocity of Mixture (υ_{sm})

The area fraction of a phase is expected to change over space and time, so the average velocity of the flow varies depending on the volume fraction of each phase and its respective velocity. In this case, the average velocity of each phase is defined at its part of the cross-section [14].

Superficial velocity of gas, oil or water is given by:

$\upsilon = Q/A$, unit is meter per second

where Q is the volumetric flow in cubic meters per second, and A is the cross section are in meters sq.

Superficial velocity of Gas (υ_{SG}):

$$\upsilon_{sg} = \alpha_g \upsilon_G = \frac{Q_g}{A_g} = \frac{Q_g}{\alpha_g A} = \frac{\dot{m}_g}{\rho_g A} \tag{2.69}$$

Superficial velocity of liquid (υ_{SL}):

$$\upsilon_{SL} = \alpha_L \upsilon_L = \frac{Q_L}{A_L} = \frac{Q_L}{\alpha_L A} = \frac{\dot{m}_L}{\rho_L A} \tag{2.70}$$

Superficial velocity of oil (υ_{SO}):

$$\upsilon_{SO} = \alpha_O \upsilon_O = \frac{Q_O}{A_O} = \frac{Q_O}{\alpha_O A} = \frac{m^{\bullet}_O}{\rho_O A} \quad (2.71)$$

Superficial velocity of water (υ_{SW}):

$$\upsilon_{SW} = \alpha_W \upsilon_W = \frac{Q_W}{A_O} = \frac{Q_O}{\alpha_W A} = \frac{m^{\bullet}_W}{\rho_W A} \quad (2.72)$$

Superficial velocity of solid (υ_{SS}):

$$\upsilon_{SS} = \alpha_S \upsilon_S = \frac{Q_S}{A_S} = \frac{Q_S}{\alpha_S A} = \frac{m^{\bullet}_S}{\rho_S A} \quad (2.73)$$

Thus, the mixture velocity is provided by:

$$\upsilon_M = \frac{Q_{total}}{A} = \upsilon_{Sg} + \upsilon_{SO} + \upsilon_{SW} + \upsilon_{SS} \quad (2.74)$$

where $m^{\bullet}_g$, $m^{\bullet}_L$, $m^{\bullet}_O$ and $m^{\bullet}_S$ are mass rates of gas, liquid, oil and solid phases, respectively.

The volumetric flow rate (Q) at the whole cross-section area (A) determines the superficial velocity of the phase. This tends to be lower than the average velocity of the flow [14].

2.5.4 Mass Flux of Mixture (G_m)

The total mass flux mixture is given by:

$$G_m = \sum_{K=1}^{N} \rho_K \upsilon_k \quad (2.75)$$

The solid particle mass is given by:

$$M_S = \frac{\pi}{6} d_p^{\,3} \rho_S \quad (2.76)$$

where (P_S) is the solid density and d_P is the solid particle diameter.

The particle density (ρ_S) is calculated as follows:

$$\rho_S = \frac{\text{sand particle weight}}{\text{sand particle volume}} = \frac{w_p}{V_p} \quad (2.77)$$

The sand particle volume (V_p) is calculated as follows:

$$V_p = \frac{\pi}{6} d_p^{\,3} \quad (2.78)$$

2.5.5 Density of Mixture (ρ_m)

The density of this mixture given as:

$$\rho_m = \sum_{K=1}^{N} \alpha_K \rho_K = \alpha_g \rho_g + (\alpha_O \rho_O + \alpha_w \rho_w + \alpha_S \rho_S) \quad (2.79)$$

$$\rho_m = \alpha_g \rho_g + \rho_{slurry} \quad (2.80)$$

The definition of the density of any material is ($\rho = \frac{m}{V}$). Hence, for flowing material, it is:

$$\rho = \frac{m^{\bullet}}{Q} \quad (2.81)$$

The continuity equation is met as:

$$m^{\bullet} = \rho_m \upsilon_m A = \rho_m Q \quad (2.82)$$

$$m^{\bullet} = m_g^{\bullet} + m_o^{\bullet} + m_w^{\bullet} + m_s^{\bullet} \quad (2.83)$$

2.5.6 Viscosity of Mixture (μ_m)

Slurry is a mixture of solids and liquid in water and oil. Slurry viscosity can be quickly tested using Marsh Funnel Viscometer:

$$\mu_{slurry} = \rho\,(t\text{-}25) \quad (2.84)$$

The viscosity of the slurry and gas mixture is given as:

$$\mu_{mix} = \mu_{slurry} + \mu_g \quad (2.85)$$

2.5.7 Solid Density(ρ_s)/Specific Gravity(SG_s)

The density of the solid particles is stated as the specific gravity. This value, SG_s, is determined by dividing the density of the solid particles by the density of water.

2.5.8 Water Density(ρ_w)/Specific Gravity (SG_w)

The density of water is assumed as1000 kg/m^3 and the specific gravity of water is assumed as 1.0 at 20°C, although these values can vary som. The value varies somewhat with temperature.

2.5.9 Specific Gravity of Slurry (SG_{slurry})

Specific gravity is the density of a particular material normalized by the density of water.

The density of sand is normally 2600 kg/m^3 and the specific gravity of sand is less than 2.6.

To determine the specific gravity of the slurry, we use the formulas below:

$$SG_{slurry} = 1 + C_V\,(SG_s - 1) \quad (2.86)$$

or $$SG_{slurry} = \frac{SG_s}{SG_s - C_S(SG_s - 1)} \quad (2.87)$$

where (SG_{slurry}) is the specific gravity of the slurry, (SG_s) is the specific gravity of the solid particles and (C_V) is the concentration of solid particles by volume in the slurry (v%).

2.5.10 Slurry Density (ρ_{slurry})

Slurry is a mixture of solids and a liquid. The density of a slurry can be calculated as

$$\rho_{slurry} = \frac{1}{\frac{C_s}{\rho_S} + \frac{(1-C_s)}{\rho_l}} \quad (2.88)$$

where (ρ_{slurry}) is the density of the slurry (lb/ft^3, kg/m^3), (C_S) is the concentration of solids by weight in the slurry (wt.%), (ρ_s) is the density of the solids (lb/ft^3, kg/m^3) and (ρ_l) is the density of liquid without solids (lb/ft^3, kg/m^3).

Chapter 3

Experimental Set-Up

3.1 Development of Multi-Phase Flow Experimental Set-Up

In the present study, the experiments were conducted in a 25 m long clear PVC pipe open-cycle system flow loop pipeline. The liquid was pumped from the tank through 20 mm diameter clear PVC pipe. Clear PVC piping was used specifically for visual enhancement. To form three- and four-phase flows, air was added from the air line, which supplies air from the lab air supply at 670 kPa liquid/slurry liquid (oil, water, and sand) is pumped by a high-speed pump from the tank through the flow loop horizontal pipeline, and gas was added from a gas cylinder. For the solid phase, spherical sand particles (0.0006-0.0008 m) with a density of around 2600 kg/m^3 were added to the liquid tank at 2-6 wt.% concentrations. For equipment, the present study adopted instruments that were able to measure different locations of set-up flow meters, pressure transducers, and temperatures thermocouple sensors. The flow meters allowed for separate measurements of liquid and gas flows. Also, the addition of manual control valves helped the liquid meter control conditions and to form a variety of flow types. Omega PX603-300G5V pressure transducers ranged from 0 to 1378.95 kPa (0-300 psi) in the pipeline. The gas flow range is about 140 L/min to 600 L/min (Approx.), and the liquid flow range is almost 15 L/min to 20 L/min. At this range, the experimental set-up mostly gives slug flow for multi-phase flow, but it also gives bubble flow and wavy flow at some range. The flow loop was connected to a data acquisition system as well. Figure 3.1 presents a schematic representation of the experimental set-up.

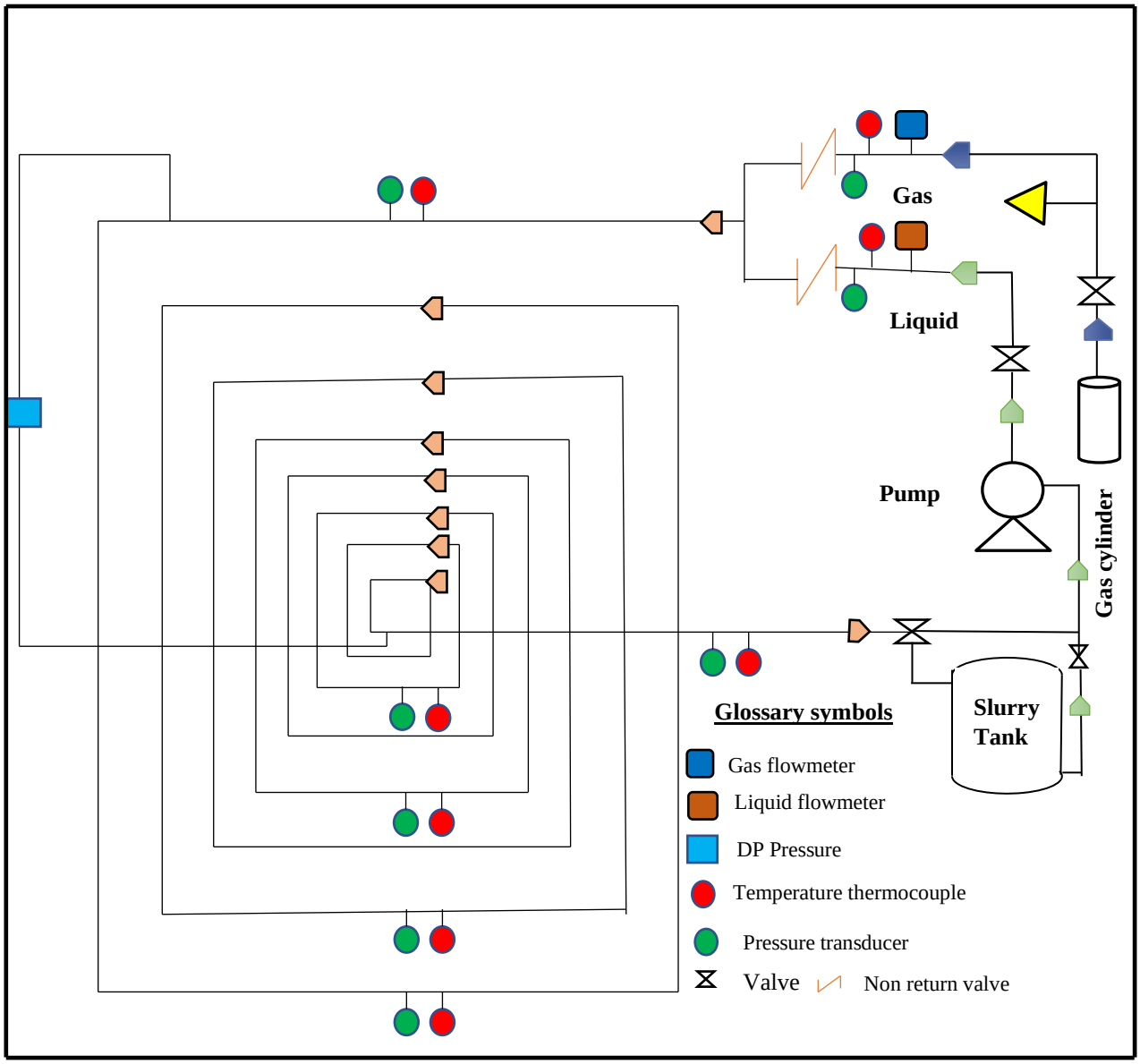

Figure 3.1 Schematic Diagram of Flow Loop Pipeline Set-Up.

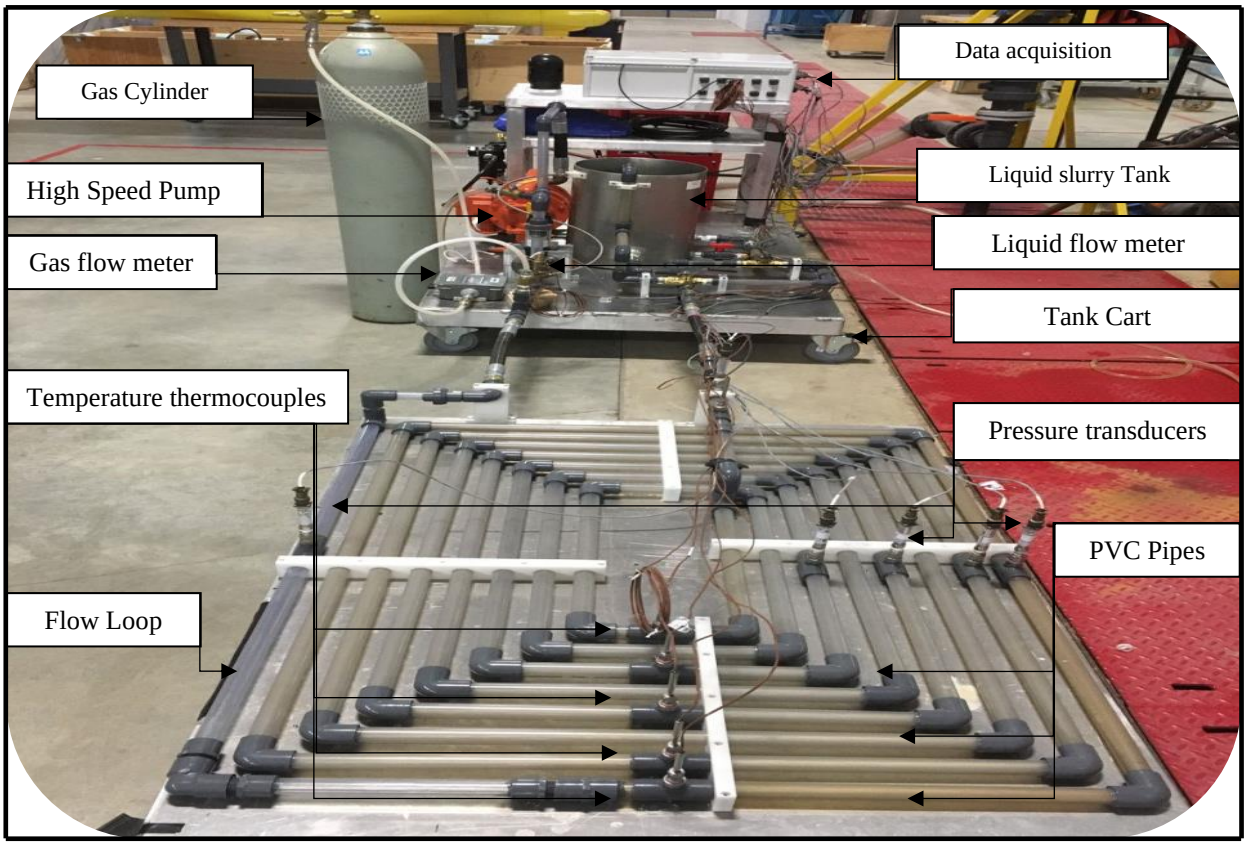

Figure 3.2 Picture of Flow Loop Pipeline Set-Up.

3.2 Process Flow Loop Pipeline

The flow loop pipeline experimental set-up (Figure 3.1 and Figure 3.2) is designed to investigate the two/three/four-phase flow in a pipeline. The set-up also contributes to basic multi-phase experiments to study different flow behavior through a continuous flow of fluids include gases (e.g., CO_2, air, etc.), liquids (water, oil, etc.) and solids (sand) at different temperatures, pressure conditions and flow patterns (slug, bubbly, stratified, etc.) by incorporating a mixture of different gases, liquids, and/or solids. This set-up also further facilitates the current available experimental set-up to conduct multi-phase flow experiments on different pipe geometries. Specifications of the test facility are given in Table 3.1.

Table 3.1 Material and Experimental Characteristics for Pipeline Flow Loop

Material and Experimental Characteristics	**Value**
Pipe material	PVC
Flow loop length	25 m (82 ft)
Liquid pipe diameter	20 mm (0.75")
Gas pipe diameter	10 mm (0.35")
Flow loop operating condition	Pressure: less than 300 psia (2070 kPa)
	Temperature: -5 to 35 ^{O}C
Pump	High speed pump
Gas flow meter	5 to 20 ft^3/min (1.75 kg/s to 7 kg/s)
Liquid flow meter	15 to 100 lpm (0.113 kg/s to 0.75 kg/s)
Pressure transducer	Seven pressure transducers
Thermocouple	Seven thermocouples
Liquid tank	5 gallons
Gas cylinder	Carbon dioxide (CO_2)
Data acquisition	Software program

3.3 Different Components of the Flow Loop Pipeline Set-Up

3.3.1 Air Flow Line Components

The air flow lines of the pipeline flow loop are constructed with a flexible 1inch diameter clear PVC pipeline. These lines consist of components such as air flowmeter, pressure sensors, air check valve, air control valve, and air filter. The fittings involved in the connectivity of this piping include a throttle valve and a pressure regulator that is positioned just in front of the point where the air is injected into the pump. The air is fed into the flow loop from the main lab air supply through a high-pressure hose. The lab air supply has a pressure of 670 kPa (100 psi). Figure 3.3 shows the gas (compressed room air) injection system.

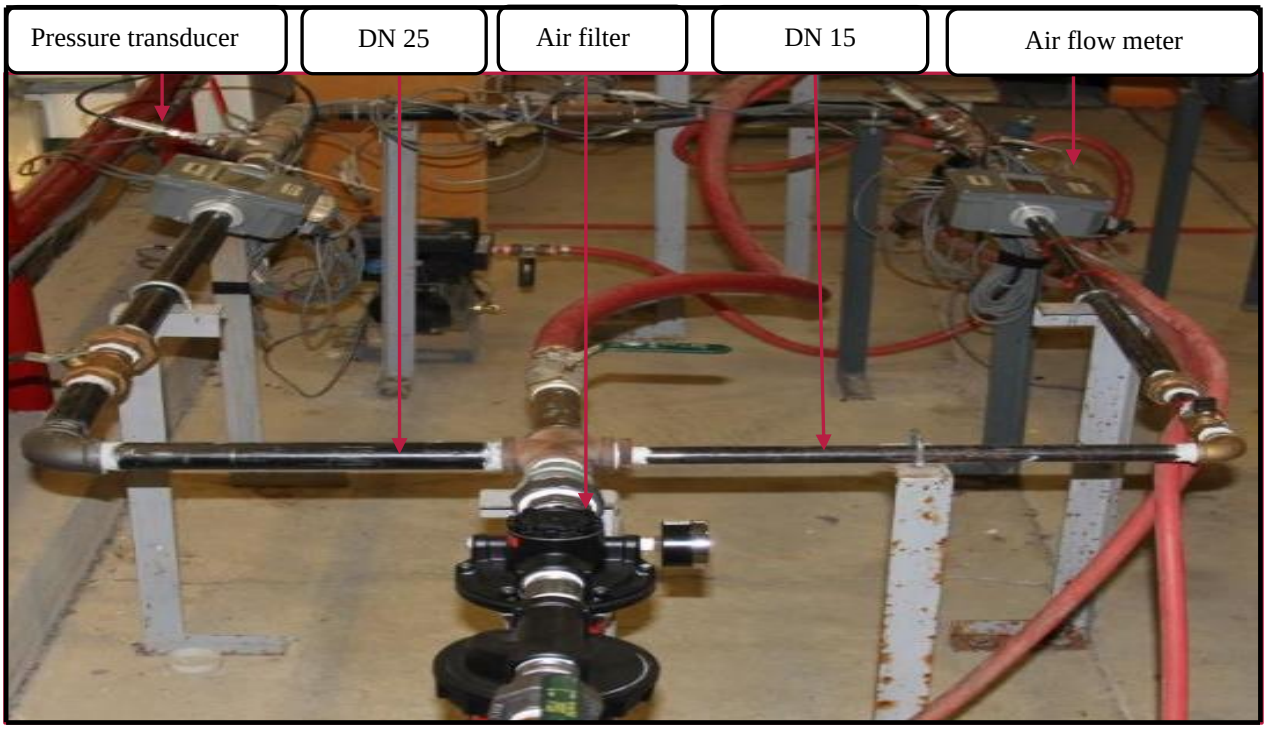

Figure 3.3 Air Flow Lines.

3.3.2 Tank

The pipeline flow loop requires a 5-gallon steel tank for the liquid/slurry liquid. The tank is connected to the circulation pump via a 0.75-in pipe. Figure 3.4 shows the tank that was used.

Figure 3.4 Tank of the Experimental Flow Loop Pipeline.

3.3.3 Pump

The pump used in this set-up is a high-pressure pump that is designed to circulate a large volume of liquid at a high-volume flow rate through the pipeline flow loop. The pump is Wilden's H200 25mm (1") high-pressure pump; the maximum flow rate of this pump is 94 lpm (25 gpm), making it a reliable pump that, is able to transfer viscous solid laden slurries from high discharge pressures up to 300 psig (3:1 ratio of liquid discharge pressure to air inlet pressure). The high-pressure pump is able to transfer solids of maximum size 6.4 mm (1/4"). The model number of the pump is H200/WWWAA/FWS/WF/MWF. The pump discharge rate can be controlled by limiting the volume and/or pressure of the air supply to the pump. An air regulator is used to regulate air pressure. The described high pressure-pump is shown in Figure 3.5.

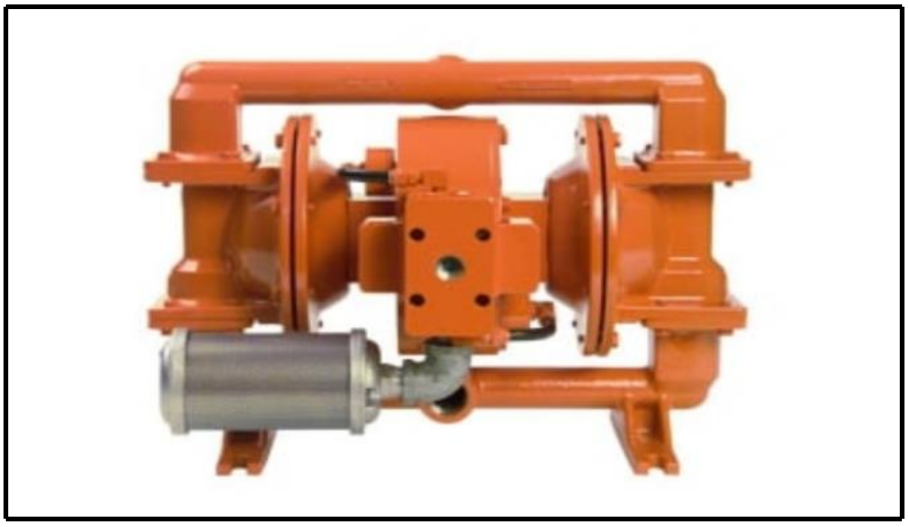

Figure 3.5 High-Pressure Pump.

Table 3.2 High-Pressure Pump Specifications

Brand	**H200 High Pressure Pump Wilden**
Pump Model Number	H200/WWWAA/FWS/WF/MWF
Inlet	25 mm (1")
Outlet	25 mm (1")
Height	343 mm (13.5")
Width	450 mm (17.7")
Depth	305 mm (12.0")
Stainless Steel	37 kg (81 lbs.)
Air Inlet	13 mm (1/2")
Max. Flow rate	94 lpm (25 gpm)
Max. Size Solids	6.4 mm (1/4")
Max. inlet air pressure	6.9 bar (100 psig)
Max. discharge pressure	20.7 bar (300 psig)

3.3.4 Pressure Regulator

TOPRING (52.360) produced an air pressure regulator with a gauge that, was installed on the system. The pressure regulator design is high flow and includes a T-handle for pressure adjustment. Further, it has the ability to maintain continual downstream pressure. Its maximum pressure is 300 psia, and its maximum air flow is 400 SCFM at 100 psia. The body and the spring cage are made out of zinc. The pressure regulator represents a specialized control valve for reducing the upstream supply pressure level to a determined constant downstream pressure. This is accomplished despite changes in flow through the valve and variations in the upstream pressure. It is important to point out that if the pneumatic equipment is used at a higher-pressure level than recommended, the energy for generating the pressure is wasted. In addition, the pressure regulator may result in a safety hazard and the early wearing out of the equipment. Also, the pressure should be calibrated as recommended to save the air pipes from rust and corrosion resulting from dirt and water found in the air flow pipes. Hence, it is critical to precisely control air pressure so that air-powered equipment can operate efficiently.

3.3.5 Air Filter

An air filter was installed in the system along with an air pressure regulator (shown in Figure 3.6). TOPRING is the manufacturer of the air filter, and its model number is 52.160-filter 1 and other contaminants Manual Zinc HIFLO. The air filter has a high flow design; it is able to remove water through centrifugal force and an automatic drain. Zinc was used to make the body; the bowl is also made out of Zinc and has a sight gauge, which is necessary to filter contaminants created during the compression cycle.

Figure 3.6 Air Filter and Pressure Regulator.

3.3.6 Liquid Flow Meter

Flow meters are required to monitor the flow rates of the fluids in the flow loop. Separate meters for the liquid and gas flows are required. Each meter is positioned on its respective line ahead of, prior to the point where the two streams are joined.

In the liquid line, the Water Magnetic Flow Meter (Flow Tube, Rosemount Model 8711-Model # 8711SHAOU1NOG1) was installed (see Figure 3.7). The accuracy of this meter is up to 0.15% of volumetric flow with a rate accuracy of over 13:1. The flow turndown is 0.25% over a 40:1 flow turndown and is feasible with 0.15-8 inches (4-200 mm). The liquid flowmeter has the capacity to measure around 5-500 L/min liquid flow rate at an accuracy of ±1% (Full Scale) [21].

Figure 3.7 Display of Rosemount Model 8711 Liquid Flow Meter.

Figure 3.8 Installed Rosemount Model 8711 Liquid Flow Meter.

3.3.7 Gas Flow Meter

A separate omega brand gas flow meter (Model # FLR6725D) is used to cover the complete range of gas flow in the gas lines of the flow loop. The flow meter is installed in the same clear PVC pipe. Each flow meter has an attached signal conditioner which interfaces each meter with the DAQ system. Furthermore, the flow rate is shown on the display of each flow meter. The flow measurements are taken by a hall sensor, counting the pulses per minute. The sensor can be screwed open to change the basic settings The flow meter has been installed in the DN15 pipe Omega FLR6725D (2 to 25 SCFM flow rate) [22].

Figure 3.9 shows the Omega FLR6725D gas flow meter.

Figure 3.9 Gas Flow Meter.

3.3.8 Pressure Transducers

The pipeline flow loop is equipped with seven pressure transducers. Figure 3.10 shows the Omega sensors installed in the pipe system.

The positions of the pressure and temperature sensors in the flow loop are shown in Figure 3.2. All the pressure and temperature sensors are Omega brand sensors, which allow the condition of the flow loop to be measured

at several locations along the loop. The pressure and temperature sensors in the gas lines are necessary to convert actual flow rates to standard conditions.

The pressure transducers are Omega PX603 series cable style transducers. These sensors are compatible with both liquid and gas. The model is PX603-300G5V and can function from 0 to 1378.95 kPa (0-300 psia) in the gas line. These transducers produce a 1-5 V output signal and are connected to the data acquisition system. Each of them transducers is equipped with a DN 8 (1/4 in) male National Pipe Thread Taper (NPTT) fitting which can be used for the installation into the flow loop [22]. Figure 3.10 shows the installed pressure transducer from Omega. The pressure gradients are evaluated by measuring the pressure at the beginning and the end of a test section.

Figure 3.10 Pressure Transducers Sensor.

3.3.9 Thermocouples

The pipeline flow loop is equipped with seven thermocouples. The temperature transducer is of the Omega TC-(*)-NPT Series, which are pipe plug probe style T-type thermocouples. The 304SS sheath has a 6.4 mm (1/4") diameter that extends (1/2") from the end of the 1/4 NPT pipe plug. The thermocouple-grade lead wires are stranded 20 American Wire Gauge (AWG), fiberglass insulated, and stainless steel over braided with stripped leads. To tighten mounting threads on the pipe connection clamp, there is a hex section that is 22 mm (0.56 ") across flats that are 5.8 mm (0.23") wide [22]. Figure 3.11 shows one of the temperature sensors used. They produce a millivolt signal related to the temperature.

Connecting of the thermocouples to the DAQ system board requires extra wire, made of different metals, from Omega. To install the transducers, fittings are used for the pipelines, the steel air lines, and the PVC liquid lines. Tees with DN 8 bushings allow both thermocouples and pressure transducers to be installed in each airline. The transducers are mounted to the PVC pipe by using clamp-it saddles which seal around the pipe with an O-ring. A bushing is inserted into a socket, where a hole has been previously drilled into the pipe to measure the pressure inside the pipe [23].

Figure 3.11 Temperature Thermocouples Sensor.

3.3.10 Data Acquisition (DAQ) System

The data acquisition (DAQ) system was purchased from National Instruments (NI). The system was designed and created using the National Instrument Data Acquisition Module NI 9319 DSUB, 4ch, 24 bit, 100S/s/ch, dynamic universal AIC series module. The program has a graphical user interface and interprets incoming signals from the flow meters, pressure sensors and thermocouples [24]. The following figures show the user interface of the National Instrument DAQ system. The screen displays the numeric values of the flow rate for all active sensor inputs.

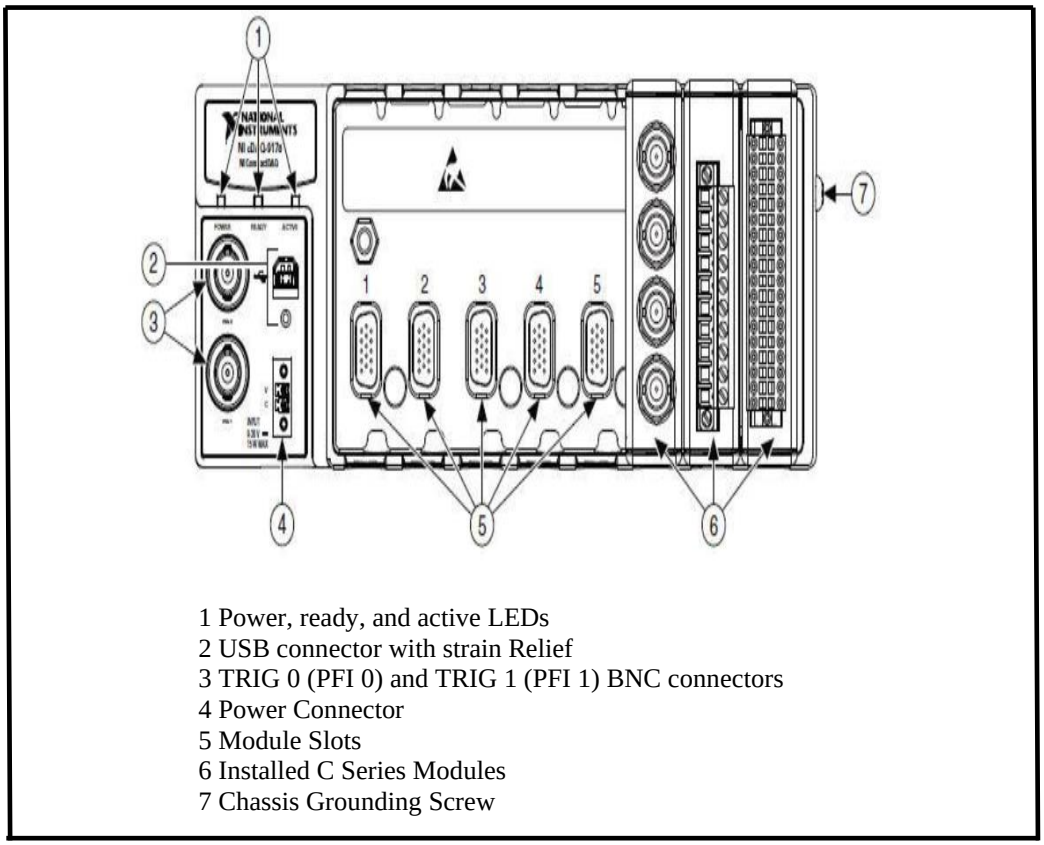

Figure 3.12 DAQ System Set-Up Options [24].

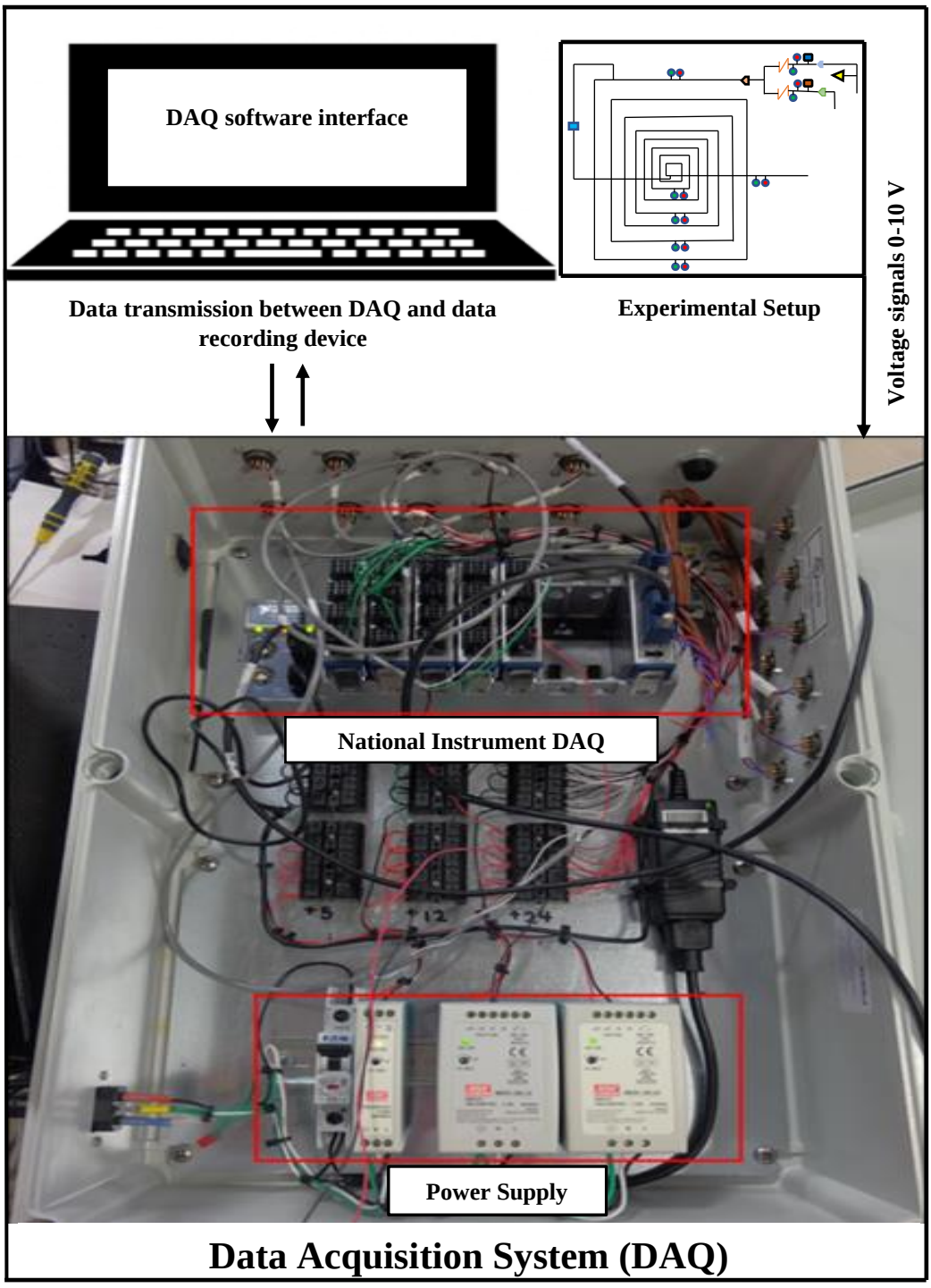

Figure 3.13 National Instrument DAQ System.

The Universal DAQ System from National Instruments has been used to collect all types of data from flow meters and sensors. This System has four NI 9319 universal modules with four channels that each gives 100 samples per second. The modules have been attached with an NI cDAQ-9178 USB chassis. NI Signal Express 2014 has been used as data-logging software from Data Acquisition Modules.

The DAQ System collected the input signal as voltage for pressure transducers, thermocouple sensors and gas/liquid flow meters through low noise cables. The NI signal express software processes the data and gives an output in kPa and Liter/min units. This software can also record data for the required time and compile it directly in an Excel sheet.

3.3.11 High-Speed Camera

The Mega-Speed MS55K Digital Camera System was used for high-speed image capture. This camera performs well when used in scientific and industrial imaging applications, packaging, and machine visions. Its main advantages are high image quality, robust design, easy connectivity, and small size. The software package includes options to control different functions, such as the command set-up, loading and saving files, single frame advance, reverse, forward, playback rate, trigger type, shutter speed, and frame rate. It is also possible to download, save and re-arm sequences to automatically start the capture as defined by the user. As the Mega Speed Digital Camera System is compact, it can be easily placed and integrated into various kinds of imaging environments [24]. The Standard Mega Speed MS55K Digital Camera System is user-friendly and flexible as can be seen in Figure 3.14.

Pictures were taken, and videos of the flow regimes were recorded by using the reflector light and the Mega Speed MS55K Digital Camera System so as. The purpose was to obtain improved visualization through the pipeline flow loop.

The High-Speed Imaging Software is a user-friendly image capture program, yet with a high capacity. The software is used for rapid identification, diagnosis, and problem solving by taking videos. The images transformation in the PC occurs in real time.

Figure 3.14 High-Speed Camera.

3.3.12 Sand Particles Bin

The multi-phase flow system must contain slurry, which is a mixture of solid particles and liquid, typically water. Irrespective of Newtonian or non-Newtonian flow the slurry must contain certain amounts of solid particles. The experimental analyses performed by the several research groups indicate that in creating to create slurry flow, spherical sand particles were preferred. A schematic diagram of the sand injection system developed in the experiment is shown in Figure 3.15.

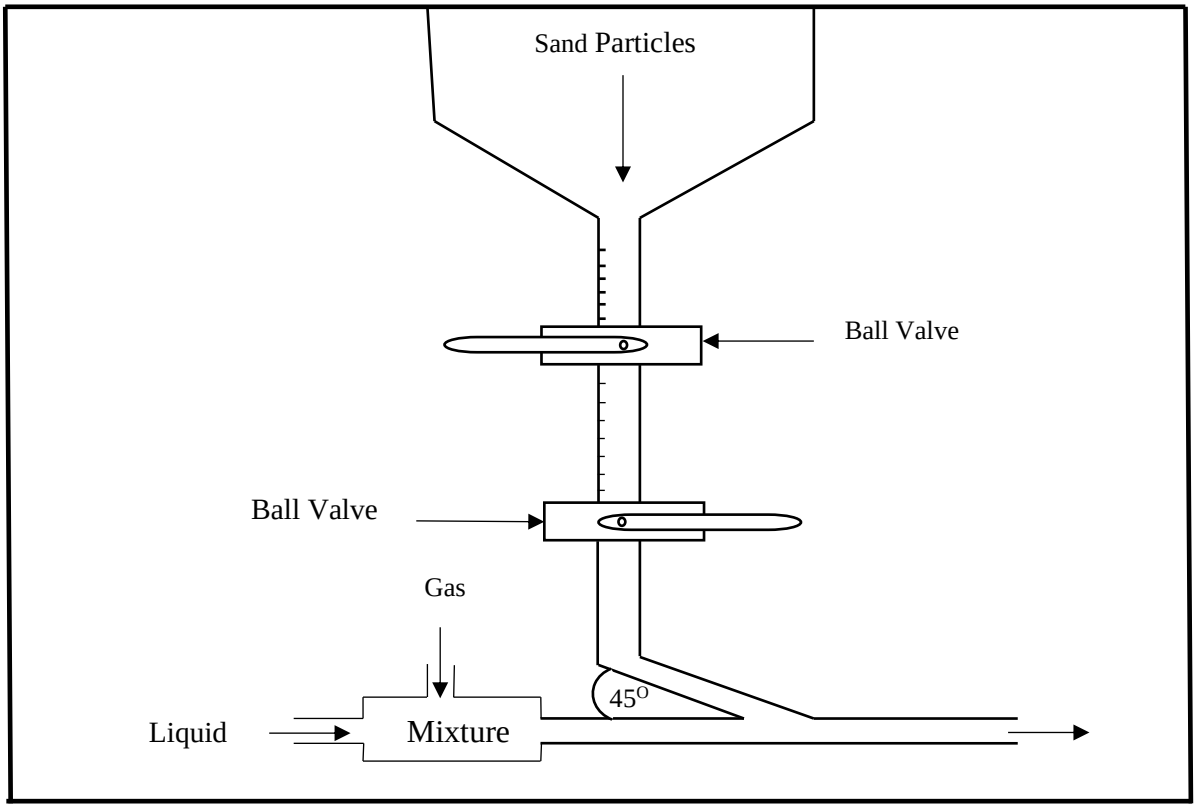

Figure 3.15 Schematic Diagram of Sand Particle Bin.

Figure 3.16 Picture of Sand Particle Bin.

Table 3.3 Specifications of Solid Particle Used in Different Experiments

Author (Year)	Phases	Pressure	Solid Parameters				
			Type	Diameter	Reynolds Number	Density	Avg. Density
Gul et al. (2017)	liquid-gas-solid	-	Industrial sands	2.75 mm	-	2762 kg/m^3	2600 kg/m^3
Al-lababidi et al. (2012)	Water-gas-sand		Sand	0.2 mm	-	2650 kg/m^3	
Oudeman et al. (1993)	Air-water-sand	above atm.	Sand grain	0.15 -0.30 and 0.69 mm	-	-	
Kelessidis (2007)	liquid-gas-solid	atm.	Glass beads	2 mm	-	2590 kg/m^3	
Shadizadeh et al. (2012)	liquid-gas-solid	-	Sandstone + limestone	3.23, 2.03 and 1.02 mm	-	2400 kg/m^3	
Duan et al. (2006)	liquid-gas-solid	-	Rock cuttings	0.45, 1.4 and 3.3 mm	-	-	
Han et al. (2010)	liquid-gas-solid	-	Sand particles	1 mm	-	2550 kg/m^3	
Ju Kim et al. (2008)	liquid-gas-solid	-	Sand particles	1 mm	-	2550 kg/m^3	
Osho et al. (2012)	Water-gas-sand	-	Sand	0.27 mm	-	2650 kg/m^3	
Bello et al. (2005)	Water-gas-sand	atm.	Sand	0.6–0.8 mm	84.00	2600 kg/m^3	
Avila et al. (2008)	liquid-gas-solid	-	Commercial gravel	2.77 mm	-	2300 kg/m^3	
Zhou et al. (2004)	liquid-gas-solid	185-500 psia	Cuttings	3 mm	-	2610 kg/m^3	
Naganawa et al. (2002)	liquid-gas-solid	-	Cuttings	3.66 mm	-	2400 kg/m^3	
Walker et al. (2000)	liquid-gas-solid	-	Sand	0.15–7 mm	-	2600 – 2710 kg/m^3	
Adari et al. (2000)	liquid-gas-solid	-	Sandstone cuttings	3.175 mm	-	2560 kg/m^3	

3.2.13 CO_2 Gas Cylinder

The main components of a carbon dioxide gas cylinder are the cylinder valve cap, adjustable belts for cylinder rack systems, and a regulator, which includes: 1) a low-pressure gauge to read the amount of internal pressure, and 2) a high-pressure gauge that indicates existing pressure in the CO_2 cylinder. The regulator can be used for a range of different gases, including CO_2, oxygen, argon, helium, and nitrogen. Figure 3.17 shows the main components of a carbon dioxide gas cylinder. The specifications of a carbon dioxide gas cylinder are shown in Table 3.4.

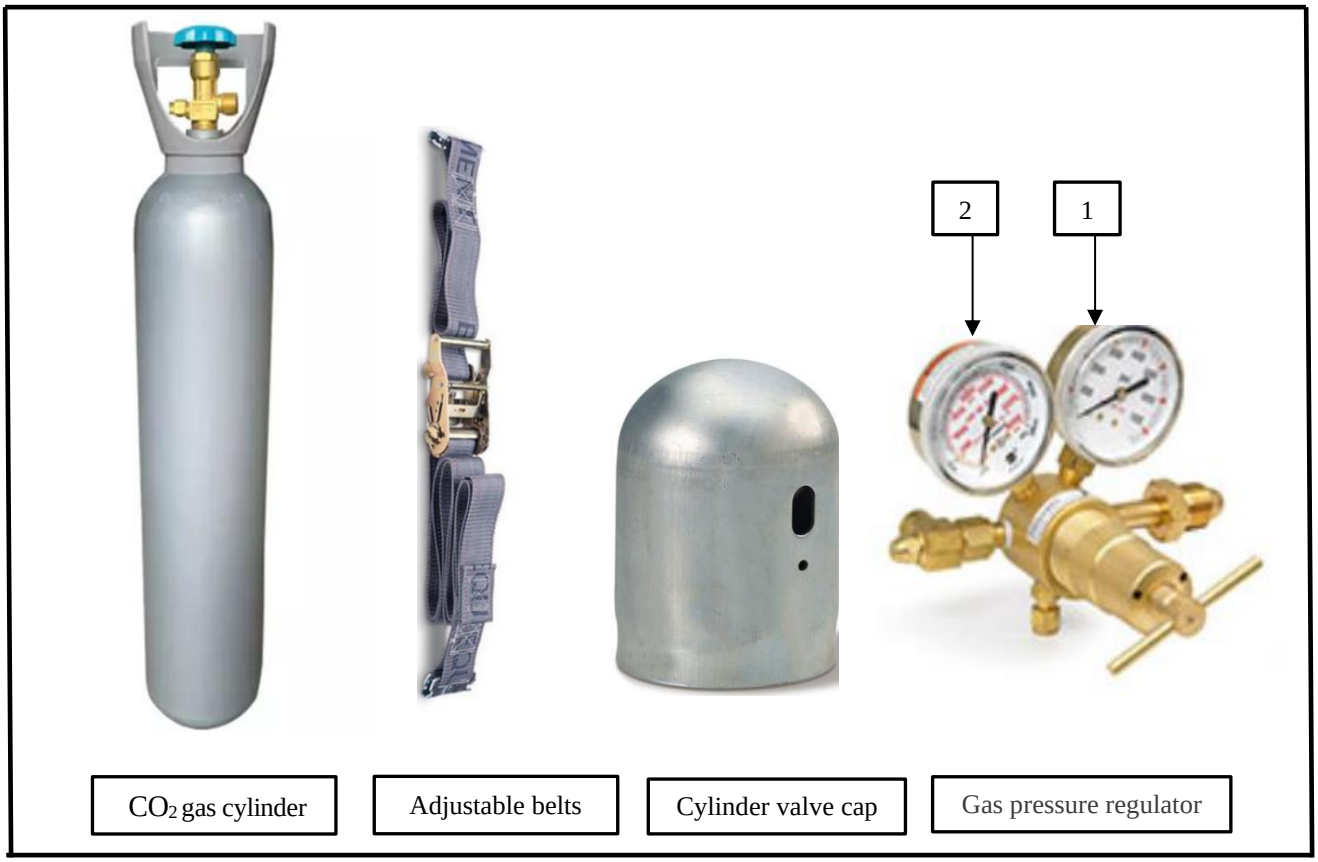

Figure 3.17 Carbon Dioxide Gas Cylinder and Accessories.

Table 3.4 Carbon Dioxide Gas Cylinder Specifications

Items	Carbon Dioxide Gas Cylinder
Weight	26 lbs
Dimensions	9 × 9 × 28 in
Gas Type	CO_2
Material	Aluminum
Capacity	20 lb / 9.1 kg
Service Pressure	1800 psia / 124 bar
Test Pressure	3000 psia / 207 bar
Length	23.3" / 592 mm
Diameter	8" / 203 mm

3.3.14 Snubber in the Pressure Transducer

The omega pressure snubber shown in Figure 3.18 has been used with each pressure transducer to protect the pressure sensor from water and solid particles. It has a porous metal disc and large filter surface which reduces the risk of sensor orifice clogging.

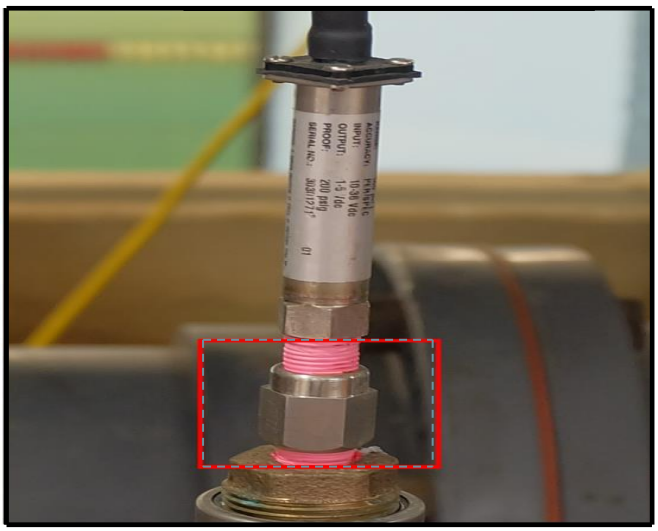

Figure 3.18 Snubber for Pressure Transducer.

3.3.15 Pressure Relief Valve

The pressure relief valve (A DN 40 Jaybell) is installed after the pump in the pipeline flow loop to ensure that the output of the pump does not exceed the pressure rating of the PVC pipeline. The valve of the series 69 is from Aquatrol Inc in Elburn, IL. It is an industry standard relief valve used for liquid relief and by-pass. The valve is engineered and designed for heavy duty, industrial, and commercial usage with a single piece bonnet to eliminate leakage while also allowing for simple cleaning. The pressure can be adjusted on the sealed hex-cap [19]. Figure 3.19 shows the installed pressure relief valve.

The relief valves are calibrated (set to a pressure of 100 psia) based on a range of flow rates in gallon per minute (GPM) versus seat size and set pressure. Should the pressure exceed 100 psia, the valve opens and the liquid flows into the drain. The valve is set at 100 psia. Therefore, the maximum pressure in the pipe cannot exceed the working pressure rating of the pipe.

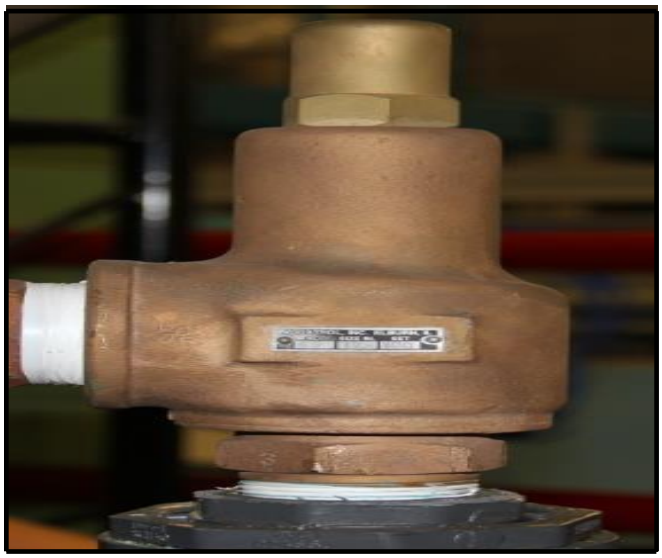

Figure 3.19 Pressure Relief Valves

3.4 Experimental Procedures

The experimental procedures are as follows:

1. Initially validate the calibration of all sensors and flow meters with basic experiments for single/two/three/four-phase flow.
2. Clear all the liquid/slurry liquid from the test section in the flow pipeline.
3. Pressurize and cool down the test section in the flow pipeline at the required test conditions/parameters.
4. Circulate water and/or oil at a constant flow rate to obtain a steady-state liquid temperature and pressure profile.
5. Inject gas (air or CO_2) at a constant flow rate for a suitable time period.
6. Gas and liquid temperature, pressure, and flow rates are measured and logged via a data acquisition system.
7. Pictures, and videos are taken of the flow regimes by using a reflector light and a high-speed digital camera system.

Table 3.5 Multi-Phase Flow Conditions and Characteristics [20]

Properties / Compounds	Liquid		Gas	Solid
	Oil	**Water**	**CO_2**	**Sand particle**
Density (kg/m^3)	900	1000	1.98	2600
Dynamic viscosity kg/(m.s)	0.018	0.001	0.000148	-
Surface tension (N/m)	oil- gas: 0.031	oil-water: 1E-6	oil- gas: 0.031	gas-liquid-solid: 0.0236
	oil-water: 1E-6	gas-water: 0.074	gas-water: 0.074	
Solid particle size (mm)	-	-	-	0.6-0.8
Particles mean diameter (mm)	-	-	-	0.6
Solid fraction wt.%	-	-	-	2

3.5 Calibration of Pressure Sensors

3.5.1 Calibration of Pressure Sensors

To calibrate the omega pressure sensors used in the experimental set-up, a metal adapter was designed and constructed to connect the sensor to the set-up. The designed adapter was built by the technical service of Memorial University. Figure 3.20 presents the designed adapter. On one side the adapter is connected to the Festo pressure hose system, while on the other side, there is a ¼ national pipe thread (NPT) to connect the Omega pressure sensor to the calibration set-up.

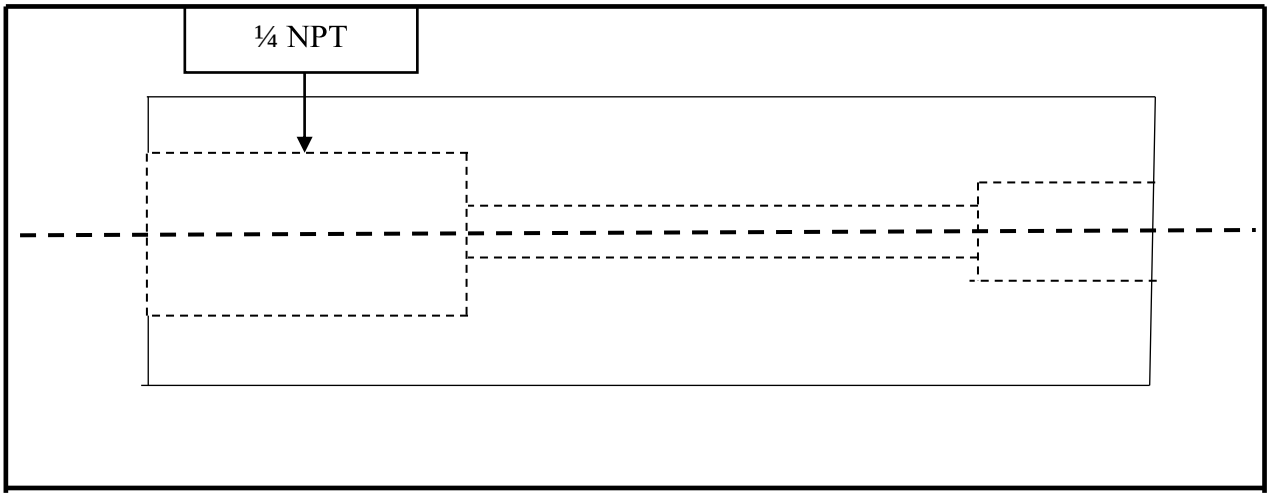

Figure 3.20 Schematic Diagram of Adapter for Pressure Sensor Calibration [25].

The calibration set-up which is shown in Figure 3.21 consists of a pressure bottle filled with compressed air at 2,000 psi, a Festo LR-D-MINI pressure regulator, and a small Festo valve to remove the pressure from the system post-calibration. The regulator works at a pressure range of 0.5 to 12 bars and has a maximal hysteresis of 0.2 to 0.4 bars [25]. All the parts are connected with Festo pressure hoses. The calibration is carried out as follows: - Different pressures are generated with the regulator, and the out-put voltage of the sensor is measured with a voltmeter. The calibration is carried out over the entire pressure range of a sensor. The pressure range is 9 bars for all sensors.

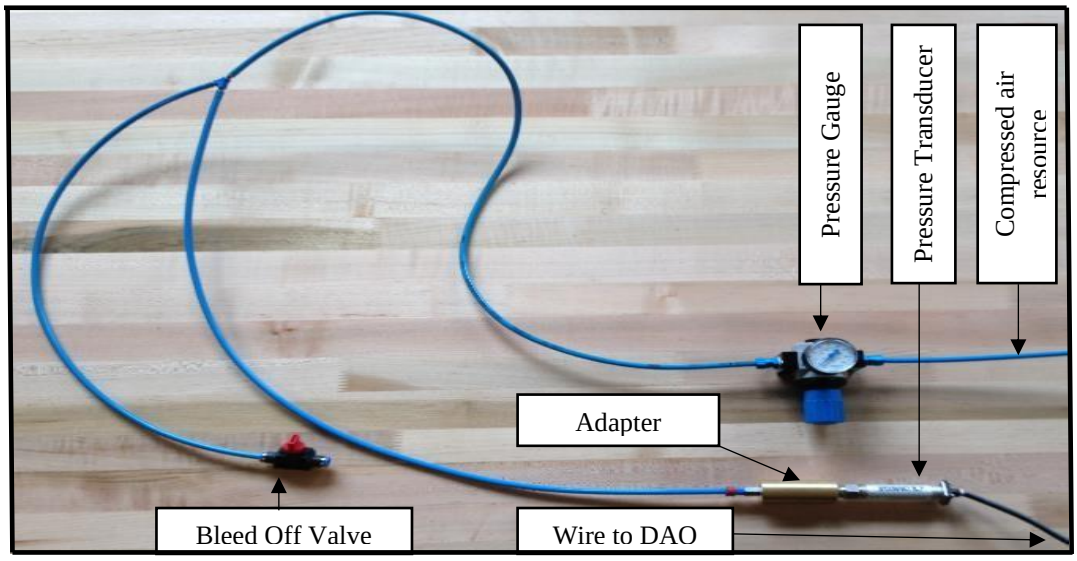

Figure 3.21 Calibration Set-Up for Pressure Sensor Calibration [25].

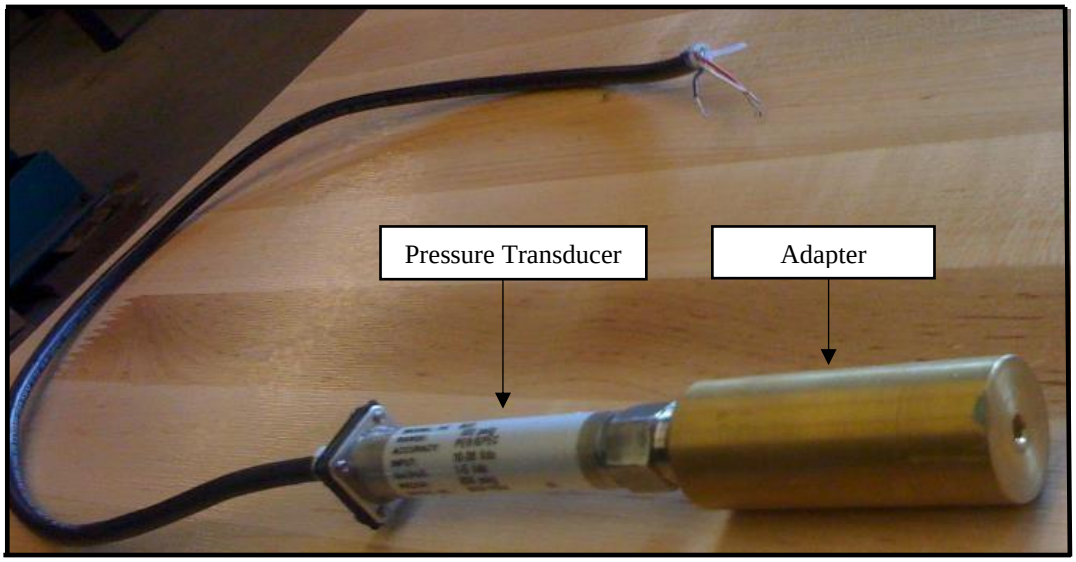

Figure 3.22 Adapter for Pressure Sensor Calibration [25].

3.5.2 Calibration Curves of Pressure Sensors

The calibration curves for every sensor are added to the DAQ system. All the calibration curves of pressure sensors from PT101 to PT106 are illustrated in Figures (3.23-3.28). The sensor voltage (VDC) output is plotted over the pressure (bar).

Calibration of Sensor PT101

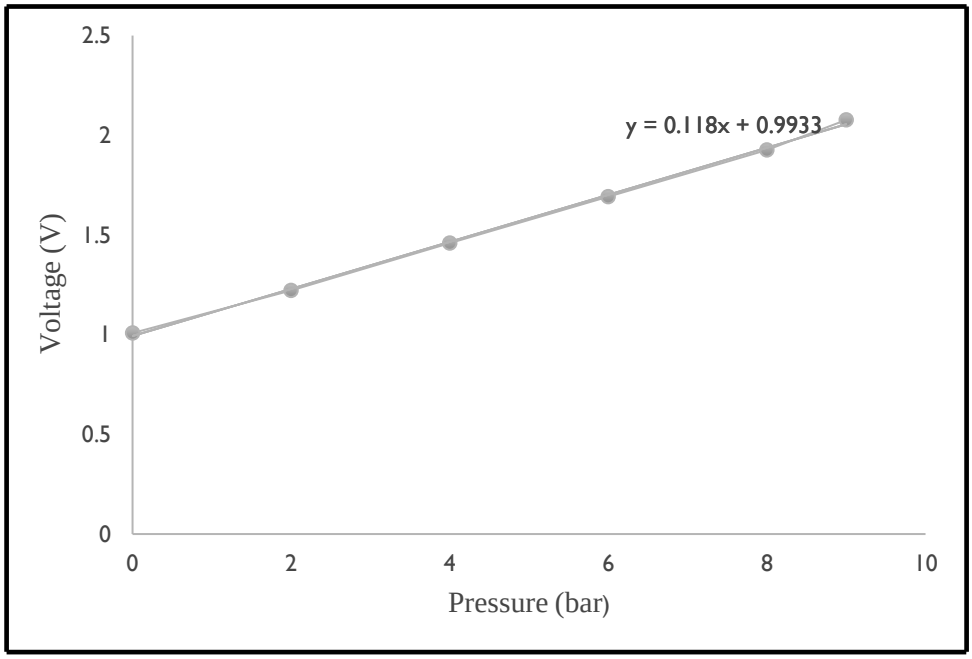

Figure 3.23 Calibration Curve of Omega Pressure Sensor PT101.

Calibration of Sensor PT102

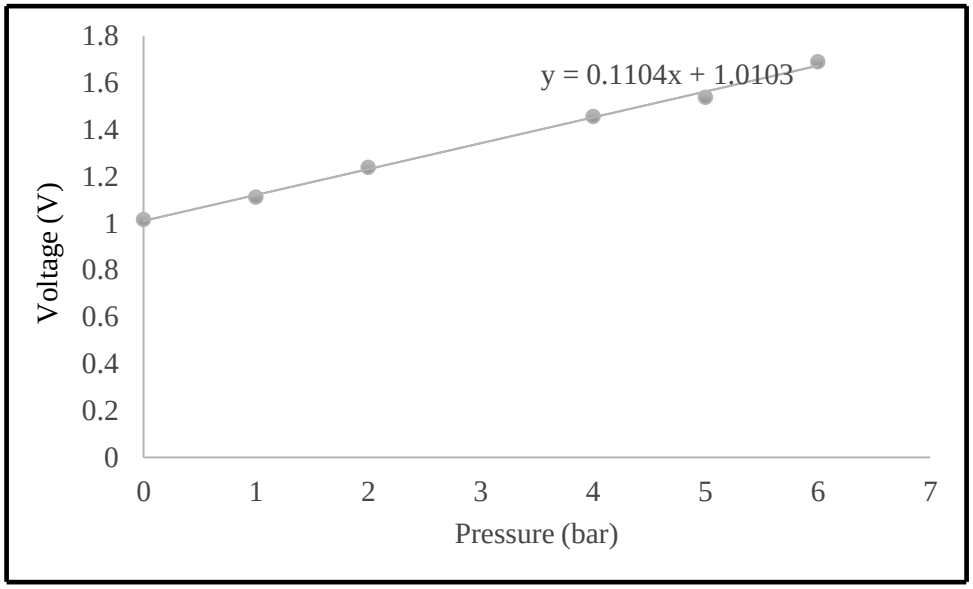

Figure 3.24 Calibration Curve of Omega Pressure Sensor PT102.

Calibration of Sensor PT103

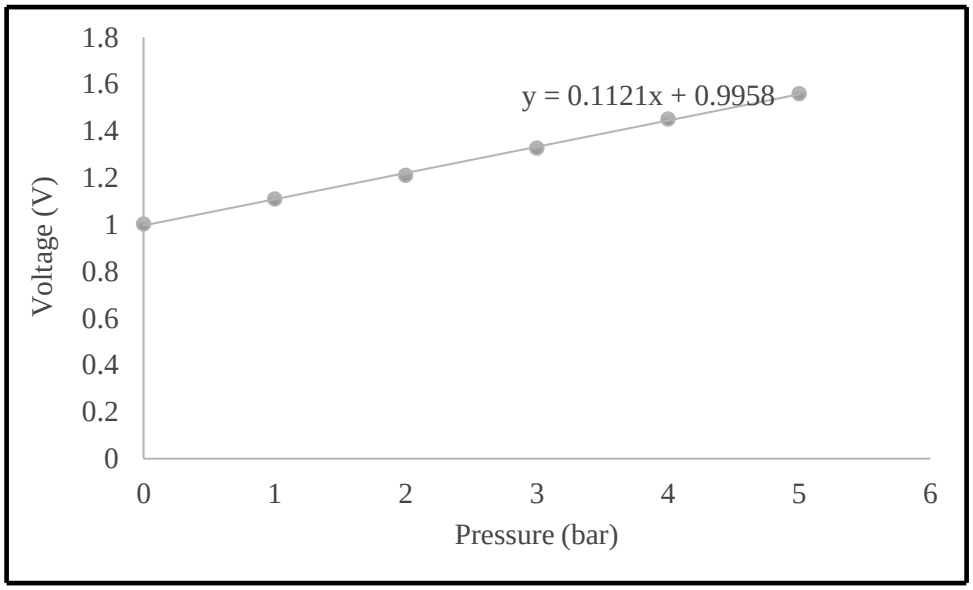

Figure 3.25 Calibration Curve of Omega Pressure Sensor PT103.

Calibration of Sensor PT104

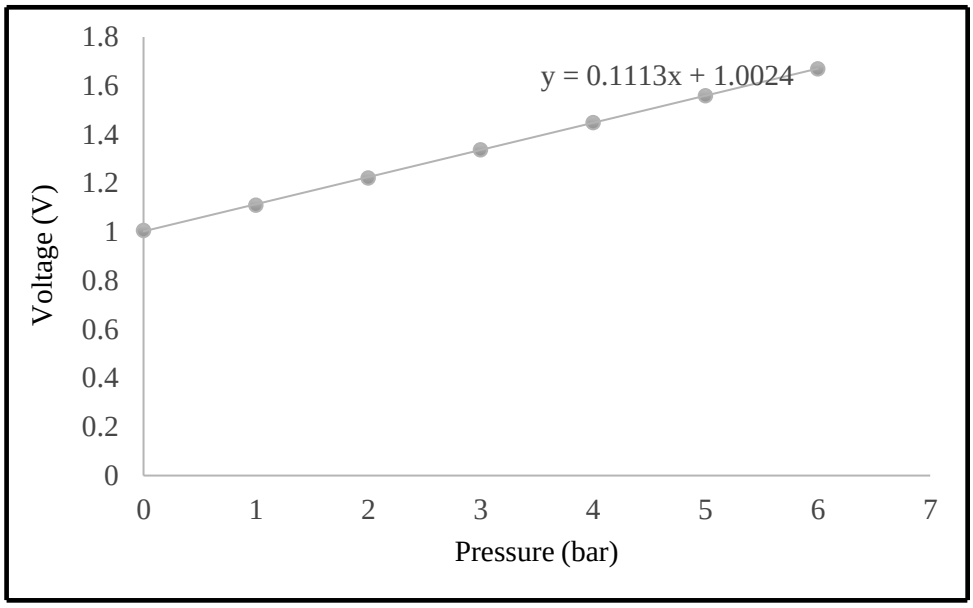

Figure 3.26 Calibration Curve of Omega Pressure Sensor PT104.

Calibration of Sensor PT105

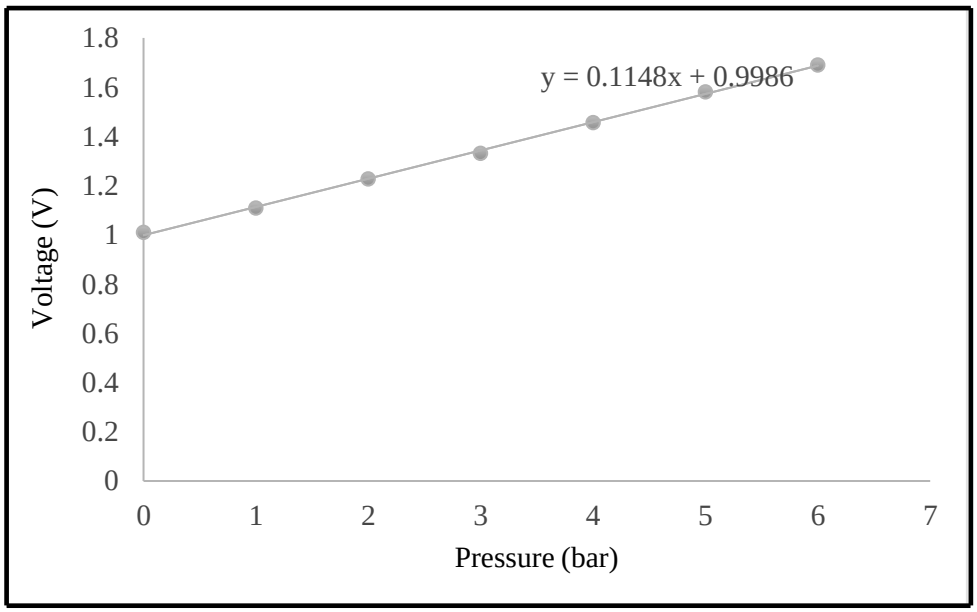

Figure 3.27 Calibration Curve of Omega Pressure Sensor PT105.

Calibration of Sensor PT106

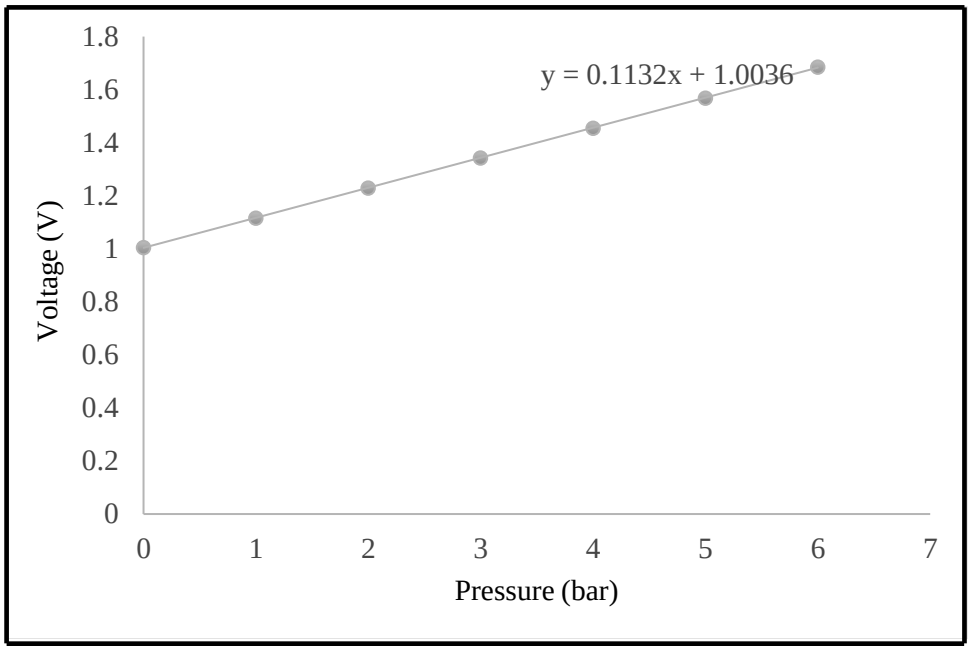

Figure 3.28 Calibration Curve of Omega Pressure Sensor PT106.

The sensor voltages (VDC) output vs input pressure sensors from PT101 to PT106 are shown in Figures (3.23-3.28). As can be seen, there is an increase in pressure sensor with increasing output voltages for all sensors.

3.6 Rheology Measurement Equipment

The following equipment and apparatuses are used to carry out the rheology measurement experiment:

3.6.1 An Electronic Weighing Scale

The mass of solid particles that should be added per liter of water was measured by this scale (Figure 3.30).

Figure 3.29 Electronic Weighing Scale.

3.6.2 Graduated Beakers

Graduated beakers are used to measure the volume of water that should be added to the solid particles to make precise concentrations, as seen in Figure 3.30.

Figure 3.30 Graduated Beaker.

3.6.3 Marsh Funnel Viscometer

The Marsh Funnel Viscometer is a simple device for measuring viscosity by observing the time it takes a known volume of liquid to flow from a cone through a short tube, specifically, time required for 1000 mL of fluid to flow from the orifice of a standardized funnel. Viscosity tested by the Marsh Funnel is shown in Figure 3.31.

Figure 3.31 Marsh Funnel Viscometer.

3.6.4 Density of Slurry Balance

The slurry balance is shown in Figure 3.32. The specific gravity of the solid particle solution was estimated by using it.

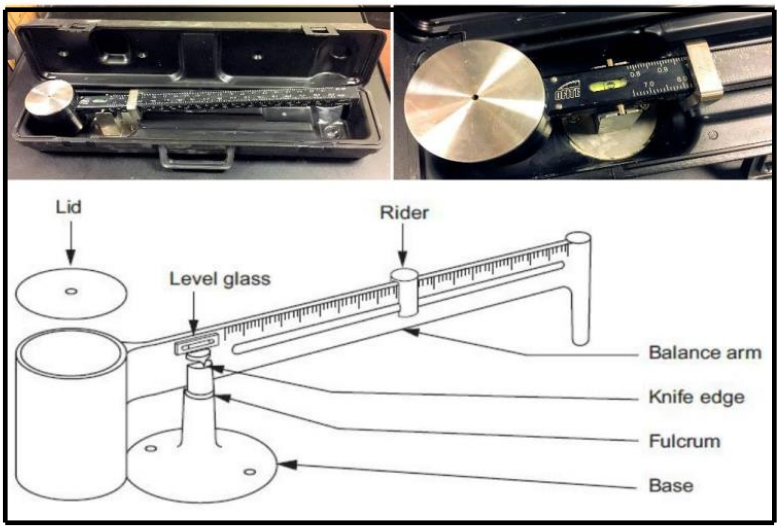

Figure 3.32 Density of Slurry Balance.

3.6.5 High-Speed Mixer

The solid particle solution was mixed uniformly and evenly using the high-speed mixer shown in Figure 3.33.

Figure 3.33 High-Speed Multi-Mixer.

3.6.6 Rotary Viscometer

The rotary viscometer used in the experiment is shown in Figure 3.34. The viscosity of the solid particle solution at different speeds is determined by the rotary viscometer.

Figure 3.34 Rotary Viscometer.

3.6.7 Concentration of Solids

The concentration of particles in the slurry can be measured as a volume percentage, C_V (v%), and a weight percentage, C_S (wt.%). The slurry concentration by weight can be measured by evaporating a known weight of slurry and measuring the weight of dried solids.

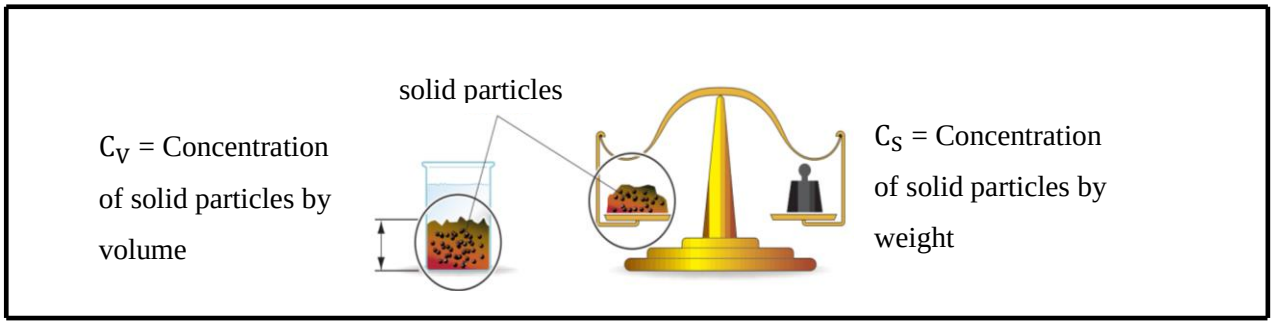

Figure 3.35 Concentration of Solid Particles in the Slurry.

Chapter 4

Experimental Investigation of Pressure and Temperature Gradient and Flow Regime in Four-phase Multi-phase Flow in a Complex Horizontal Pipeline

4.1 Introduction

The widespread existence of multi-phase flow and its importance in industrial units has prompted extensive research in this field. This type of flow occurs in pipelines, oil-producing wells and associated flow lines, separators, dehydration units, evaporators, and other processing equipment. The nature of multi-phase flow is extremely complicated due to the existence of various flow patterns and different mechanisms governing them.

Therefore, it is important to understand the nature and behavior of flow in multi-phase systems. In the initial stages of an oil well, the flow consists of mainly oil and natural gas. As the reserves of oil and gas in the oil wells decrease, seawater and gas are pumped into the well for enhanced recovery purposes.

This chapter presents a laboratory-based investigation of four-phase flows of oil, gas, sand, and water (i.e., liquid-gas-solid-liquid) through a horizontal pipeline loop system. The present study on pressure reductions in four-phase flows in horizontal pipeline flow loop systems is carried out on an (oil/gas/sand/water) mix. The investigation also tested the pipeline used in 20 mm I.D., set experimentally for atmospheric temperature and pressure. Test outcomes indicate changes in flow for particles in the four-phase flow mix in accordance with changes in operational conditions in horizontal pipelines that have bends and jumpers. The results and discussions presented in this chapter have been published in paper number seven mentioned at the beginning of this thesis.

The major objective of this experimental investigation is to understand the multi-phase flow behavior of (sand/water/gas/oil) four-phase flow through pipelines with multiple bends and jumpers. This study also aims to investigate temperature and pressure gradients in a pipeline handling for four-phase flows.

4.2 Experimental Set-Up of Flow Loop Horizontal Pipeline

The experiments were conducted on a 25 m length clear PVC pipe, as represented by the flow loop horizontal pipelines shown in Figure 4.1. The clear PVC pipe was chosen for its visualization abilities. The three and four-phase flows were created by adding water and oil from the liquid line and CO_2 gas from the gas cylinder. Sand particles measuring 0.6 mm were added to the liquid tank as the solid phase at 2-6 wt.% concentrations.

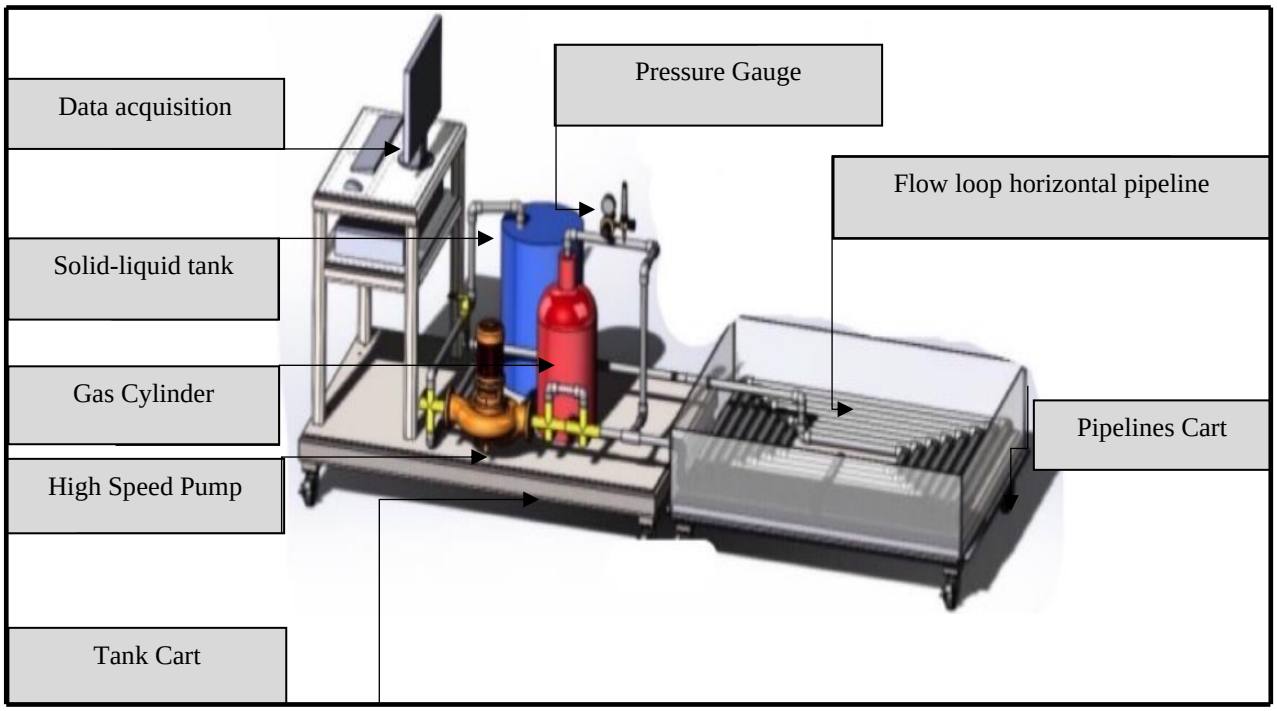

Figure 4.1 Multi-Phase Flow Loop Horizontal Pipeline Set-Up.

Table 4.1 Four-Phase (CO_2/Oil/Water /Sand) Flow Conditions and Characteristics

Property / Compounds	Solid	Gas	Liquid	
	Sand particles	CO_2	Oil	Water
Density (kg/m^3)	2600	1.98	900	1000
Dynamic viscosity kg/(m.s)	-	0.000148	0.018	0.001
Surface tension (N/m)	Gas-liquid-solid: 0.0236	Oil-gas: 0.031	Oil-gas: 0.031	Oil-water: 1E-6
		Gas-water: 0.074	Oil-water: 1E-6	Gas-water: 0.074
Solid particle size (mm)	0.6-0.8	-	-	-
Particles mean diameter (mm)	0.6	-	-	-
Solid fraction wt.%	2-6%	-	-	-

Table 4.1 presents the four-phase (CO_2/oil/water/sand) flow conditions and characteristics in a complex horizontal pipeline.

4.3 Four-Phase (CO_2/Oil/Water/Sand) Flow Experimental Procedure

4.3.1 Rheology Determination of Newtonian and Non-Newtonian Test Fluid

The experiment, was conducted in the geo-mechanic laboratory of Memorial University over days, adhering to all required safety procedures, as follows:

- The electronic weighing scale was used to measure the following masses of solid particle: 0.5 g, 1.0 g, 1.5 g, 2.0 g, 2.5 g and 3.0 g.
- Each mass was placed in a separate beaker (1000 mL), which was then filled with water. The water and solid particles were mixed and the settling process of settling lasted for 24 hours.

- After the water and solid particles settled, they were mixed again. The, density slurry balance (shown in Figure 3.33) was then used to measure the density of each solid particle concentration.
- The preliminary test of estimating viscosity trends in all solid particle concentrations was conducted using the Marsh Funnel Viscometer as shown in Figure 3.32. Each liter of solid particle solution was drained through the Marsh Funnel Viscometer, the time required to drain was recorded. Therefore, it is possible to estimate the viscosity using the formula:

$$\mu = \rho\,(t\text{-}25) \tag{4.1}$$

where:

μ = Viscosity (cp)

ρ = Density of solid particle (g/cm^3)

t = Time to drain (second)

Lastly, the rotary viscometer was used to estimate the viscosity of each solid particle solution. Various rotary speeds provided various dials, and all were recorded.

The rotary viscometer includes a rotor for stirring the solid particle solution in order to produce a shearing effect and create a dial read, as presented in Figure 3.35. As the theory suggests, there is a tendency of non-Newtonian fluids to vary in viscosity once the fluid is under the exposure of a shear strain or a shear rate, resulting in a shear stress. Six shear rates are produced by using the six following speeds of the rotary viscometer: 3 rpm, 6 rpm, 100 rpm, 200 rpm, 300 rpm, and 600 rpm. When this kind of viscometer is used, the rotor rotating at a constant rate causes a shear rate. The constant rate is given in rpm (revolutions per minute). The following relationship is used to determine the shear rate:

$$\gamma = rpm * 1.70 \tag{4.2}$$

$$\tau = \mu * \gamma \tag{4.3}$$

where:

rpm = N-rotational velocity

γ = shear rate (s^{-1})

τ = Shear stress (lb/100 ft^2)

τ should be multiplied by 0.4788, to convert, lb/100ft^2 to Pascals (Pa).

First, the dial readings for all speeds were recorded. Then, the conversion mentioned above was used to convert it to shear rate and shear stress, after which the shear stress was plotted against the shear rate. In general, the viscosity of the solid particle solution at various shear rates and rpm is acquired through the slope of the shear stress-shear rate curve. Deriving from the shear stress-shear rate graph, the rheology of the solid particle solution is related to the Herschel-Bulkley model and in particular to shear thinning (pseudo-plastic).

The following equation is used to calculate the plastic viscosity μ_p:

$$\mu_p = \theta_{600} - \theta_{300} \tag{4.4}$$

where:

μ_p = Plastic viscosity (cp)

θ_{600} = dial reading of 600 rpm

θ_{300} = dial reading of 300 rpm

$$Y_B\ (Pa) = (Dial\ Read\ at\ 300 - \mu_P) * 0.4788 \tag{4.5}$$

where:

Y_B = Bingham Yield Point, lb/100ft^2 (Pa)

The true yield strength is given as:

$$Y_T = \frac{3}{4} * Y_B \quad (4.6)$$

where:

Y_T = True Yield Point, (Pa)

In order to detect the range of solid particle concentrations that result in a slurry of a non-Newtonian rheology while at the same time ensuring adequacy for application in the process flow loop pipeline because of the constraints of the current pump in the system, a viscosity test was carried out. Any two values of shear stress and shear rate can serve to calculate K (consistency index) and n (flow behavior index). It is normal to acquire 3 rpm, 300 rpm, and 600 rpm from all tests which are then used to detect k and n [23].

$$n = 0.5 \log \frac{\theta_{300}}{\theta_3} \quad (4.7)$$

$$K = \frac{5.11 * \theta_{300}}{511^n} \quad (4.8)$$

where:

θ_{300} = reading at 300 rpm

θ_3 = reading at 3 rpm

4.3.2 Lab Test Fluid Rheology

The test fluid sample was taken after completing each flow testing state in the process flow loop. Subsequently, the analysis was performed to identify the viscous properties. To find the rheological parameters of the designed fluid systems, a rotary viscometer was used in the experiment. The viscosity of the samples was measured at the rotational velocity (v) of 3, 6, 100, 200, 300 and 600 rpm. A summary of the results of the measurements are reported in Table 4.2, Table 4.3 and Table 4.4.

Table 4.2 Experiment Sample Concentration Cs = 2 wt.%

RPM (v)	Dial dial reading (θ)	shear rate, γ (1/sec)	shear stress, τ (Pa)	Plastic Viscosity, μ_p (cP)	Yield Point, Y_B (Pa)	True Yield Point, Y_T (Pa)	Parameters
600	13	1020	6.641	4	2.394	1.79	
300	9	510	4.597	4	2.394	1.79	K = 0.0056 (Pa.s^n)
200	7	340	3.576	4	2.394	1.79	
100	5	170	2.554	4	2.394	1.79	
6	3	10.20	1.532	4	2.394	1.79	n = 0.948
3	1	5.10	0.510	4	2.394	1.79	

Table 4.3 Experiment Sample Concentration Cs = 3 wt.%

RPM (v)	Dial dial reading (θ)	shear rate, γ (1/sec)	shear stress, τ (Pa)	Plastic Viscosity, μ_p (cP)	Yield Point, Y_B (Pa)	True Yield Point, Y_T (Pa)	Parameters
600	24	1020	12.261	6	5.745	4.30	
300	18	510	9.195	6	5.745	4.30	K = 0.0101 (Pa.s^n)
200	15.5	340	7.918	6	5.745	4.30	
100	11	170	5.619	6	5.745	4.30	
6	5	10.20	2.554	6	5.745	4.30	n = 0.906
3	3	5.10	1.532	6	5.745	4.30	

Table 4.4 Experiment Sample Concentration Cs = 5 wt.%

RPM (v)	Dial dial reading (θ)	shear rate, γ (1/sec)	shear stress, τ (Pa)	Plastic Viscosity, μ_p (cP)	Yield Point, Y_B (Pa)	True Yield Point, Y_T (Pa)	Parameters
600	45	1020	22.989	10	11.97	8.977	
300	35	510	17.880	10	11.97	8.977	K = 0.0195 (Pa.s^n)
200	29	340	14.815	10	11.97	8.977	
100	21	170	10.728	10	11.97	8.977	
6	8	10.20	4.087	10	11.97	8.977	n = 0.891
3	5	5.10	2.554	10	11.97	8.977	

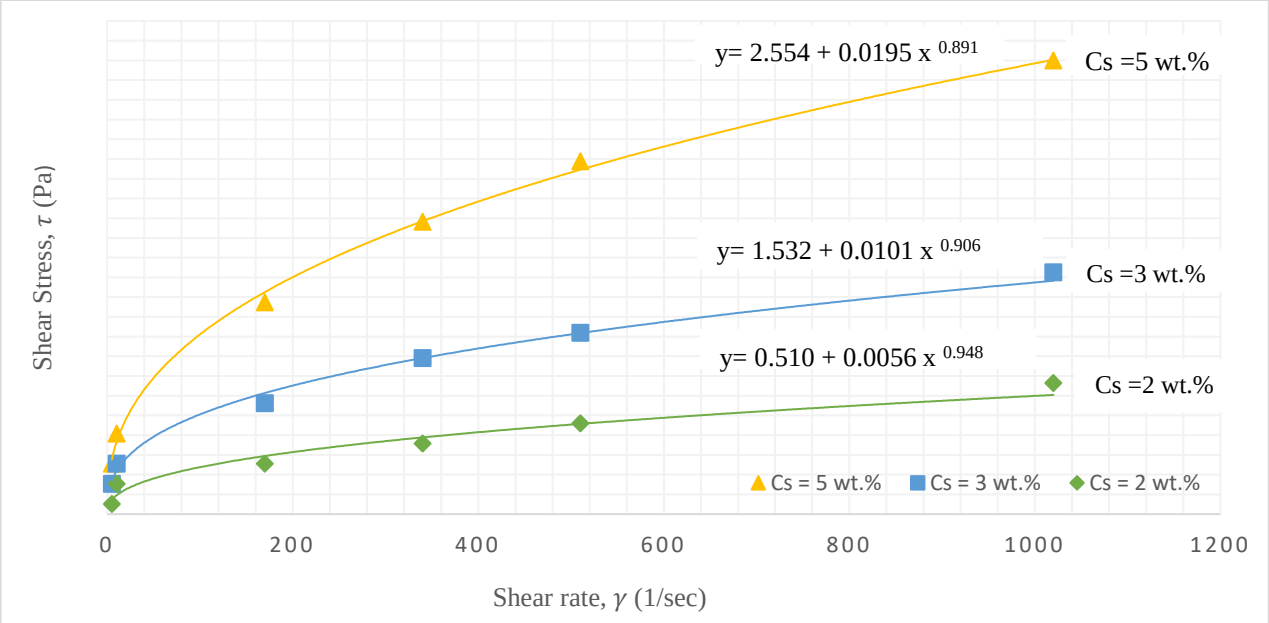

Figure 4.2 Rheogram for Experiment Sample Concentrations.

Figure 4.2 illustrates the shear stress versus shear rate relationships of the test fluids. As can be seen the shear stress increases at a higher rate when there is a higher concentration of solid particle in the solution.

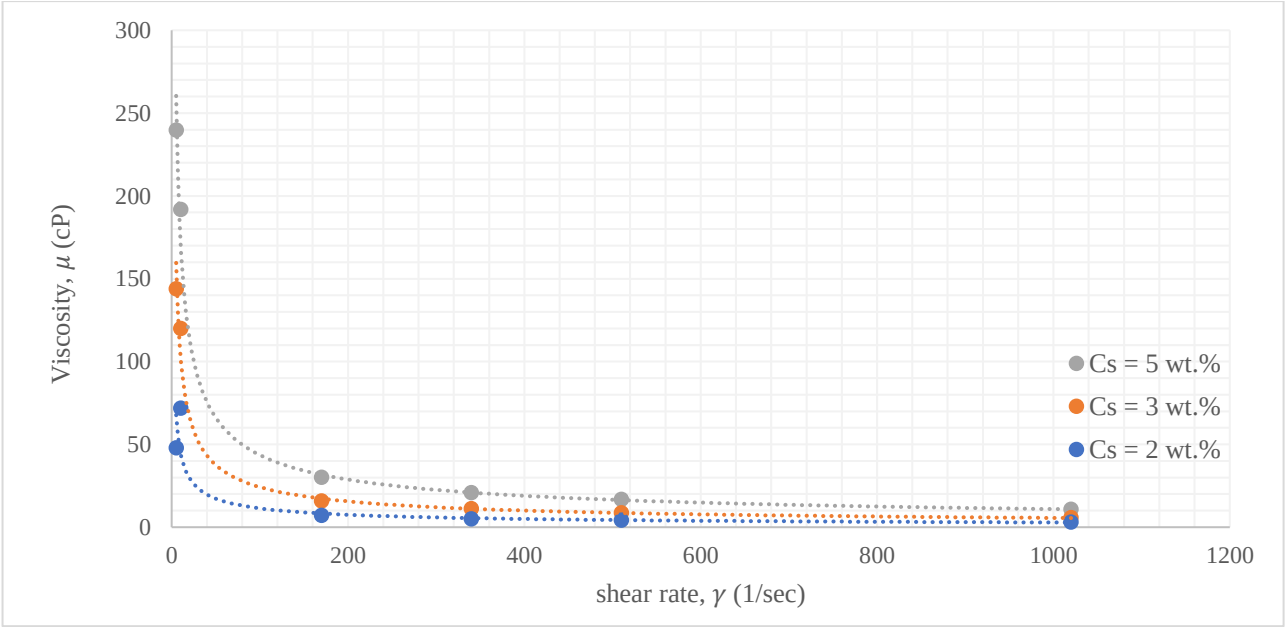

Figure 4.3 Effect of Shear Rate on Viscosity of Solid Particle Concentrations.

The impact of shear rate on the viscosity of solid particle solution concentrations (Cs = 2 wt.%, Cs = 3 wt.% and Cs = 5 wt.%) is presented in Figure 4.3. As shown, with a rise in the shear rate, the viscosity significantly decreases with the values of 0.0056, 0.0101 and 0.0195 ($Pa.s^n$), which correspond to 2 wt.%, 3 wt.% and 5 wt.% respectively, the consistency index (k) increases with the concentration of solutions. With the values 0.948, 0.906, and 0.891, which correspond to 2 wt.%, 3 wt.% and 5 wt.% respectively, the flow index (n) drops.

4.4 Four-Phase (CO_2/Oil/Water/Sand) Flow Experiments in a Complex Horizontal Pipeline.

Sand particles were used for the solid-phase in the experiments, with CO_2 used for the gas-phase, oil and water for liquid-phases. Table 4.5 presents the results for the parameters obtained from the flow loop horizontal pipelines tests of four-phase (CO_2/oil/water/sand) flows at different flow rates of gas and liquid. The results of these tests are shown in Figure 4.4 and Figure 4.5, which depict four-phase flow pressure profiles for four-phase (CO_2/oil/water/sand) flows in a flow loop horizontal pipeline. Figure 4.6 and Figure 4.7 illustrate temperature distribution for four-phase (CO_2/oil/water /sand) flow in a flow loop horizontal pipeline.

Figure 4.8 depicts linear relationships with gas flow rates for four-phase (CO_2/oil/water/sand) flow pressure gradients in a flow loop horizontal pipeline.

Table 4.5 Four-Phase (CO_2/Oil/Water/Sand) Flows at Different a Flow Rates in Flow Loop Horizontal Pipeline.

Oil flow rate gal/min	Liquid flow rate gal/min	CO_2 flow rate (L/s)	Solid fraction C_S (wt.%)	Distance from entrance	1	2	3	4	5	6	7	ΔP/L (kPa/m)	U Superficial liquid velocity (m/s)	U Superficial gas velocity (m/s)	Um mixture velocity (m/s)	$Re_m = \rho_m u_m d/\mu_m$	$N_{FRm} = u_m/(D.g)^{05}$
				Length (m)	0	4	8	12	18	20	24						
2	4	4	2	P (psia)	75	65	55	50	45	40	35	12.00	3.5	63	67	123165	272
				T (°C)	25	24	23.6	23.3	23.2	23.1	23						
		6	3	P (psia)	85	80	75	70	65	60	55	9.00		95	98	179127	400
				T (°C)	25	23.75	23.4	22.9	22.8	22.7	22.4						
		8	5	P (psia)	100	95	90	85	80	75	70	8.50		126	130	233663	529
				T (°C)	25	23.60	22.8	22.6	22.5	22.3	22.1						
4	8	10	2	P (psia)	105	90	85	80	75	70	65	7.50	4	157	161	286833	658
				T (°C)	22.7	22.6	22.5	22.5	22.4	22.3	22.2						
		12	3	P (psia)	110	95	90	85	80	75	70	7.00		189	192	338698	786
				T (°C)	22.75	22.7	22.6	22.5	22.4	22.3	22.2						
		14	5	P (psia)	115	100	95	90	85	80	75	6.50		220	224	389313	915
				T (°C)	22.7	22.8	22.7	22.0	22.3	22.2	22.1						
8	16	16	2	P (psia)	120	105	68	66	60	56	52	6.00	8	252	255	432487	1043
				T (°C)	21.7	21.6	21.5	21.4	21.3	21.2	21.1						
		18	3	P (psia)	125	110	88	84	80	75	70	5.50		283	287	487001	1172
				T (°C)	21.6	21.6	21.5	21.4	21.3	21.2	21.1						
		20	5	P (psia)	130	115	95	90	85	80	77	5.00		315	318	534170	1300
				T (°C)	21.8	21.7	21.6	21.5	21.4	21.3	21.2						

Fluid	Tube D(mm)	Viscosity μ, kg/(m.s)	Density ρ, kg/m^3	Area (mm^2)
Water	20	0.001	1000	0.28
Oil	20	0.018	900	
CO_2	20	0.000148	198	
Sand	20	-	2600	

In each experiment of four-phase (CO_2, oil, water, sand) flows, intervals were used to modify the gas, water, and oil flow rates and solid concentrations from the minimum to the maximum. To detect the data trends, the temperature distribution and the pressure drop for four-phase (CO_2/oil/water/sand) flows in the flow loop horizontal pipeline, were, plotted over the flow loop pipeline distance. It was concluded that the empirical results are reliable because the validation of the experimental results proved good predictions.

4.4.1 Temperature Gradient Four-Phase (CO_2/Oil/Water/Sand) Flow Experiments in a Complex Horizontal Pipeline

Figure 4.4 and Figure 4.5 illustrate temperature distribution profiles along the flow loop of a complex horizontal pipeline for four-phase (CO_2/oil/water/sand) flows.

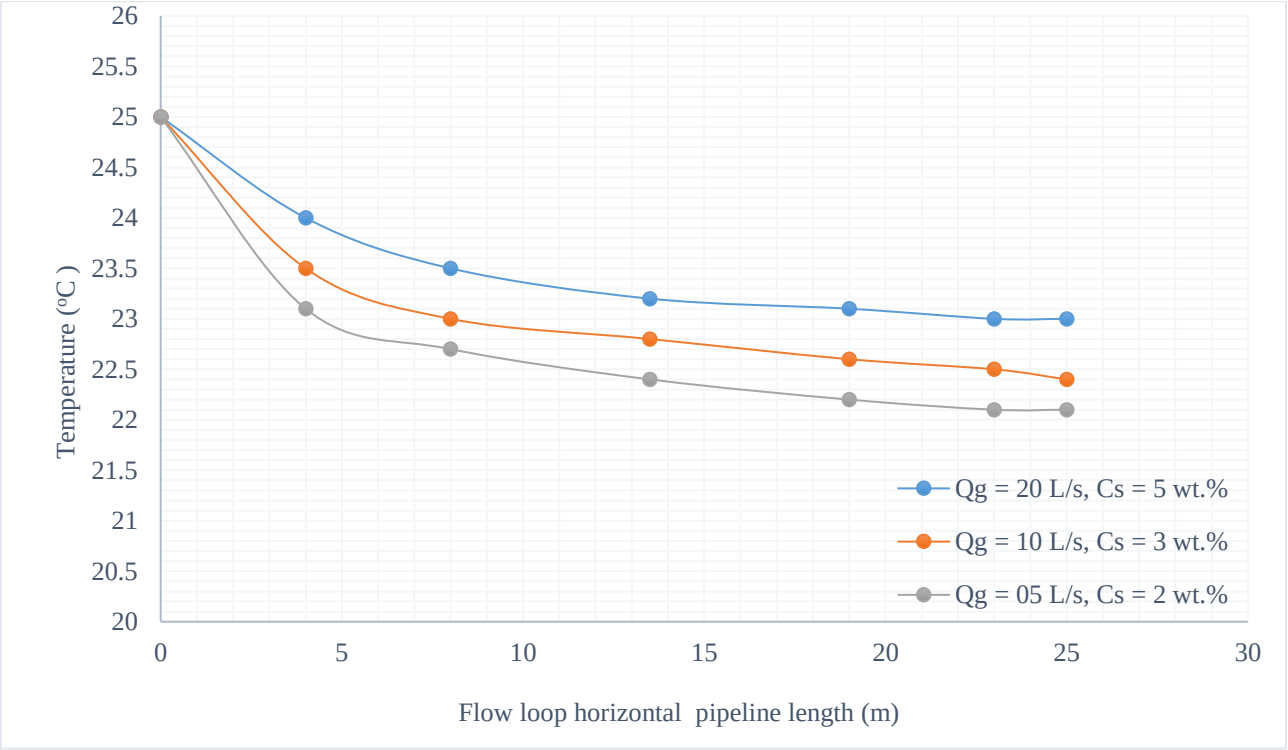

Figure 4.4 Temperature Profile Along the Flow Loop of a Complex Horizontal Pipeline for Four-Phase (CO_2/Oil/Water/Sand) Flows at Different Gas Flow Rates and Solid Weight Concentrations, with Other Variables Constant.

Figure 4.4 explains the temperature distribution along a flow loop horizontal pipeline with increasing gas flow rates (Q_g=5 L/s, Q_g=10 L/s, Q_g=20 L/s) and solid weight concentrations (Cs=2 wt.%, Cs=3 wt.% and Cs=5 wt.%). As can be seen, the temperature drops with gas flow rates, while solid fractions rise in as the flow goes along during the flow loop pipeline. This happens due to friction effecting gas flow rates and solid fractions.

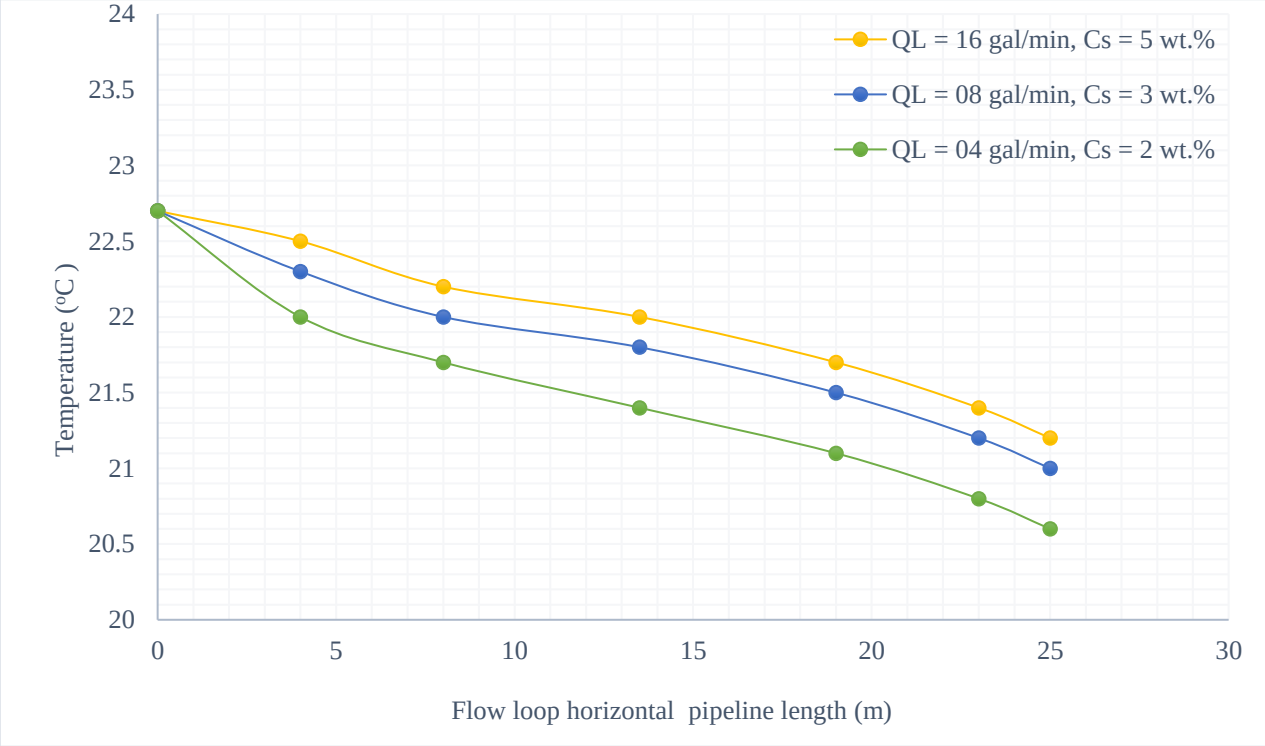

Figure 4.5 Temperature Profile Along the Flow Loop of a Complex Horizontal Pipeline for Four-Phase (CO_2/Oil/Water/Sand) Flows at Different Liquid Flow Rates and Solid Weight Concentrations, with the Other Variables Constant.

Figure 4.5 shows the temperature distribution along a clear PVC flow loop horizontal pipeline with increasing liquid flow rates (Q_L=4 gal/min, Q_L=8 gal/min, Q_L=16 gmal/min) and solid weight concentrations (Cs=2 wt.%, Cs=3 wt.% and Cs=5 wt.%) in a flow loop horizontal pipeline. As shown, the temperature distribution decreases as the distance of the low loop pipeline increases. Additionally, the liquid flow rates and solid weight concentrations rise as the flow goes along the flow loop pipeline distance. This occurs due to the friction effecting and the density of the liquid flow rate and solid fraction. As well, the temperature distribution

decreases around (2 ºC) from room temperature due to increases in the fluid-mixture along the 25 m length of the flow loop pipeline. This is due to CO_2 gas responding to cold CO_2 cylinder pressure at about 860 psia at normal room temperature (20 ºC).

4.4.2 Pressure Gradient in Four-Phase (CO_2/Oil/Water/Sand) Flow Experiments in Complex Horizontal Pipeline.

Figure 4.6 and Figure 4.7 depicts the pressure profile of (CO_2/oil/water/sand) four-phase flows in the flow loop of a complex horizontal pipeline. Figure 4.6 shows the rise of the local pressure through the flow loop horizontal pipeline caused by increasing the gas flow rate. Additionally, pressure drops increase as gas flow rates (Q_g=5 L/s, Q_g=10 L/s, Q_g=20 L/s) and solid weight concentrations (Cs=2 wt.%, Cs=3 wt.% and Cs=5 wt.%) increase when the flow goes along the flow loop pipeline. We can also observe the decline in pressure for the same flow rate when the flow reaches far points in the loop.

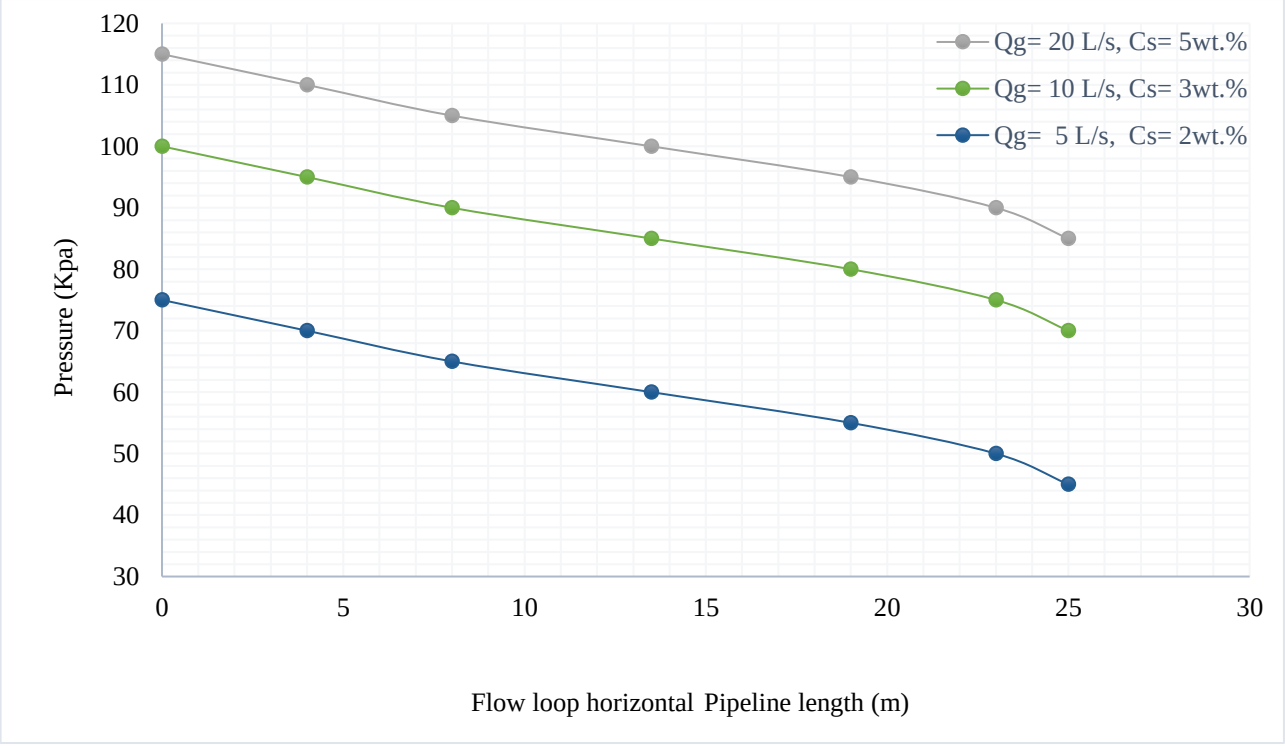

Figure 4.6 Pressure Profile Along the Flow Loop Horizontal Pipeline for Four-Phase (CO_2/Oil/Water/Sand) Flow at Different Gas Flow Rates and Solid Weight Concentrations, with the Other Variables Constant.

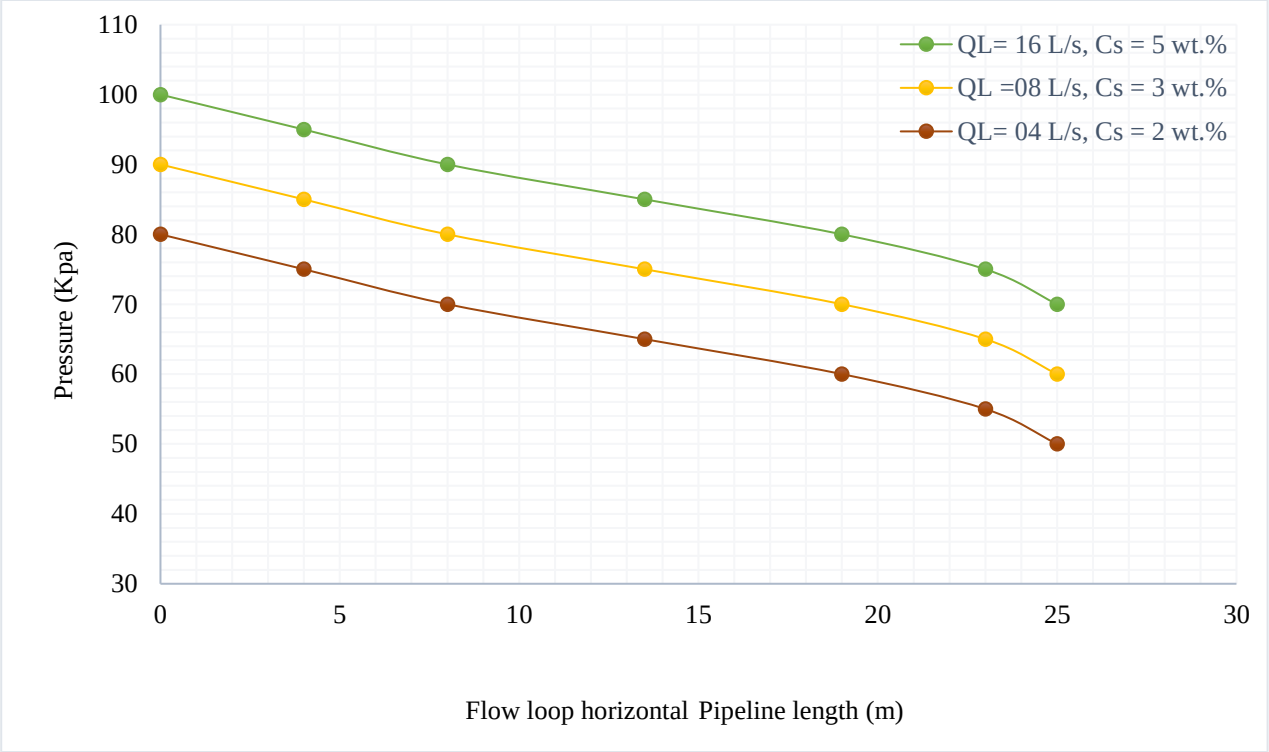

Figure 4.7 Pressure Profile Along the Flow Loop Horizontal Pipeline for Four-Phase (CO_2/Oil/Water/Sand) Flow at Different Liquid Flow Rates and Solid Weight Concentrations, with the Other Variables Constant.

Figure 4.7 explains the pressure drop of four-phase (CO_2/oil/water/sand) flow through a flow loop horizontal pipeline by increasing liquid flow rates (Q_L=4 gal/min, Q_L=8 gal/min, Q_L=16 gal/min) and solid weight concentrations (Cs=2 wt.%, Cs=3 wt.% and Cs=5 wt.%). This occurs due to the friction affecting the liquid flow rate and solid fractions. To devise a minimum velocity formula, we assume the pipeline is horizontal and has few to no inclinations. Further, we also assume that compared to the liquid flow in the pipeline, the sand's volume fraction is quite low, and that all the sand particles in the pipeline have a similar diameter and are spherical in shape.

The results, including pressure drop and temperature distribution, have been found to show good agreement. The above trends for four-phase (CO_2/oil/water/sand) flow indicate decreases in pressure drops with the length of the pipeline, which is a good indication that pressure is decreasing due to a long profile and multiple elbows. However, the temperature profile is not much affected, because the experiments were conducted at room

temperature.

The pressure gradient (pressure drop per unit length) of the four-phase (CO_2/oil/water/sand) flow data is discussed in terms of gas flow rates, liquid flow rates, sand particle weight concentrations, mixture of volume fractions, and Reynolds and Froude numbers.

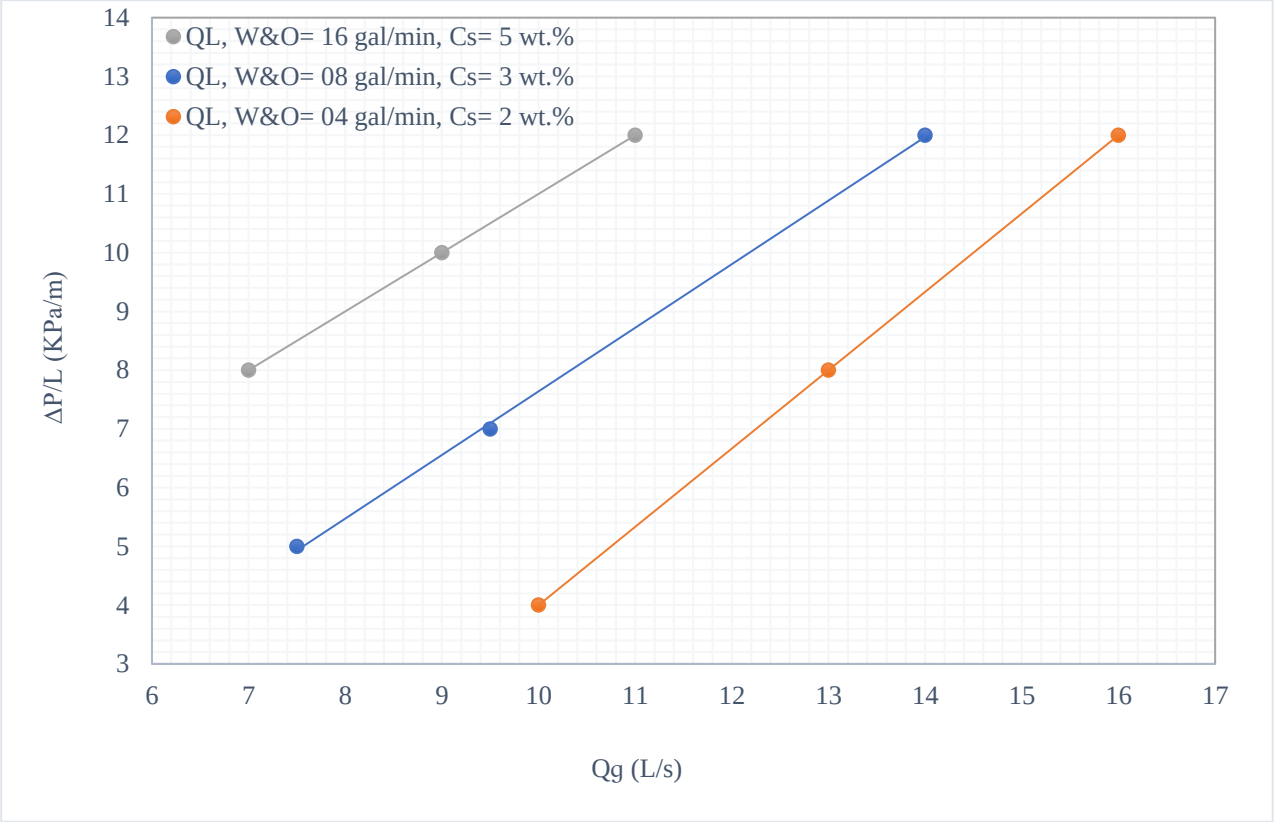

Figure 4.8 Pressure Gradient vs Gas Flow Rates for Four-Phase (CO_2/Oil/Water/Sand) Flow with Increasing Liquid (Water and Oil) Flow Rates and Solid Weight Concentrations in a Flow Loop Horizontal Pipeline.

Figure 4.8 shows the effects of gas flow rates on pressure gradients for four-phase (CO_2/oil/water/sand) flow in a flow loop horizontal pipeline. For liquid (water and oil), flow rate pressure gradient increases with increasing gas flow rates (Q_g=5 L/s, Q_g=10 L/s, Q_g=20 L/s) and solid weight concentrations (Cs=2 wt.%, Cs=3 wt.% and Cs=5 wt.%). In the above Figure 4.8 depicts linear relationships with the pressure gradient for four-phase (CO_2/oil/water/sand) flow and gas flow rates in a flow loop horizontal pipeline.

Figure 4.8 depicts pressure gradients of four-phase flow in a horizontal pipeline at different gas, and liquid velocities, and with a solid weight concentration in mixture (C_S), with the other variables fixed.

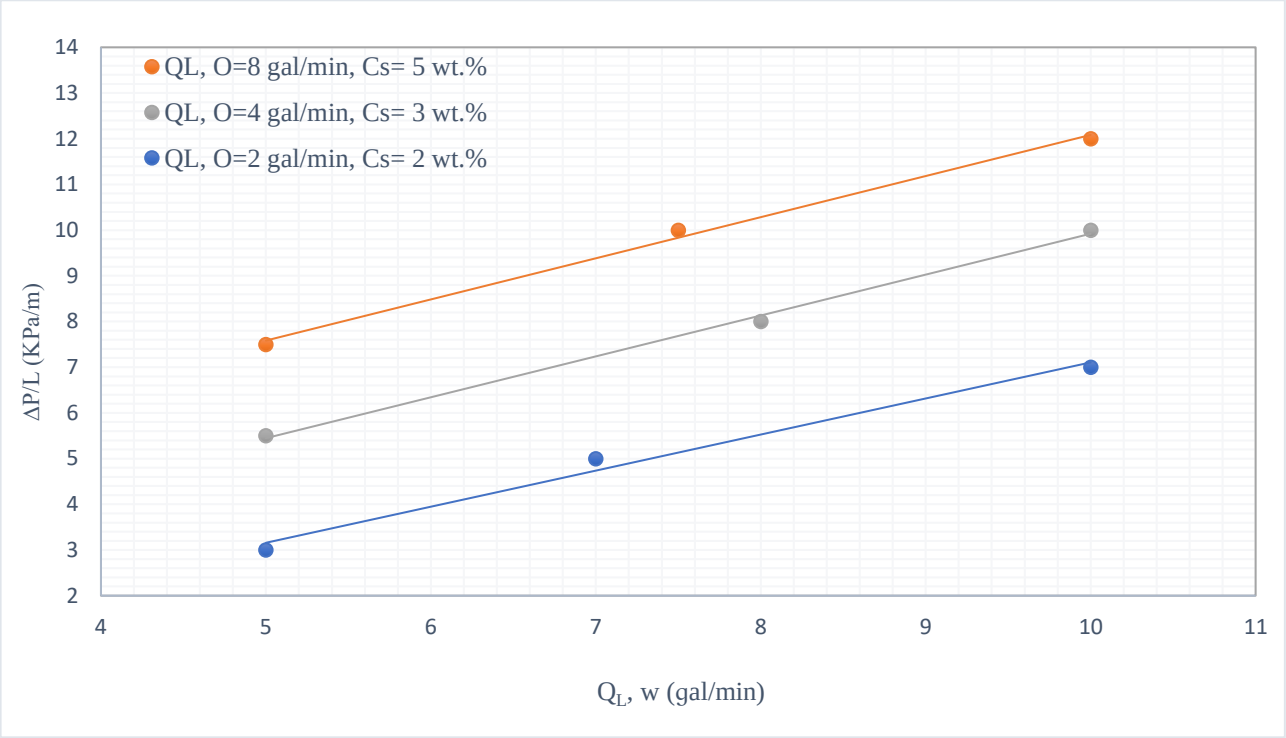

Figure 4.9 Pressure Gradient vs Water Flow Rates for Four-Phase (CO_2/Oil/Water/Sand) Flow with Increasing Oil Flow Rates and Solid Weight Concentrations in a Flow Loop of a Complex Horizontal Pipeline.

Figure 4.9 indicates the pressure gradients of four-phase (CO_2/oil/water/sand) flow at different liquid (water and oil) flow rates (Q_L=4 gal/min, Q_L=8 gal/min, Q_L=16 gal/min) and solid weight concentrations (Cs=2 wt.%, Cs=3 wt.% and Cs=5 wt.%), with the other variables constant. The pressure gradients for four-phase (CO_2/oil/water/sand) flow increases with increases in water flow rates for all tests combination, while the oil flow rates, and sand particle weight fractions were kept constant for each set of data. This occurred due to the increase in oil volume fraction.

Figure 4.10 and Figure 4.11 provide a comparison of (CO_2/oil/water/sand) four-phase flow frictional pressure gradients with sand particle weight concentrations as being perfectly linear in the flow the loop of a complex horizontal pipeline.

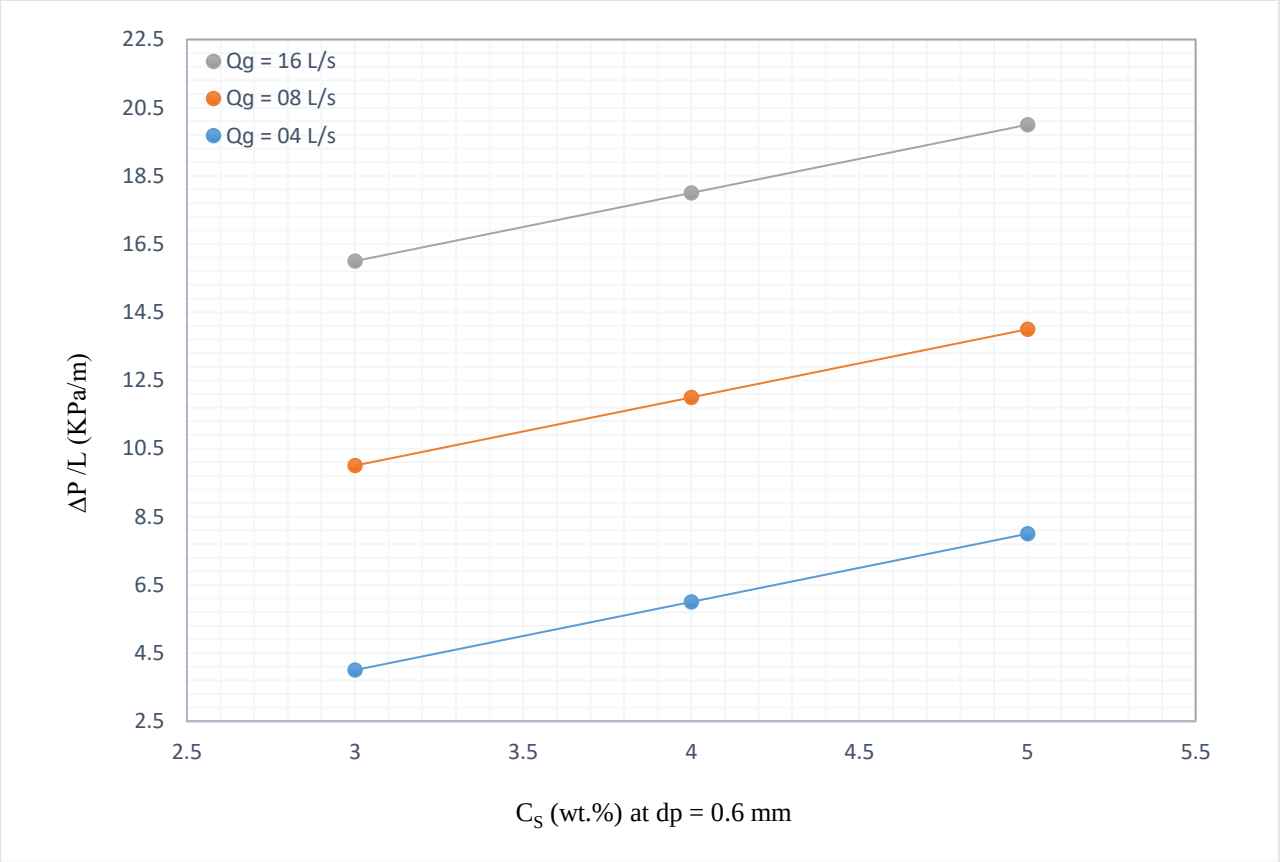

Figure 4.10 Pressure Gradient vs Sand Particle Weight Fraction of Four-Phase (CO_2/Oil/Water/Sand) Flow with Increasing Gas Flow Rates in the Flow Loop of a Complex Horizontal Pipeline.

Figure 4.10 shows pressure gradients of four-phase (CO_2/oil/water/sand) flow at different solid weight concentrations (Cs=2 wt.%, Cs=3 wt.% and Cs=5 wt.%) and liquid gas flow rates (Q_g=5 L/s, Q_g=10 L/s, Q_g=20 L/s), with the other variables constant.

Sand particles were used for the solid phase in the experiments, with CO_2 employed for the gas phase. Water and oil were used for the liquid-phases. The experimental results for the parameters in the flow loop pipeline are presented in Table 4.5.

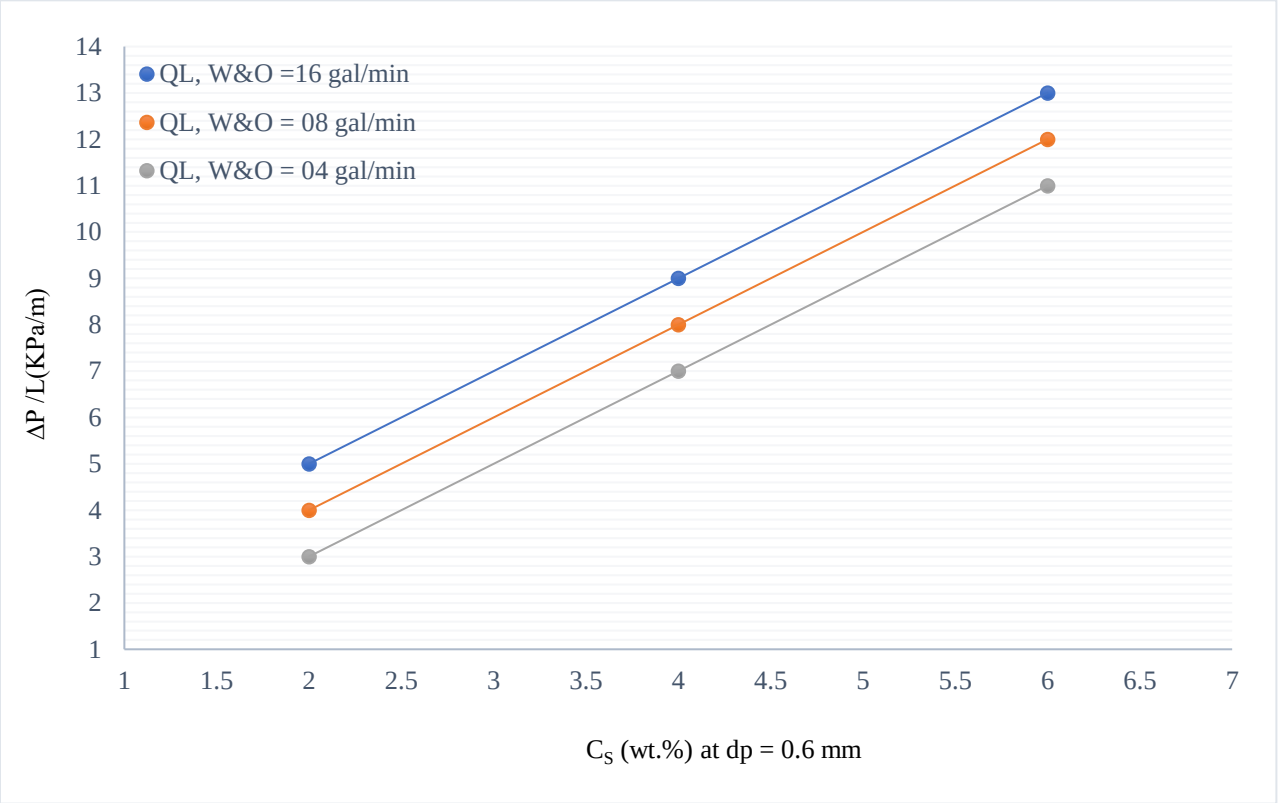

Figure 4.11 Pressure Gradient vs Sand Particle Weight Fraction of Four-Phase (CO_2/Oil/Water/Sand) Flow with Increasing Liquid (Water and Oil) Flow Rates Throughout the Flow Loop of a Complex Horizontal Pipeline.

From Figure 4.11, it can be seen that pressure gradients of four-phase fluid (CO_2/oil/water/sand) flows increase with solid weight concentration (Cs=2 wt.%, Cs=3 wt.% and Cs=5 wt.%) in slurry throughtout the horizontal pipeline. Also, this analysis shows the usage of gas injections in slurry flows to reduce horizontal pipeline blockage by slurry near pipeline bottom and bends.

Figure 4.12 shows a comparison of four-phase (CO_2/oil/water/sand) flow frictional pressure gradients with increasing liquid (water and oil) flow rates throughout a flow loop horizontal pipeline vs. mixture volume fraction as being perfectly linear.

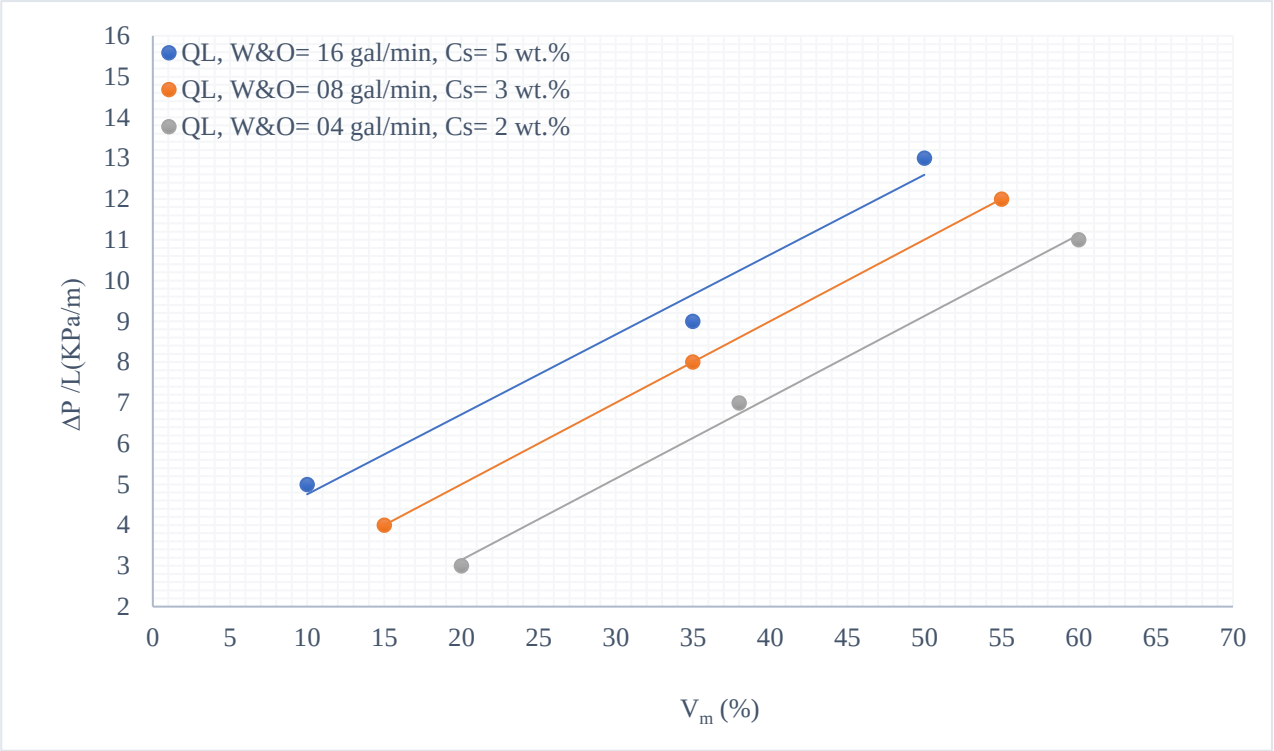

Figure 4.12 Pressure Gradient vs Mixture of Volume Fraction of Four-Phase (CO_2/Oil/Water/Sand) Flow at Different Liquid (Water and Oil) Flow Rates in a Flow Loop of a Complex Horizontal Pipeline.

Figure 4.12 depicts pressure gradients of four-phase (CO_2/oil/water/sand) flows at different solid weight concentrations and, volume fractions of mixture and liquid (water and oil) flow rates, with the other variables constant.

The pressure gradient in the horizontal pipeline increases with the gas and liquid flow rates, and with the concentration of solids in mixtures. According to the Darcy-Weisbach equation:

$$\frac{\Delta P}{L} = f \frac{\rho}{D} \frac{v^2}{2} \tag{4.9}$$

where, ΔP is pressure drop, L is pipe length, D is internal diameter of the pipeline, f is friction factor, ρ is fluid density, and v is fluid velocity.

From Equation (4.9), we can see that pressure gradient is directly proportional to the square of fluid velocity, if other variables are kept constant. We can also see that, pressure gradient decreases with increases in the pipe's internal diameter. As well, increasing wall roughness increases friction near the wall, thus creating more turbulence in flow and increasing pressure drops. With time, the wall roughness further increases due to sand particle deposition and moisture, damaging the wall material. Additionally, the four-phase fluid mixture density increases with solid volumetric concentration in slurry, causeing the pressure gradient to increase. The sand concentration and the fluid velocity should therefore be kept at a minimum level to maintain low pressure drops in a pipeline.

4.5 Dimensionless Quantities:

A significant quantity of dimensionless groups exists to assist multi-phase flow researchers in developing more general results and models. Many different dimensionless groups can be used to convert multi-phase flow data into more convenient forms. Dimensionless numbers provide a means for assessing the relative magnitudes of these interacting forces. The values of Reynolds and Froude numbers for mixtures have been estimated for a range of mixture velocities.

4.5.1 Reynolds Number for Mixtures ($\mathbf{Re_m}$)

The Reynolds number is the ratio of inertial forces to viscous or frictional force. This number is calculated according to Equation (4.10):

$$\mathrm{Re_m} = \frac{\rho_m u_m D}{\mu_m} \tag{4.10}$$

where v_m (m/s) is the velocity of the mixture, D (m) is the pipeline diameter, ρ_m (kg/m^3) is the density of the mixture, and μ_m (kg/(m.s)) is the dynamic viscosity of the mixture.

The Reynolds number depends on the flow rates and physical properties of the multi-phase flow.

Figure 4.13 depicts a linear relationship with the Reynolds number vs pressure gradients for four-phase (CO_2/oil/water/sand) flows in a flow loop horizontal pipeline.

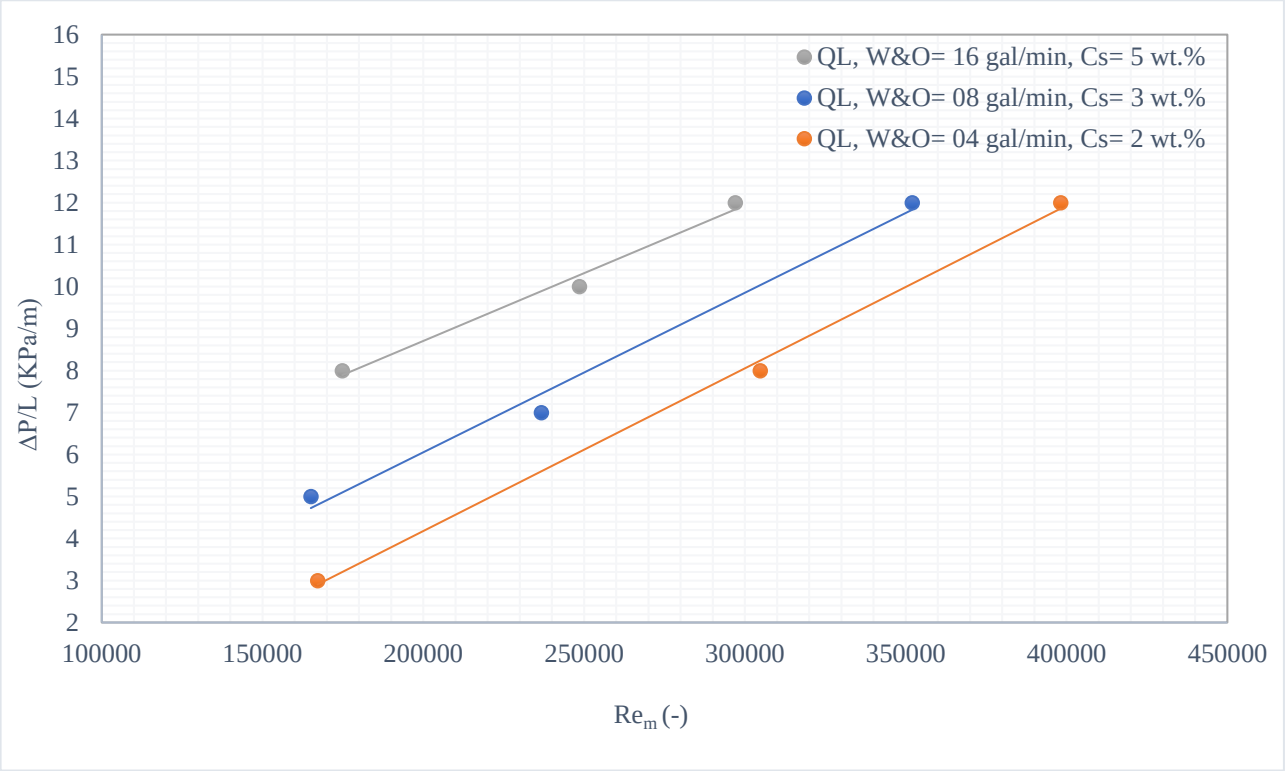

Figure 4.13 Pressure Gradient vs Reynolds Number of Four-Phase (CO_2/Oil/Water/Sand) Flow at Different Liquid (Water and Oil) Flow Rates and Solid Weight Concentrations with the Other Variables Constant, in a Flow Loop of a Complex Horizontal Pipeline.

Figure 4.13 indicates that a linear relationship is present between the pressure gradients and the Reynolds number of four-phase (CO_2/oil/water/sand) flows. The pressure gradient increases with increasing in the Reynolds number of the four-phase flows in a horizontal pipeline. Figure 4.13 shows the pressure gradient vs Reynolds number of the four-phase flows in a horizontal pipeline at different liquid (water and oil) flow rates (Q_L=4 gal/min, Q_L=8 gal/min, Q_L=16 gal/min) and solid weight concentrations (Cs=2 wt.%, Cs=3 wt.% and Cs=5 wt.%) with the other variables constant.

The values of the Reynolds number have been estimated for a range of four-phase (CO_2/oil/water/sand) flow rates. As is known, the Reynolds number (dimensionless number trends) is the ratio of inertial forces to viscous or frictional force.

From Equation (4.10), we can see that the Reynolds number for mixtures decreases with increases in fluid viscosity. These changes indicate that the fluid viscosity has a proportional relation with the friction factor and also eventually with pressure drop.

4.5.2 Froude Number for Mixture (NFR_m)

The Froude number is the second of the non-dimensional groups and can be formulated as follows:

$$NFR_m = \frac{u_m}{\sqrt{gD}} \tag{4.11}$$

where u_m (m/s) is the velocity of the mixture, D (m) is the pipeline diameter, and g (m/s^2) is the gravity force constant.

Hence, this number represents the ratio between the fluid's gravitational and inertial forces.

Figure 4.14 depicts a linear relationship for the Froude number vs. pressure gradients for four-phase (CO_2/oil/water/sand) flow in a flow loop horizontal pipeline.

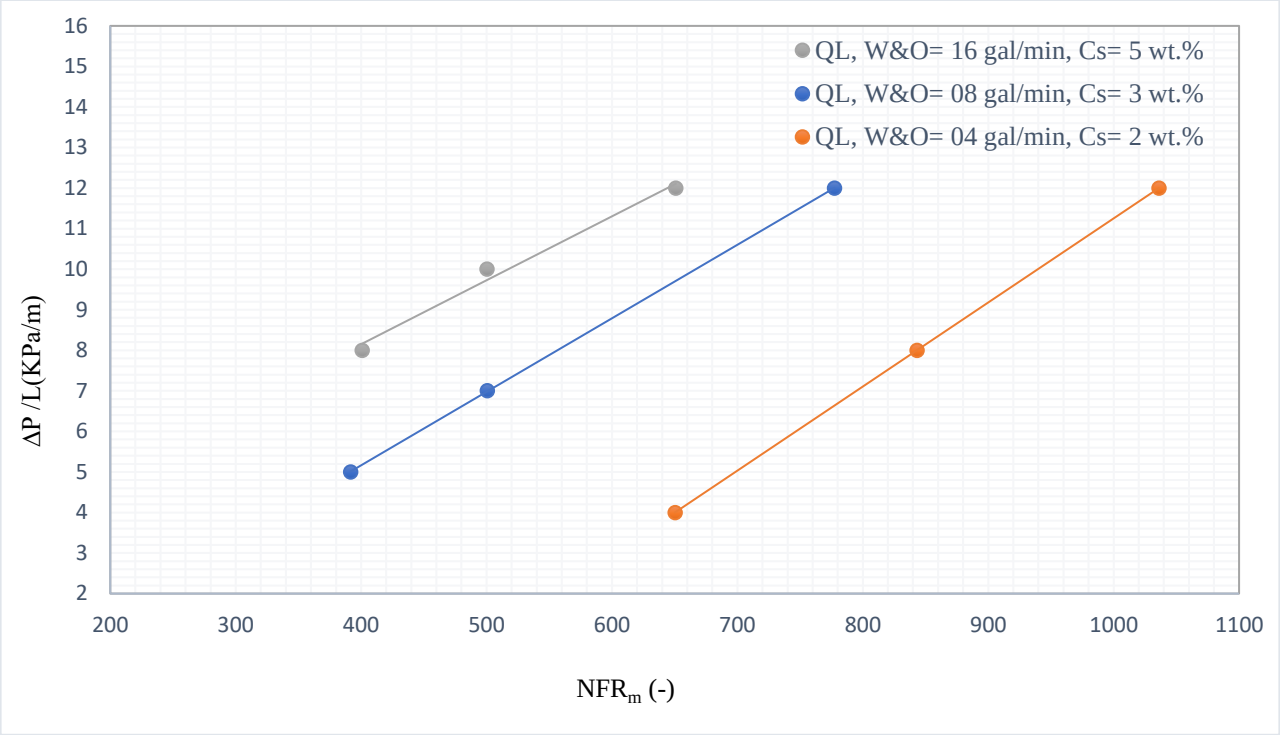

Figure 4.14 Pressure Gradient vs Froude Number in Four-Phase (CO_2/Oil/Water/Sand) Flow at Different Liquid (Water and Oil) Flow Rates and Solid Weight Concentrations, with the Other Variables Constant.

Using Equation (4.11), we can see that the Froude Number for mixtures is directly proportional to the fluid velocity, if the other parameters are kept constant. In Figure 4.14 above, the linear relationship is denoted by the pressure gradient vs the Froude number of the four-phase flow (sand, water, oil, CO_2) in a horizontal pipeline at different liquid (water and oil) flow rates (Q_L=4 gal/min, Q_L=8 gal/min, Q_L=16 gal/min) and solid weight concentrations (Cs=2 wt.%, Cs=3 wt.% and Cs=5 wt.%), with the other variables constant. The Froude number of mixtures is a linear function of the velocity of the mixture, so plotting against a Froude number is the same as plotting against velocity.

4.5.3 Weber Number for Mixtures (We)

The Weber number, which is another non-dimensional number, describes the ratio in fluids between surface tension and inertial forces. The Weber number for mixtures can be used to express this influence as follows:

$$We_m = \frac{\rho_m u_m^2 D}{\sigma_m} \tag{4.12}$$

where u_m (m/s) is the velocity of the mixture, D (m) is the pipeline diameter, ρ_m (kg/m^3) is the density of the mixture, and σ_m (N/m) is the surface tension of the mixture.

4.5.4 Four-Phase Number for Mixtures (4-Phase Nm)

Four-phase number for mixtures (4-phase Nm), which is dimensionless as well, provides the measure for the ratio of inertial forces to gravitational and viscous forces.

$$4-\text{Phase Nm} = \text{Re}_m \times \text{N}_{FR} = \frac{\rho_m u_m{}^2 D}{\mu_m \sqrt{gD}} \quad (4.13)$$

where u_m (m/s) is the velocity of the mixture, D (m) is the pipeline diameter, ρ_m (kg/m^3) is the density of the mixture, μ_m (kg/(m.s)) is the dynamic viscosity of the mixture and g (m/s^2) is the gravity force constant.

Using Equation (4.13), we can see that the Four-phase number for mixtures increases with increases in mixture density and mixture velocity and decreases in fluid viscosity. This means, that fluid viscosity has a proportional relation with the friction factor and eventually with pressure drop.

Figure 4.15 depicts a linear relationship between the Four-phase number vs. pressure gradients for four-phase (CO_2/oil/water/sand) flow at constant liquid flow (water and oil) rates in a flow loop horizontal pipeline.

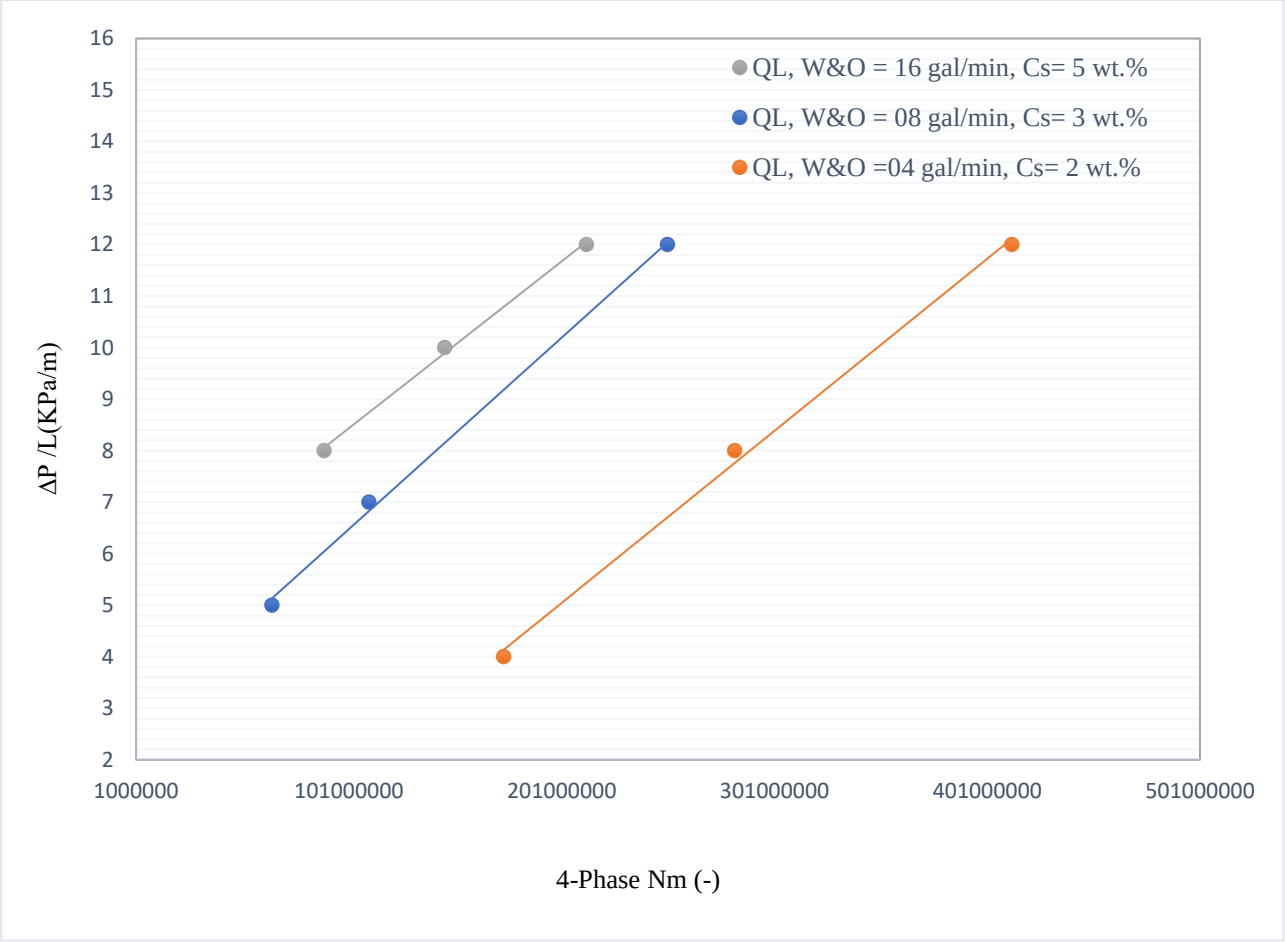

Figure 4.15 Pressure Gradient vs 4-Phase Nm in Four-Phase (CO_2/Oil/Water/Sand) Flow at Different Liquid (Water and Oil) Flow Rates and Solid Weight Concentrations, with the Other Variables the Constant in Flow Loop of a Complex Horizontal Pipeline.

Figure 4.15 indicates that the relationship between pressure gradient vs Four-phase Nm of the four-phase (CO_2/oil/water/sand) flows in horizontal pipelines is perfectly linear at different liquid (water and oil) flow rates (Q_L=4 gal/min, Q_L=8 gal/min, Q_L=16 gal/min) and solid weight concentrations (Cs=2 wt.%, Cs=3 wt.% and Cs=5 wt.%), with the other variables constant.

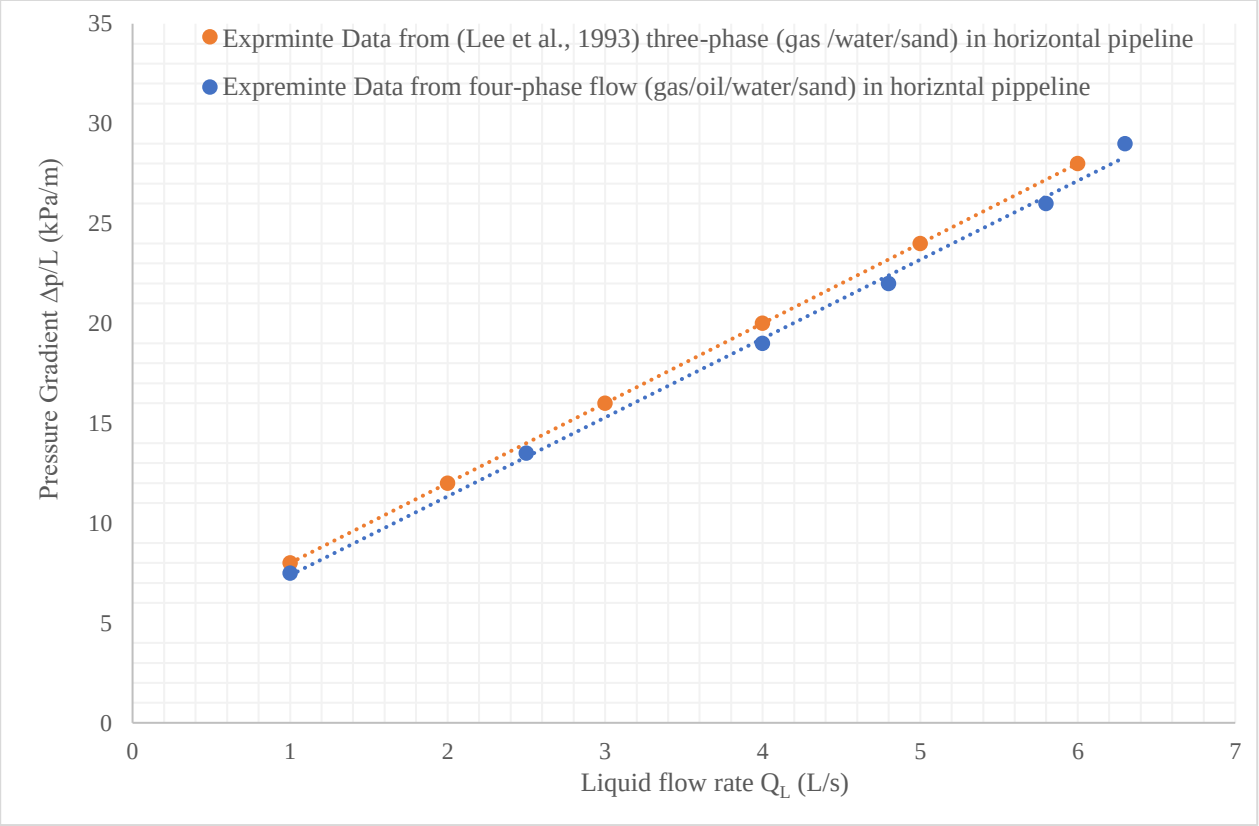

Figure 4.16 Comparison of Experimental Four-Phase flow (Gas/Oil/Water/Sand) Flow and Test Outcomes from Previous Studies (e.g., Lee et al., 1993) for Three-Phase (CO_2/Water/Sand) Flow Pressure Gradients at Different Flow Rates in a Flow Loop Horizontal Pipeline.

No experimental data are available for four-phase (liquid, liquid, solid, gas) flows in a horizontal pipeline with bends prior to this work. Comparisons are made between four-phase flow (gas/oil/water/sand) pressure gradients and test outcomes from a previous of study (Lee et al., 1993) for three-phase (CO_2/water/sand) flow in a flow loop horizontal pipeline [48].

Comparing the test results from this study with those from other study reveals a good match.

Figure 4.16 indicates that a linear relationship is present between the pressure gradient and the liquid flow rate. The pressure gradient increases with increases in the liquid flow rate of the four-phase flow in the horizontal pipeline. Figure 4.16 shows the pressure gradient vs liquid flow rate for four-phase flows in horizontal pipelines at different liquid flow rates, with the other variables constant.

4.6 Conclusions and Recommendations

A four-phase flow in a flow loop horizontal pipeline was developed in this work to study four-phase flows (CO_2/oil/water/sand) used in O&G pipelines.

The experiments applied and validated the proposed model, with the main pipeline flow properties summarized below:

- An experimental investigation has been carried out to study the pressure gradients and flow regimes of four-phase (CO_2/oil/water/sand) flows in a 20 mm ID horizontal pipeline at different flow conditions.
- A multi-phase flow loop horizontal pipeline was devised in order to carry out tests on the four-phase (CO_2/oil/water/sand) flows. This included careful calibration of sensors for both temperature and pressure.
- The pressure gradients were found to increase with rise in the gas and liquid flow rates rise.
- To effectively gauge how pressure impacts transient flow behavior, it was necessary to first analyze temperature profiles, pressure, and gas velocity in the pipeline system.
- The flow regimes show strong dependence on volume fraction, gas, and liquid flow rates.
- The pipeline's material should routinely be inspected and reinstalled to maintain a minimum wall roughness, as the pressure gradient increase with increases in wall roughness.
- The temperature surrounding of the pipelines should be kept at room temperature to maintain a minimum pressure loss and for safety issues.
- Comparisons were made between a four-phase flow (CO_2/oil/water/sand) pressure gradient in a flow loop horizontal pipeline and test outcomes from previous studies (e.g., Lee et al., 1993) that used three-phase flow (CO_2/water/sand) pressure gradients at different flow rates in a flow loop horizontal pipeline. The comparisons in Figure 4.16 showed a good match.

Chapter 5

CFD Modeling and Simulation of Multi-Phase flow Phenomena for Four-Phase (Gas/Liquid/Liquid/Sand) Flow in a Complex Horizontal Pipeline

5.1 Introduction

Multi-Phase flows such as production fluid from reservoirs typically include sand with water. The inclusion of sand in this mixture is concerning, as it not only leads to increased levels of pipeline erosion but also causes sand to accumulate at the bottom of the pipe, blocking the pipe or at the very least hindering the flow.

Oil pumped to the surface from subsea offshore reservoirs is typically comprised of a fluid mixture of gas-oil-water, which is moved to onshore oil and gas processing sites via pipes. Due to the excessive temperatures and pressures of the oil transport pipeline system, the main pipes include shorter pipes (bends and jumpers) that are attached to the manifold at the well. These shorter pipes are used to enable expandability and to prevent system failure. However, the functionality of bends and jumpers can be challenged by extreme internal flow hydro-dynamic loads and internal pressure. The heavy flow loads, and immense pressure can cause major pressure gradient, leading to compromised safety levels and reduced system reliability.

After the fluid mixture has been transported onshore, multi-phase flow separators can be used to separate the mixture. The separation of the fluid into its various elements eliminates most pressure gradient issues. Unfortunately, such fluid separation is too costly to be carried out in offshore facilities. Sand particles are often included in the mixture being transported to shore, which can restrict flow rates or even block the flow altogether. To resolve this dilemma, the sand can be flushed from the bends and jumpers by injecting a high-pressure flow, but this process can be expensive to employ over time, especially when the volume fraction of the sand is relatively high [30].

An alternative approach considers various system inputs and outputs as a means to gauge how well the fluid frequency matches the pipeline's natural frequencies. Based on data analysis, flow rates, phase numbers and phase volume fractions can be adjusted to lessen the flow's impact on bends and jumpers. To accommodate this approach, a standard guideline should be developed for O&G companies to determine flow-induced pressure gradients occurring in pipelines. By assisting in the estimation of multi-phase flow impacts in pipeline systems, such a guideline would enable the O&G industry to better monitor pipeline structure and thus exert enhanced control over the production phase.

The presence of different phases in a multi-phase flow pipeline makes it extremely complicated to model. While other modelling techniques have been developed in recent decades to simulate single and two-phase flow regimes, understanding the physics governing a four-phase flow still poses great challenges to researchers. Not surprisingly, given these inherent difficulties, very little research has been conducted to explain and formulate the behaviour of four-phase (gas, oil, water and sand) flow. This flow regime is of particular interest in petroleum industries, because the entire flow regime from the reservoir to the processing facilities falls into this category.

Untreated reservoir production normally consists of oil, produced water, associated gas, and solids, the latter mainly in the form of sand particles. Sand particles in the pipeline must be kept moving to mitigate the formation of a stationary sand bed at the pipe bottom. A stationary sand bed can jeopardize the integrity and performance of a pipeline by partially or completely blocking the pipe. It may also be a corrosion risk, due to Microbially Induced Corrosion (MIC). Early investigations into liquid/sand flows were all based on visual observations in laboratories. Vocaldo and Charles [31], along with Parazonka et al. [32], observed and classified several flow patterns in liquid/solid horizontal flow.

In a three-layer model, the sand bed is divided into two layers: the stationary sand bed and the moving sand bed. This assumption was confirmed by experimental results, showing that while the upper layer of the sand bed is moving, the lower layer can be stationary. The three-layer model has proven to be a sophisticated approach for two-phase flow, capable of predicting geometrical properties for each layer, including liquid

and sand holdups, phase velocities and pressure drops for the entire field. The results match with the experimental data [33-40].

However, no model has been developed to consider the four-phase flow of (gas, oil, water, and sand), a flow which is dominant in the petroleum industry. In this chapter, for the first time (to the best of our knowledge), a four-phase (gas, oil, water and sand) flow model has been formulated using a mathematical framework.

5.1.2 Objective

The purpose of this work is to develop a mathematical model of four-phase (gas, oil, water, and sand) flow for pressure and flow regimes in a horizontal pipeline. This work also provides a methodology for pressure and force in pipeline components when internal multi-phase flow (oil-gas, oil-gas-water, oil-gas-water with sand particles) is injected into a horizontal pipeline.

5.2 Mathematical Model Description of Four-Phase (Gas-Oil-Water-Sand) Flow

A model has been developed to consider the stratified four-phase (liquid/liquid/gas/solid) flow of pipelines, consisting of five separate layers of gas, oil, water, moving sand bed and stationary sand bed, as illustrated Figure 5.1.

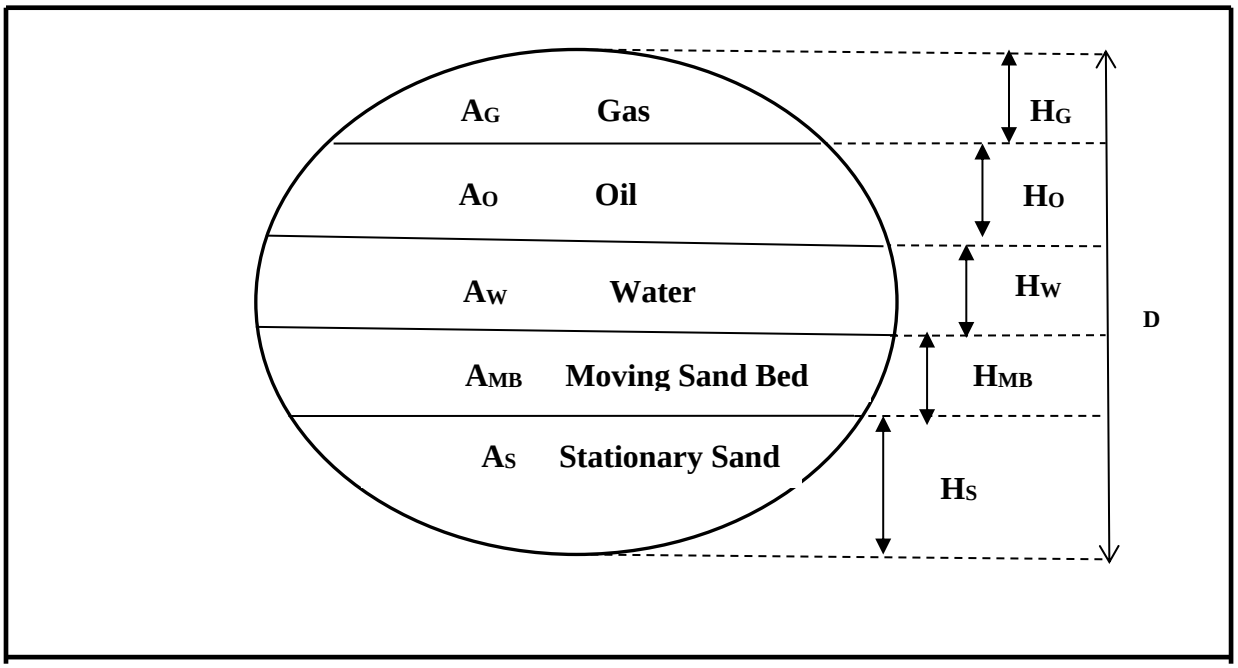

Figure 5.1 Geometrical Illustration of Four-Phase Model.

Water is heavier than oil and flows in the vicinity of the sand bed. If a moving layer of sand bed exists, it will be between the stationary sand bed layer and the water layer. Oil is always on top of the water layer and beneath the gas layer.

H_i represents the height of the layer, and the subscript "i" is one of the following indexes: stationary sand bed or sand phase (S), moving sand bed layer (MB), water layer or water phase (W), oil layer or oil phase (O), gas layer or gas phase (G). Both gas layer and stationary sand bed layer have interfaces with the pipe

wall and with at least one other layer. The middle layers, i.e. moving sand bed, water and oil, each have interfaces with two layers [39].

5.2.1 Mathematical Model Formulation

Since the introduction of the "mathematical" approach by Taitel and Dukler [41] was first used to predict the behaviour of two-phase liquid/gas flow using physical phenomena instead of experimental correlation, their modelling approach has gained considerable attention among researchers.

One of the main advantages of their model is its simplicity. Taitel et al. [41] then used the same approach to develop a model for stratified three-phase liquid/liquid/gas flow. The two-layer model in Doron et al. [38] and the three-layer model developed by Doron and Barnea [38] used the same principles as Taitel and Dukler [42] to simplify the momentum conservation equations for each layer. In this chapter, for the first time, we are proposing a set of formulations using a combination of the Taitel et al. [42] approach towards liquid/liquid/gas and Doron and Barnea's [39] three-layer model for liquid/sand, to model the entire sand/water/oil/gas field, as detailed in Figure 5.1.

Gas bubbles are assumed to be absent inside the oil or water layers, and oil and water are assumed to be fully separated. Hence there is no oil droplet in the water layer and there is no water droplet in the oil layer. It is further assumed that there are no sand particles in the gas phase [43]. Sand particles are considered to be water-wetted and are therefore only transported by the water layer. Also, the entire system is assumed to be isothermal.

5.2.2 Construction of Mathematical Model

In this chapter, we construct a mathematical model by first, theoretically analyzing hydraulic and particle transport features in oil-sand, gas-oil-sand and gas-oil-water-sand multi-phase pipeline flows and then applying some governing equations. The equations, which pertain to distributions of hold-up, flux and mass rate as well as particle velocity, distributions of critical velocity, and optimal transport velocity, all derive from what-phenomenology refers to as a distinct philosophical tradition that implies a specific methodology

of multi-phase flow behaviour in pipelines. Our mathematical model will include balanced equations obtained from laws on momentum conservation and mass, along with factors such as gravitation, buoyancy, drag force, and interaction forces (here, particle-liquid, particle-particle, and particle-pipe wall).

The fourth order Runge-Kutta numerical method will be used to solve the governing equations, with the computational algorithm being implemented as visual basic computer code. Our proposed model offers a guideline for a range of decision-making processes, as it employs optimization strategies to achieve an optimal transport velocity that will inhibit the deposition of sand, sand erosion, and pressure drops. It will also assist in decisions pertaining to downtime and maintenance costs, aiming for overall reductions while retaining peak productivity. As well our proposed mathematical model will be able to discern the best designs among competing options [44].

In constructing our model, we take into consideration existing (gas-oil-water-sand) multi-phase production as well as pipeline transport systems that must function using high-pressure rates.

5.3 Conservation Equations of Four-Phase Flow in Pipeline

Conservation equations for continuity, momentum, and mass use for the turbulent flow of four-phase (gas-oil-water-sand) flow through a horizontal pipeline can be written as follows:

5.3.1 Continuity Equations

The continuity equations for each phase have been developed as per the following:

Solid-phase continuity equation:

$$\frac{\partial}{\partial t}(\rho_S)+\frac{\partial}{\partial x}(\rho_S V_S)=0 \tag{5.1}$$

Water-phase continuity equation:

$$\frac{\partial}{\partial t}(\rho_w)+\frac{\partial}{\partial x}(\rho_w V_w)=0 \tag{5.2}$$

Oil-phase continuity equation:

$$\frac{\partial}{\partial t}(\rho_O)+\frac{\partial}{\partial x}(\rho_O V_O)=0 \tag{5.3}$$

Gas-phase continuity equation:

$$\frac{\partial}{\partial t}(\rho_G) + \frac{\partial}{\partial x}(\rho_G V_G) = 0 \quad (5.4)$$

Equations (5.1 to 5.4) represent the continuity equations for solid/water/oil/gas-phase transport go four-phase flow through a horizontal pipeline.

where the first term indicates accumulated mass in the pipe's interior, and the second term denotes total mass flow in the pipe. In the present work, the final term equals zero, as none of the flow passes through a horizontal pipeline wall and out the other side.

5.3.2 Mass Conservation

The mass conservation equations for each phase have been developed as per the following:

Sand-phase:

$$(U_W\ C_{S.W}\ A_W) + (U_{MB}\ C_{S.MB}\ A_{MB}) = (U_{inlet}\ C_{S.inlet}\ A) \quad (5.5)$$

Water-phase:

$$U_W\ (1 - C_{S.W})\ A_W + U_{M.B}\ (1 - C_{S.MB})\ A_{MB} = (U_{inlet}\ C_{W.inlet}\ A) \quad (5.6)$$

Oil-phase:

$$(U_O\ A_O) + (U_G\ C_{O.G}\ A_G) = (U_{inlet}\ C_{O.inlet}\ A) \quad (5.7)$$

Gas-phase:

$$U_G\ (1 - C_{O.G})\ A_G = (U_{inlet}\ C_{O.inlet}\ A) \quad (5.8)$$

In Equations (5.5) to (5.8), $C_{i.K}$ is the average volumetric concentration of phase i in phase k, e.g., $C_{S.W}$ is sand concentration in the water phase or $C_{O.G}$ is oil droplet volumetric concentration in the gas phase. Index "inlet" refers to the pipe inlet conditions. $C_{S.MB}$ sand particle concentration in the moving bed layer is assumed to be 0.52 for cubic packing [45].

5.3.3 Momentum Conservation

To calculate pressure drops $\frac{dP}{dX}$, the momentum continuity equations are written for all the moving layers. τ_S^k is the shear stress between phases k and I, while τ_i is the shear stress between layer "i" and the pipeline wall.

Gas-phase:

$$(A_G \cdot \frac{dP}{dX}) = -(\tau_G \cdot S_G) - (\tau^{G}_{O} \cdot S^{G}_{O}) \quad (5.9)$$

Oil-phase:

$$(A_O \cdot \frac{dP}{dX}) = -(\tau_O \cdot S_O) - (\tau^{O}_{W} \cdot S^{O}_{W}) + (\tau^{G}_{O} \cdot S^{G}_{O}) \quad (5.10)$$

Water-phase:

$$(A_W \cdot \frac{dP}{dX}) = -(\tau_W \cdot S_W) - (\tau^{W}_{MB} \cdot S^{W}_{MB}) + (\tau^{O}_{W} \cdot S^{O}_{W}) \quad (5.11)$$

The shear stresses between different phases and between the flowing layers and the pipe wall are shown in Figure 5.2.

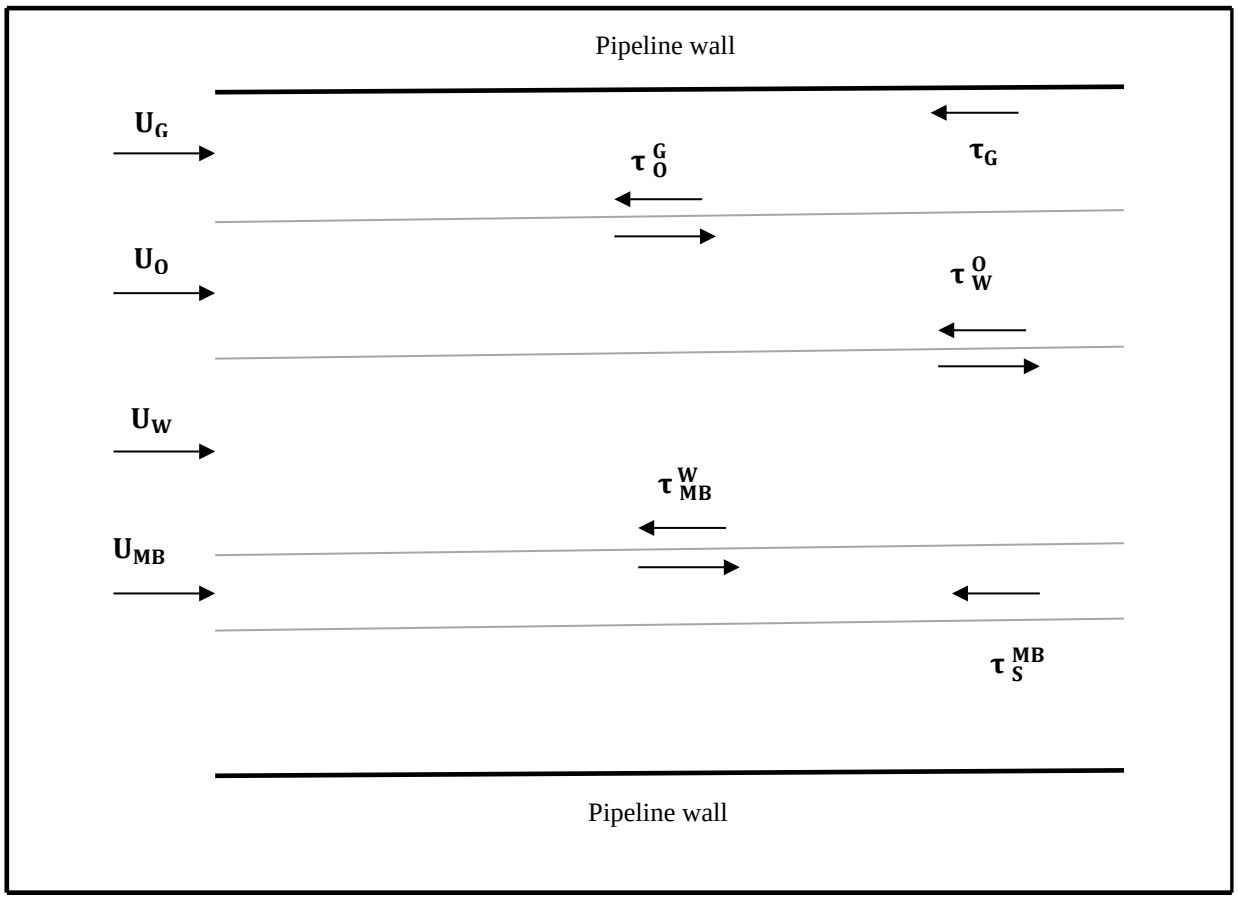

Figure 5.2 Shear Stress Between Moving Phases.

Shear stresses between the gas, oil or water phases and the pipeline wall are:

$$\tau_i = \frac{1}{2} (\rho_i) (f_i) (U_i^2) \tag{5.12}$$

where f_i is the friction coefficient and is calculated using the following:

$$f_i = \begin{cases} 16\, Re_i^{-1} & Re_i \leq 2000 \\ 0.046\, Re_i^{-0.2} & Re_i > 2000 \end{cases} \tag{5.13}$$

The water, gas, and oil Reynolds numbers in Equation (5.13) are:

$$Re_W = 4\ U_W\ A_W\ \frac{[(C_{SW}\rho_S)+(1-C_{SW})\rho_W]}{(S_W \mu_W)} \tag{5.14}$$

$$Re_G = 4\ U_G\ A_G\ \frac{[(C_{OG}\ \rho_O)+(1-C_{OG})\rho_G]}{(S_O+ S_O^G)[(C_{OG}\ \mu_O)+(1-C_{OG})\ \mu_G]} \tag{5.15}$$

$$Re_O = 4\ U_O\ A_O\ \frac{\rho_O}{(S_O \mu_O)} \tag{5.16}$$

Sand particles in the water phase and oil droplets in the gas phase are assumed to be travelling with the same velocity as their carrier phases, i.e., water and gas, respectively. Hence, there will be no shear stress between suspended phases and carrier phases. The effect of the presence of sand particles in the water phase on mixture viscosity has also been neglected. Shear stress between gas and oil layer τ_O^G can be calculated as:

$$\tau_O^G = \frac{1}{2} [(C_{OG}\rho_O) + (1 - C_{OG})\rho_G] (U_G - U_O)|U_G - U_O| f_O^G \tag{5.17}$$

where f_O^G is the largest value between 0.014 and f_G, as calculated by Equation (5.13). The same principle is used to calculate the shear stress between the oil and water layer τ_W^O.

$$\tau_W^O = \frac{1}{2} \rho_O (U_O - U_W)|U_O - U_W| f_W^O \tag{5.18}$$

f_W^O is the largest value between 0.014 and f_O, as calculated by equation (5.13). The shear stress between the water phase and the moving sand bed layer is

$$\tau_{MB}^W = \frac{1}{2} [(C_{SW}\ \rho_S) + (1 - C_{SW})\rho_W] (U_W - U_{MB})|U_W - U_{MB}| f_{MB}^W \tag{5.19}$$

where U_{MB} IS calculated using Equation (5.20) and the friction coefficient from the equation below [36]:

$$\frac{1}{\sqrt{2\, f_{MB}^{W}}} = -\, 0.86 \ln\left[\frac{\left\{ d \Big/ \left(4 \frac{A_W}{S_W + S_{MB}^{W}} \right) \right\}}{3.7} + \frac{2.51}{Re_W \sqrt{2\, f_{MB}^{W}}}\right] \tag{5.20}$$

Re_W in Equation (5.20) is calculated using Equation (5.14), but $\frac{A_W}{S_W}$ in Equation (5.14) will be replaced by $\frac{A_W}{S_W + S_{MB}^{W}}$ to consider the interface perimeter in hydraulic diameter calculation. The momentum continuity equation for the sand moving bed layer has a slightly different form than Equations (5.9) to (5.11), due to the solid friction forces between the moving bed layer and the stationary bed.

$$\left(A_{MB} \cdot \frac{dP}{dX}\right) = -\left(\tau_S^{MB} \cdot S_S^{MB}\right) + \left(\tau_{MB}^{W} \cdot S_{MB}^{W}\right) - \left(\tau_{MB} \cdot S_{MB}\right) - F_{friction} \tag{5.21}$$

$F_{friction}$ in Equation (5.20) is the summation of friction between the moving bed layer and the stationary layer, and the friction between sand particles in the moving bed layer and pipe wall, which is calculated using the formulation of Doron and Barnea [38] and Doron et al. [43]. The shear stress between the moving bed and the stationary bed τ_S^{MB} is

$$\tau_S^{MB} = \frac{1}{2}\left[(C_{S.MB}\, \rho_S) + (1 - C_{S.MB})\rho_W\right] U_{MB}^{2}\, f_S^{MB} \tag{5.22}$$

The friction coefficient in Equation (5.13) is calculated using a formulation similar to Equation (5.20), with the only difference being that the hydraulic diameter and Reynolds number in Equation (5.29) should be replaced by $4\, \frac{A_W}{S_W + S_{MB}^{W}}$ and $4\, U_{MB}\, A_{MB}\, \frac{[(C_{S.MB}\, \rho_S) + (1 - C_{S.MB})\rho_W]}{(S_W + S_{MB}^{W})\, \mu_W}$, respectively. The shear stress between the moving bed layer and the pipe wall is calculated similar to Equations (5.12) and (5.13).

In all the previous mathematical models, including the three-phase model of Taitel et al. [41] and the three-layer model of Doron and Barnea [40], the entire flow is described by a set of nonlinear equations. The total number of these nonlinear equations varies, based on the developed model. For example, the Taitel et al. [41] model is represented by two nonlinear equations, while Doron and Barnea's [40] three-layer model is made up of six nonlinear equations.

In all of these cases, the number of equations can be reduced even further by combining and rearranging the equations. They can then be solved them numerically by estimating one of the variables as a complex and employing an iterative trial and error method to solve other variables [38].

The present four-phase model is described by eight unknowns, which are seven holdups in the form of H_i, pressure drops $\frac{dP}{dX}$. These eight unknowns are represented by the nonlinear Equations (5.14)-(5.20) and (5.21).

The arrangement and dependency of these eight equations are in such a way that none of these unknowns can be identified as a priori. Therefore, the whole set of eight equations must be solved simultaneously. Solving these eight nonlinear equations in the form of a system of equations has its own challenges. The possibility of having multiple roots for these nonlinear equations has been reported by some researchers [40, 45], which means solving this system of equations may not result in a unique set of results.

In order to have physically feasible results, they must satisfy a set of criteria. For example, the summation of all the heights should be equal to the internal pipe diameter, and none of the heights should be negative. It is assumed that the water, oil and gas layers always exist. However, the stationary sand bed may or may not be formed, depending on operating conditions. Sand particles may be all-moving or suspended in the water layer, which would result in a reduction of the number of unknowns and Equations. In this case, equation (5.21) should be modified to remove the friction force between the moving bed and the stationary bed. If the water layer's velocity is greater than the hindered settling sand's velocity, as detailed in Doron et al. [37], then it can be assumed that all the sand particles are fully suspended in the water layer, in which case the moving bed and the stationary bed disappear.

When solving the equations, if it is determined that any or both of the stationary and moving beds are non-existent, then all of the geometrical equations must be modified accordingly.

5.4 Multi-Phase Flow in a Horizontal Pipeline

Emerging from reservoir productions, sand particles are introduced into multi-phase pipelines, since sand particles can affect the integrity of the structure of pipeline when flow assurance problems such as erosion, corrosion, pressure build-up, and critical flow patterns occur in oil and gas lines. It is important to control transportation or production, with the main concern being the deposition of sand particles at the bottom of the pipe, which depends on the minimum critical velocity of the continuous flow, the sand volume fraction, and the flow regimes. Although sand management is important for optimizing the performance and operation of the multi-phase pipelines, only a few experimental investigations have been carried out thus far and insufficient analytical methods to predict the effect of sand particles. Al-lababidi et al. (2012) conducted experiments on the transportation of sand to analyze deposition characteristics in horizontal and inclined pipelines [10].

Six different sand concentrations were used in tests, with a sand particle of approximately 0.2 mm in diameter flowing in a pipe with an inner diameter of 0.05 m. It was observed that the sand minimum transport condition (MTC) in horizontal and +5 deg inclined pipelines were similar in water flow tests. For air-water experiments, while the MTC in the horizontal pipe occur in stratified wavy and hydrodynamic slug flow patterns, the MTC in the inclined pipe habited a terrain slug flow regime. This latter flow pattern is more likely to occur in hilly pipes, and the deposition of sand is prevented due to the turbulent motion of continuous fluid flow. All of the previous criteria should be considered when designing a pipeline to avoid flow assurance issues that can cause a decrease in oil production or failure of the pipeline [10].

In the design of oil-gas-sand multi-phase flow pipelines, sand holdup is one of the important conditions that can affect the mass flux, pressure drops, and even flow regime. Most of these parameters are influenced by liquid and solid characteristics such as sand particle weight, gas superficial velocity, and liquid superficial velocity. Bello, Reinicke and Teodoriu studied the effect of sand-loading and the of phases velocity by performing an experimental work that measured the local sand holdup in an air-water-sand three-phase slug flow. Static and dynamic pressure distributions were also measured using a particle size diameter of

approximately 0.6 mm.

According to the results of three-phase slug flow in the pipeline, the axial distribution (from the bottom to the top of the pipe) of the sand holdup showed a non-linear behavior with its highest values at the walls and a peak at the center for gas superficial velocities of 0.505 m/s and 0.606 m/s. Further, the sand particle distribution depended on the collision of gas bubbles and sand particles and the vortex motion of the slug. As expected, the sand holdup decreased with increasing superficial gas velocity [11].

For the remaining contents, the percentages of water and sediments were limited to 0.5 percent in crude oil transmission pipelines with deposits of sand particles and oil. However, these sediments can contribute to a corrosive environment when water volume fraction exceeds 10% [12].

5.4.1 Flow-Induced Turbulence

Turbulence flow is usually generated by high flow rates or the presence of flow discontinuities such as bends or tees. The flow at the center of the pipe usually has high kinetic energy in the form of large eddies, and it dissipates into the turbulent boundary layer of the pipe in the form of small eddies with heat and potential energy (Figure 5.3). This energy is then transferred to the wall in the form of pressure. In the turbulent zone, a broadband excitation of the kinetic energy occurs, but with low frequency.

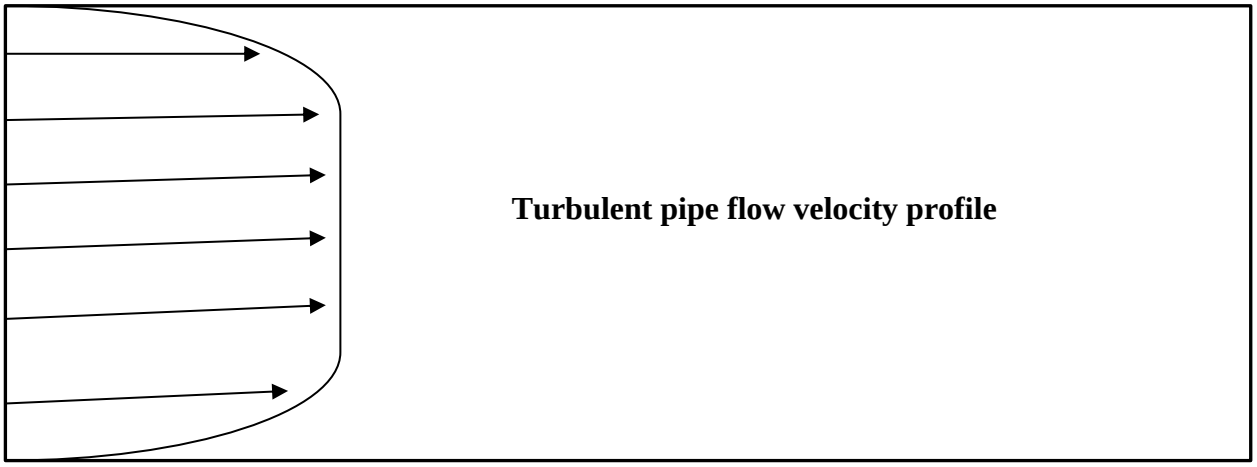

Figure 5.3 Turbulence Eddies in a Horizontal Pipeline (Source: www.isa.org).

Resolving the small scales of the turbulence becomes important when the viscosity has a significant effect. The dissipation rate ϵ of the kinetic energy and the viscosity υ are the two factors that determine the scales at which the energy is dissipated. Kolmogorov developed a relationship to relate these two variables to the smallest scale in turbulent flows:

$$\eta = (\frac{\upsilon}{\epsilon})^{1/4} \tag{5.23}$$

This is called the Kolmogorov length scale. Kolmogorov also found a relationship with the largest length scales, as follows:

$$\eta = (\frac{\upsilon^2 L}{U^3})^{1/4} \tag{5.24}$$

where U is the kinetic energy of the flow. A specific turbulence model was used to resolve the scales in the free stream and near the wall, where the sub-viscosity boundary layer is located. Although it is expected that the effect of flow-induced turbulence is much less than the effect of multi-phase flow, the methodology of this study considers both phenomena to prevent any high risk in the likelihood of failure.

5.5 Methodology of Multi-Phase Flow Through Horizontal Pipelines

There is no standard procedure or methodology for analyzing multi-phase flow through short sections of horizontal pipelines that have multiple bends and jumpers. Instead, such analysis is usually based on very conservative guidelines for fluid-induced fatigue in onshore piping. The challenge is to create a methodology that engineers can follow to identify the risk of failure according to preliminary flow analysis and then perform a more detailed assessment that tells if the flow conditions need to be modified. This latter approach is preferred due to its accuracy, but it usually requires a long computation time, even with the availability of good computational resources. Computational Fluid Dynamics (CFD) diagrams of multi-phase flow through short sections of a horizontal pipeline are presented in Figure 5.4.

5.5.1 Computational Fluid Dynamics (CFD) Model

As the solutions to a multi-phase flow can highly complex and comprehensive, CFD is implemented as a numerical method to simulate realistic flow conditions and achieve accurate results. ANSYS fluent version

16.2 is used to do the simulation, while the Eulerian approach using the Reynolds Stress Model (RSM) turbulence closure is adopted to analyze multi-phase fluid flow.

CFD has the advantage of capturing multiple flow outputs in the same analysis for a better understanding. It can also reduce costs and overcome limitations that are typical of experimental tests, particularly with regard equipment and set-up. In general, CFD tools, follow a workflow to perform flow simulations. A sample workflow is given blow:

- Create model and import the geometry.
- Specify the boundary conditions (i.e., type of boundary: velocity inlet, or pressure outlet).
- Select the appropriate meshing models and mesh size.
- Select the physics of the model (turbulent model, flow regime, multi-phase or single-phase, steady, or unsteady).
- Specify the time step and physical time of the simulation.
- Create reports and plots to monitor the solution and then run the solution.
- Analyze the results.

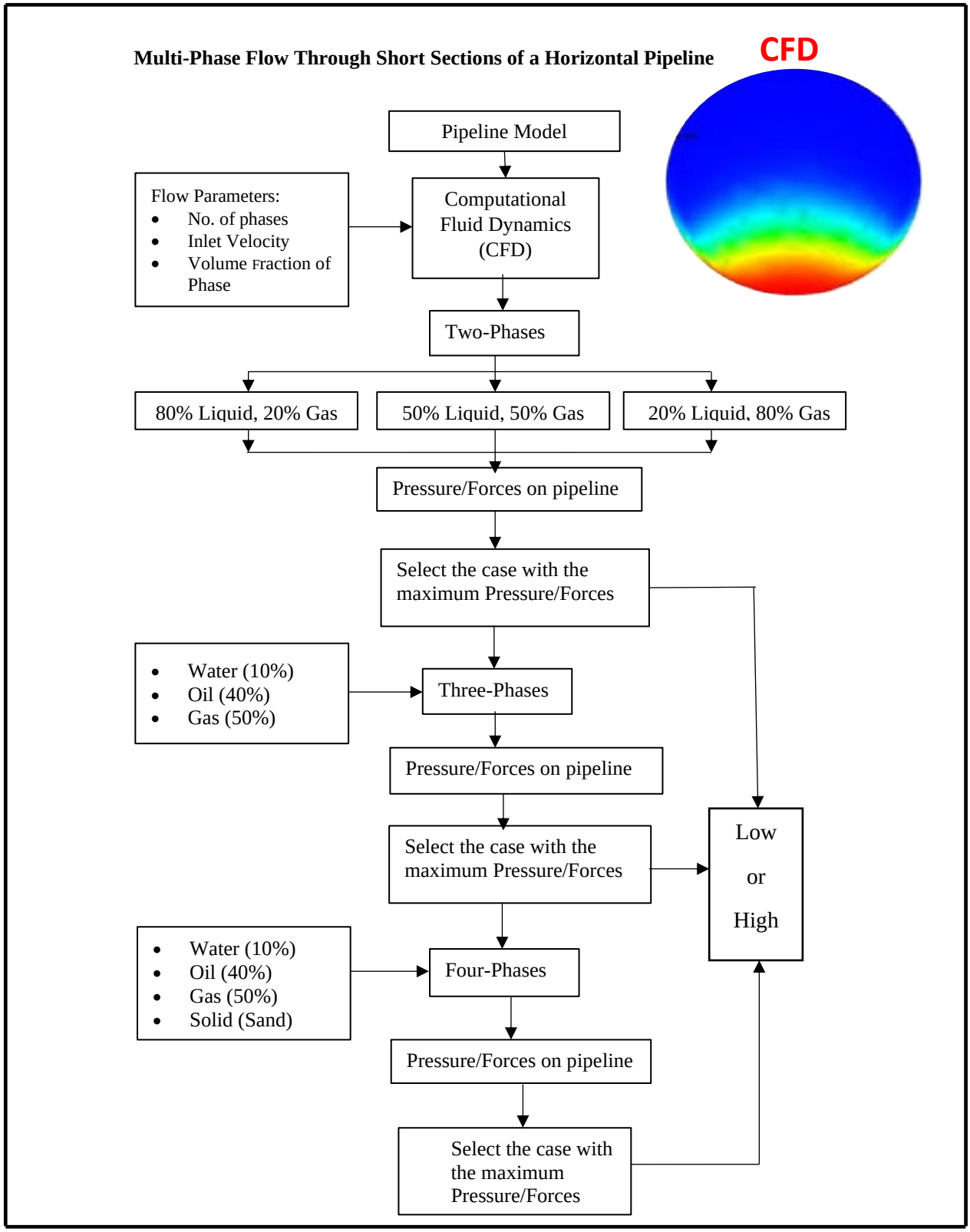

Figure 5.4 Computational Fluid Dynamics (CFD) Diagrams of Multi-Phase Flow Through Short Sections of a Horizontal Pipeline.

5.5.1.1 Fluid Domain

A U-shaped horizontal pipeline was modeled. For the boundary conditions, the left end is defined as the velocity inlet while, the right end is set as the pressure outlet.

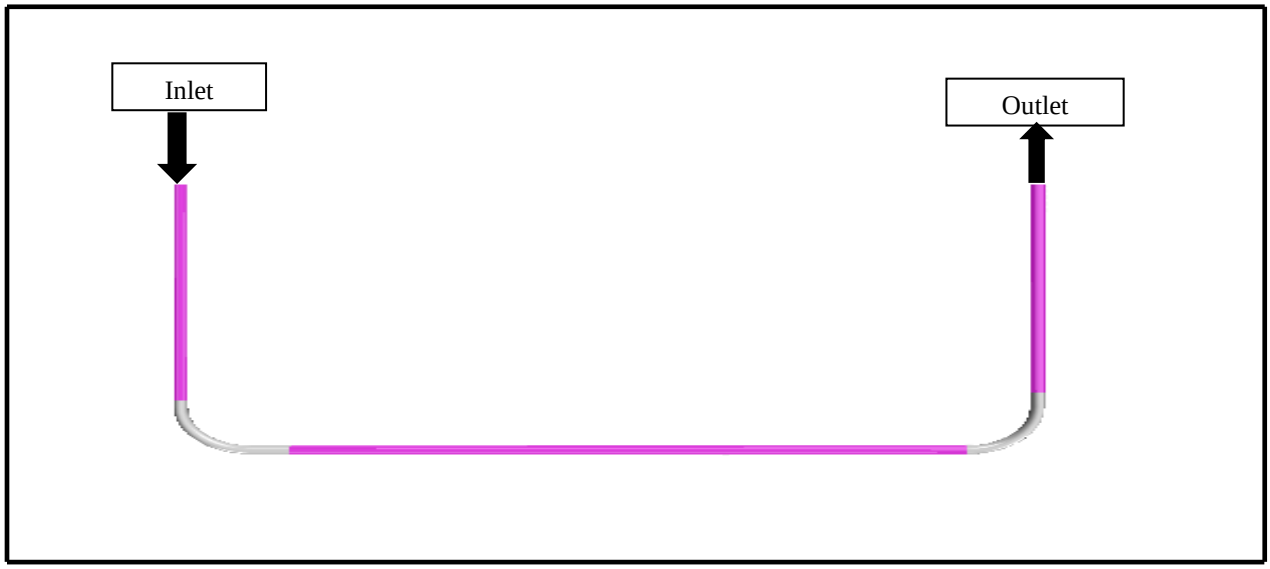

Figure 5.5 Fluid Domain Partition for Short Sections of a Horizontal Pipeline with Bends Model.

5.5.1.2 Turbulence Model

Turbulence models are available to solve unclosed systems with mean flow equations. Of the three turbulent methods available, the Reynolds-Averaged Navier-Stokes (RANS) is the most efficient due to its balance between simulation time and accuracy. RANS solves the Navier-Stokes (NS) Equations into its time-averaged ($\bar{u}i$) and fluctuating term (ui'). Therefore, the instantaneous velocity can be expressed as:

$$ui = \bar{u}i + ui' \tag{5.25}$$

This model solves two extra transport equations with the variables k and ω defined independently in a simple form, as follows:

Turbulent Kinetic Energy $$k = \frac{3}{2}(Iv) \tag{5.26}$$

Specific turbulent dissipation rate $$\omega = \frac{\sqrt{K}}{L.\beta^{\frac{1}{4}}} \tag{5.27}$$

where ν is the local velocity magnitude, I is the turbulence intensity, L is the turbulent length scale, and β is the coefficient of the model. Those parameters are usually defined at the recommended default values in the CFD tool.

5.5.1.3 Volume of Fluid (VOF)

This is a multi-phase model that simulates the interaction between two or more phases. It solves the interface between phases using numerical grids that track the volume fraction of each phase at each small volume. VOF is an Eulerian method in which the grid is fixed while the flow material passes through the mesh.

5.5.1.4 Lagrangian Multi-Phase

Multi-Phase flows with solid particles are modeled and solved using Lagrangian method. A Lagrangian phase is a dispersed phase modeled in a Lagrangian framework, such as sand particles. This approach allows selection of phase models and the setting of phase boundary conditions.

The Lagrangian method is suitable for very small particle sizes and is also more appropriate when the aim is to prevent long computational times.

5.5.1.5 Implicit Integration and Time Step

Solving complex problems requires selecting an appropriate numerical method that considers how accurate and stable the solution needs to be. A time step sensitivity analysis was performed to estimate the appropriate time step based on the Courant number (CFL). This is used as an estimate of the time step depending on the mesh size and average velocity, as follows:

$$\Delta t = \frac{CFL \cdot \Delta x}{u} \tag{5.28}$$

The purpose is to converge the solution at a faster rate. CFL is recommended to be no more than 1. Therefore, a balance between the mesh size and the time step must be achieved. The recommended time step based on this criterion is 0.005 seconds.

5.5.1.6 Meshing

There are two types of mesh that can be assigned to solve the multi-phase flow: Eulerian mesh and

Lagrangian mesh. Eulerian mesh has a fixed grid with the flow moving through the mesh. This type of mesh is the most common for single flow or multi-phase mixture flows. Lagrangian mesh deforms or moves with the flow.

In our experiments, the mesh was modified to have a better control on the number of cells along the length of the horizontal pipeline and the proximity to the wall. A directed mesh was applied at the inlet of the jumper and bends and then the surface mesh was extruded along the length of the jumper and bends similar to the process of the generalized mesher. Mesh-independent results could be produced for node-counts exceeding 150,000.

As shown in Figure 5.6 (a), the pressure drops are almost constant with increases in the number of nodes to above a certain value (here, 150,000). The simulation of numerous others similar data points showed that the minimum number of nodes required to ensure mesh independency for pipelines was 140,000. Inflations near all the walls were added for to obtain precise solutions for different parameters.

Table 5.1 presents some of the mesh parameters and their reference values for the CFD simulations.

Table 5.1 Meshing Parameters for CFD Model

Mesh Parameters Value	**Mesh Parameters Value**
Base size (mm)	14
Number of prism layers	4
Prism Layer Stretching	1.25
Prism Layer Thickness (mm)	7.5

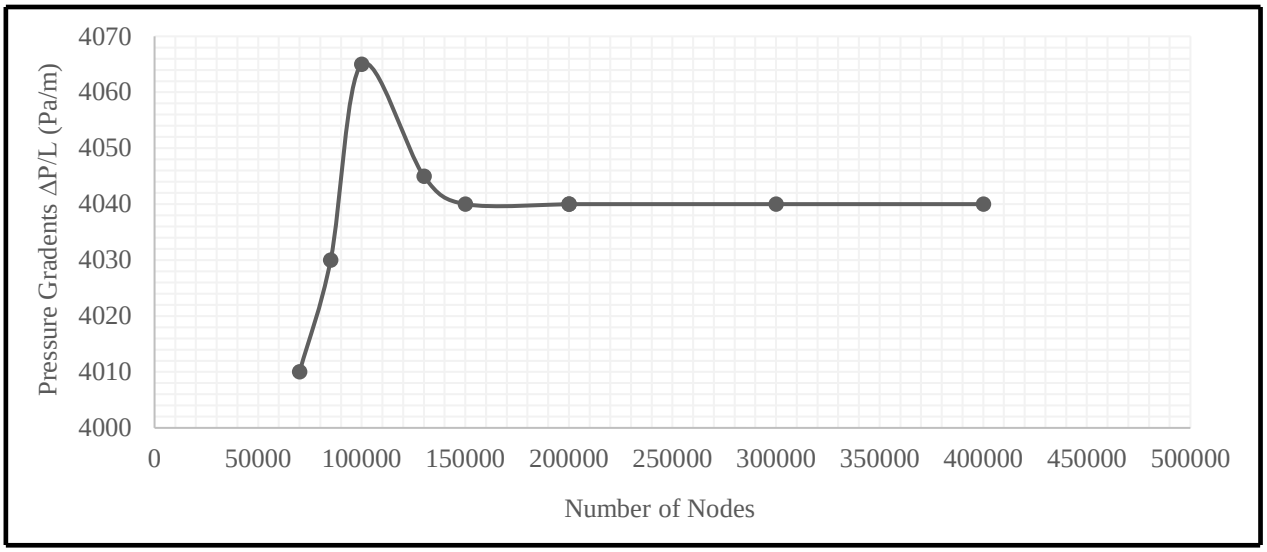

(a)

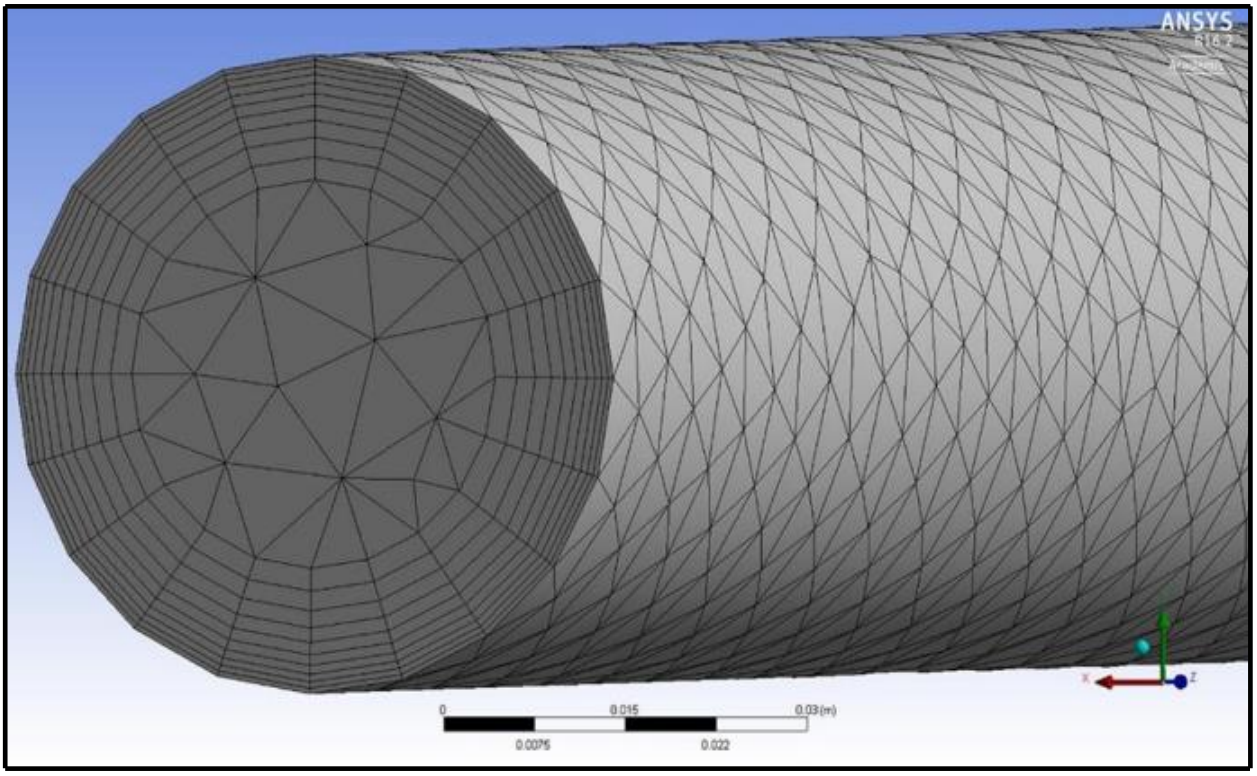

(b)

Figure 5.6 Demonstration of Mesh Distributions in Horizontal Pipeline Geometry (Number of Nodes: 150,000; Wall Inflation Layers:10).

5.5.1.7 Boundary Conditions

For the flow in a pipe, the following boundary conditions are specified:

- Velocity Inlet: An initial velocity is provided at the entrance of the pipe.
- Pressure outlet: A static pressure is specified at the exit of the pipe.
- Wall: The inner surface of the pipe is treated as a no-slip smooth wall.

5.5.1.8 CFD Physics Models

The physics models selected for solving the multi-phase flow are:

- Three dimensional.
- Implicit Unsteady: Iterative time-dependent analysis.
- Multi-phase Mixture: Composed of oil, gas, and water.
- Eulerian Multi-phase.
- Volume of Fluid (VOF).
- Segregated Flow: The momentum and continuity equations are solved in an uncoupled manner.
- Lagrangian Multi-phase: This option is enabled if solid particles are modeled.
- Turbulence flow through pipeline can be modelled with this CFD methodology.
- Gravity.

5.6 Computational Fluid Dynamics Results

As specified in the methodology of multi-phase flow through short sections of horizontal pipelines, a modal analysis is performed as a first step to extract the natural frequencies. After that, CFD cases are described and explained in general for each configuration in terms of the volume fraction. The time and frequency domains of pressure and volume fraction of oil were obtained as a form of screening to assess the risk of failure.

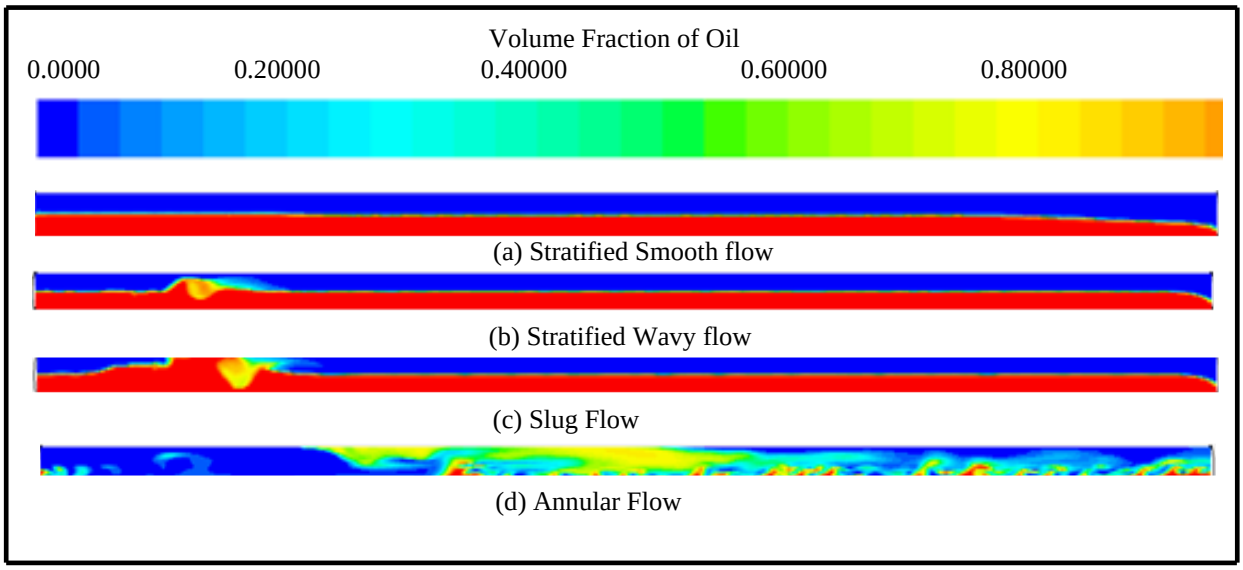

Figure 5.7 Volume Fraction of Oil for a Horizontal Pipeline:

(a) Stratified Smooth (b) Stratified Wavy
(c) Slug Flow (d) Annular Flow.

5.6.1 Two-Phase (Oil-Gas) Flow Through a Horizontal Pipeline

For the two-phase flow, oil and gas were initialized as a stratified flow. The simulation of this multi-phase flow was allowed to run until the flow reached the outlet of the pipe. The volume fraction of the phases and superficial velocity are the two parameters analyzed in this work, since they are expected to have a significant effect on the flow and the structure of pipelines. As initial conditions, it was assumed that the pipeline was filled with gas. Table 5.2 presents details modeling and analysis of oil-gas flow in a U-shaped pipeline.

Table 5.2 CFD Simulation Cases for Two-Phase Flow Through a Horizontal Pipeline

Case	Inlet Velocity (m/s)	Volume Fraction of Oil	Volume Fraction of Gas
1	1	0.2	0.8
2		0.5	0.5
3		0.8	0.2
4	2	0.2	0.8
5		0.5	0.5
6		0.8	0.2

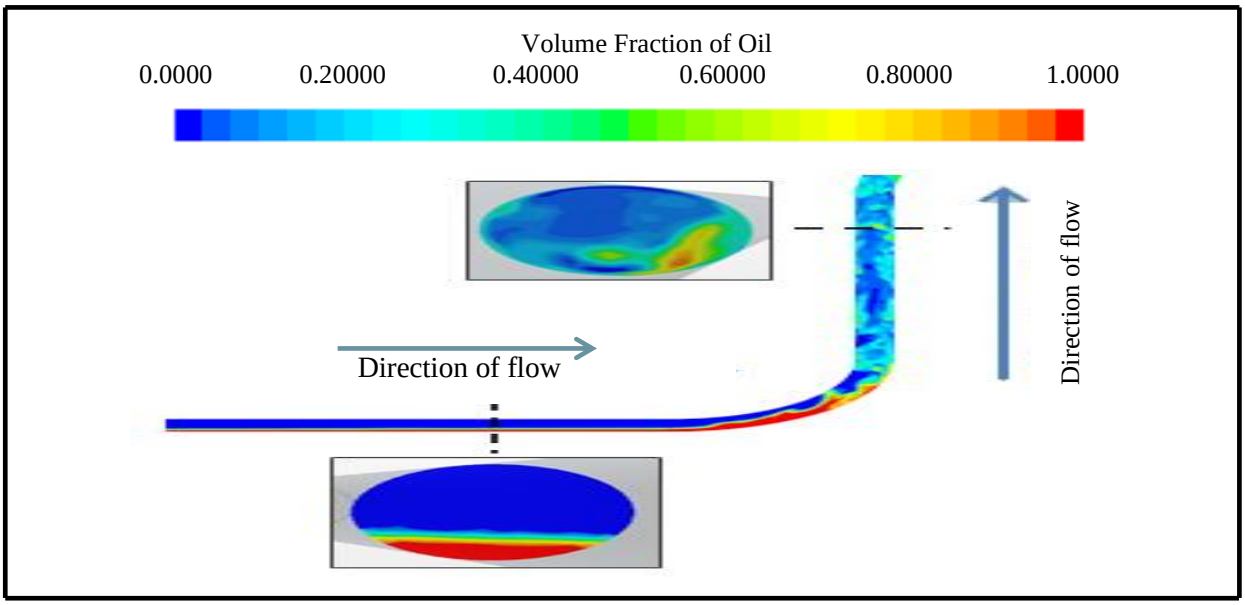

Figure 5.8 Contour of Volume Fraction of Oil for a Two-Phase (20% Oil-80% Gas) Flow (Case 1) in the Short Sections of a Horizontal Pipeline with Bends.

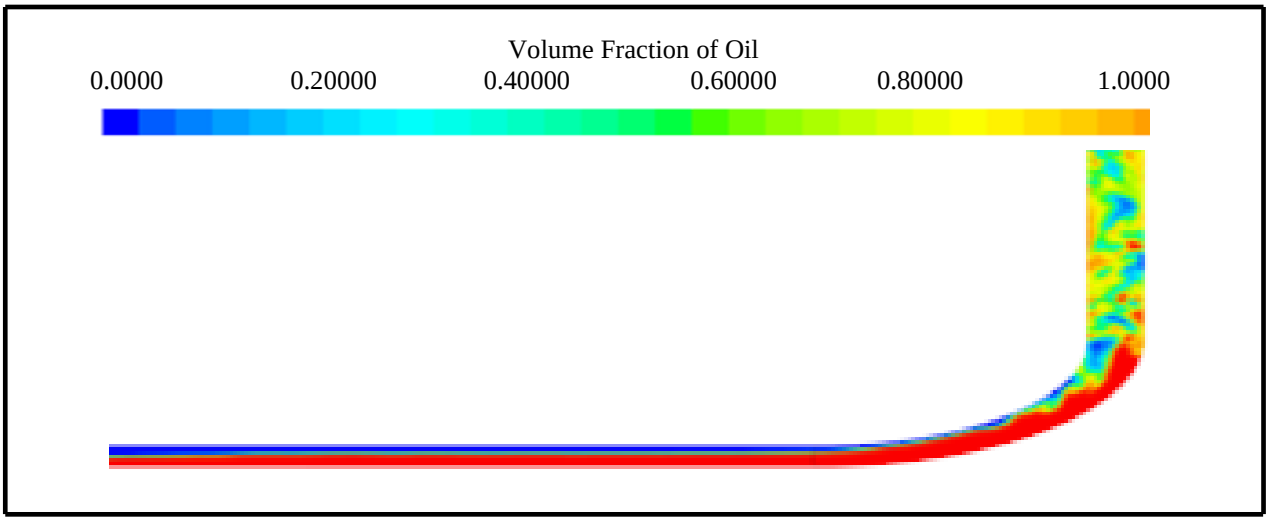

Figure 5.9 Contour of Volume Fraction of Oil for a Two-Phase (50% oil-50% Gas) Flow (Case 2) in the Short Sections of a Horizontal Pipeline with Bends.

5.6.2 Three-Phase (Gas-Oil-Water) Flow Through a Horizontal Pipeline

Adding a third phase to the flow in the short sections of horizontal pipeline with bends might produce significantly different results.

Case 7 and case 8 were considered to analyze three-phase (gas-oil-water) flow, as follows:

Case 7: 50% gas, 40% oil, 10% water, inlet velocity = 1 m/s

Case 8: 50% gas, 40% oil, 10% water, inlet velocity = 2 m/s

Table 5.3 CFD Simulation Cases for Three-Phase (Gas-Oil-Water) Flow Through a Horizontal Pipeline

Case	Inlet Velocity (m/s)	Volume Fraction of Gas	Volume Fraction of Oil	Volume Fraction of Water
7	1	0.5	0.4	0.1
8	2	0.5	0.4	0.1

Similar to the two-phase flow, the oil-gas-water three-phase flow is initialized at the inlet as a stratified flow with water at the bottom and oil and gas at the top, as shown in Figure 5.10. The flow patterns for the three-phase flow are very similar to those for the two-phase flow, with the difference being that the liquid is a mixture of oil and water. As the flow approaches the first bend, the oil is squeezed by the accumulated water.

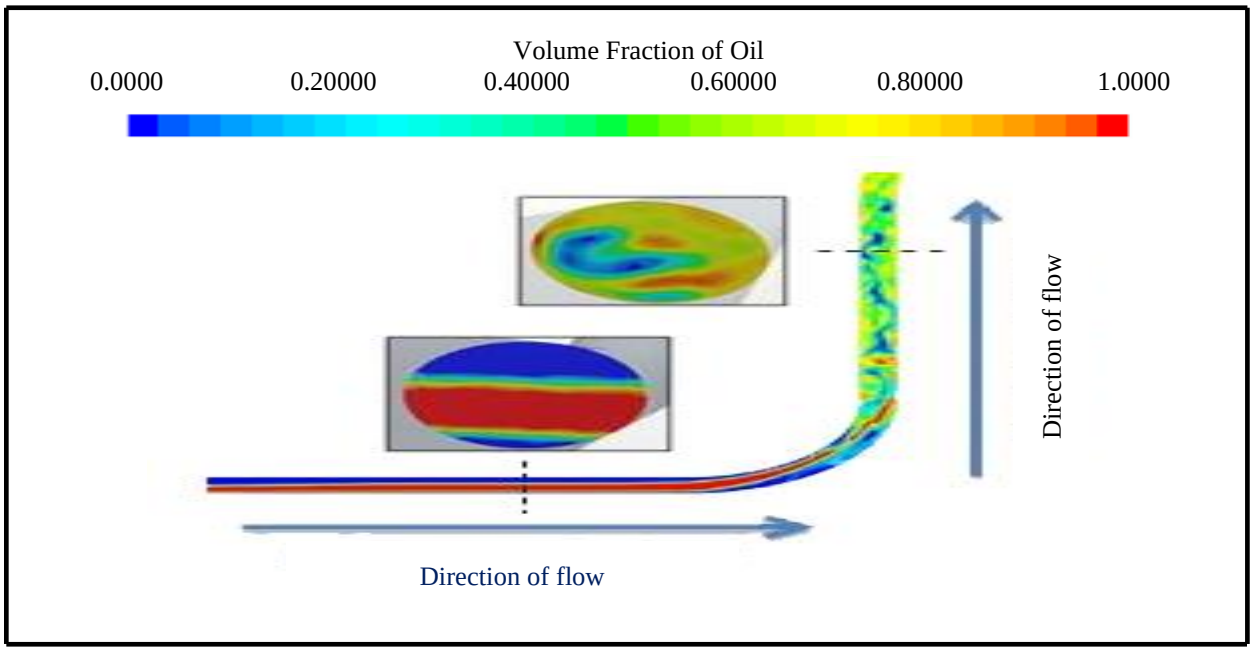

Figure 5.10 Contour of Volume Fraction of Oil for Three-Phase (Gas-Oil-Water) Flow in Short Sections of a Horizontal Pipeline with Bends for Case 7.

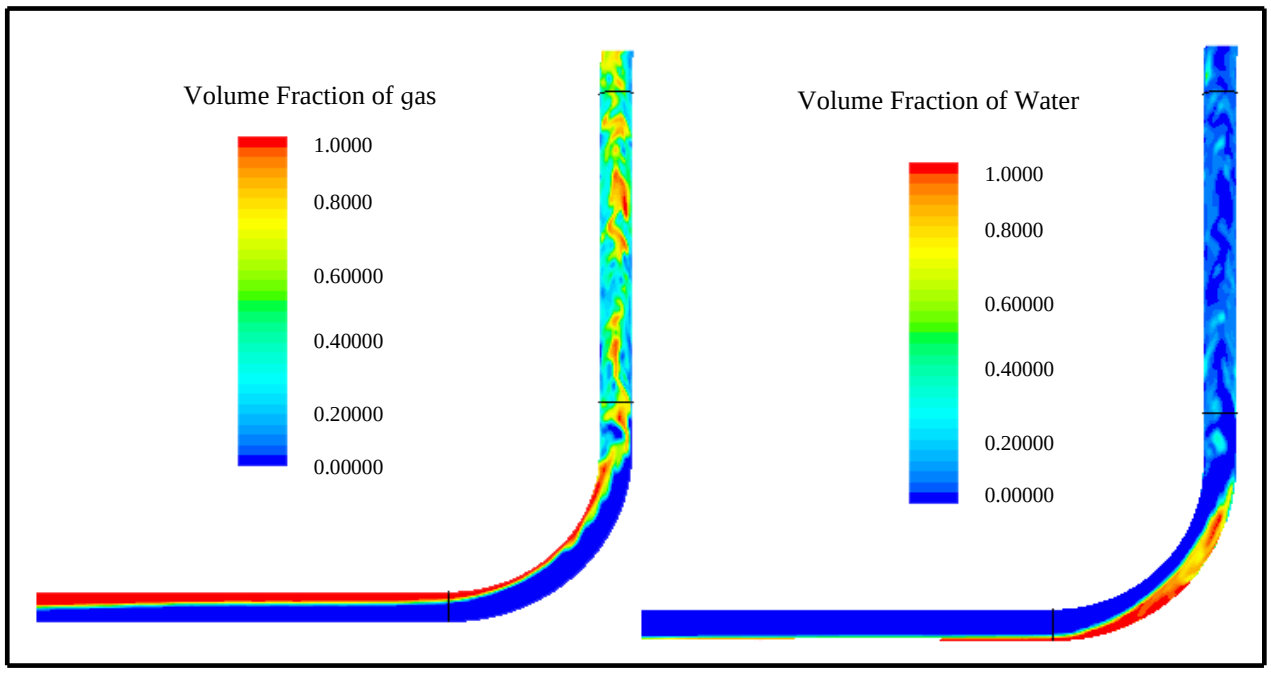

a) b)

Figure 5.11 Contour of Volume Fraction of a) Gas and b) Water for Three-Phase (Oil-Gas-Water) Flow in Short Sections of a Horizontal Pipeline with Bends for Case 7.

5.6.3 Four-Phase (Gas-Oil-Water with Sand Production) Flow Through a Horizontal Pipeline

For the same horizontal pipeline model, sand particles were simulated to flow from a distributed grid at the inlet, as shown in Figure 5.11. The purpose of this analysis is to assess the effect of having sand particles in the pipe and to identify if a four-phases flow can be modeled and treated as a three-phase flow or a two-phase flow. The locations where the deposition of particles or blockage of the pipe occurs will be analyzed based on the velocity and pressure. Table 5.4 presents the cases that were studied.

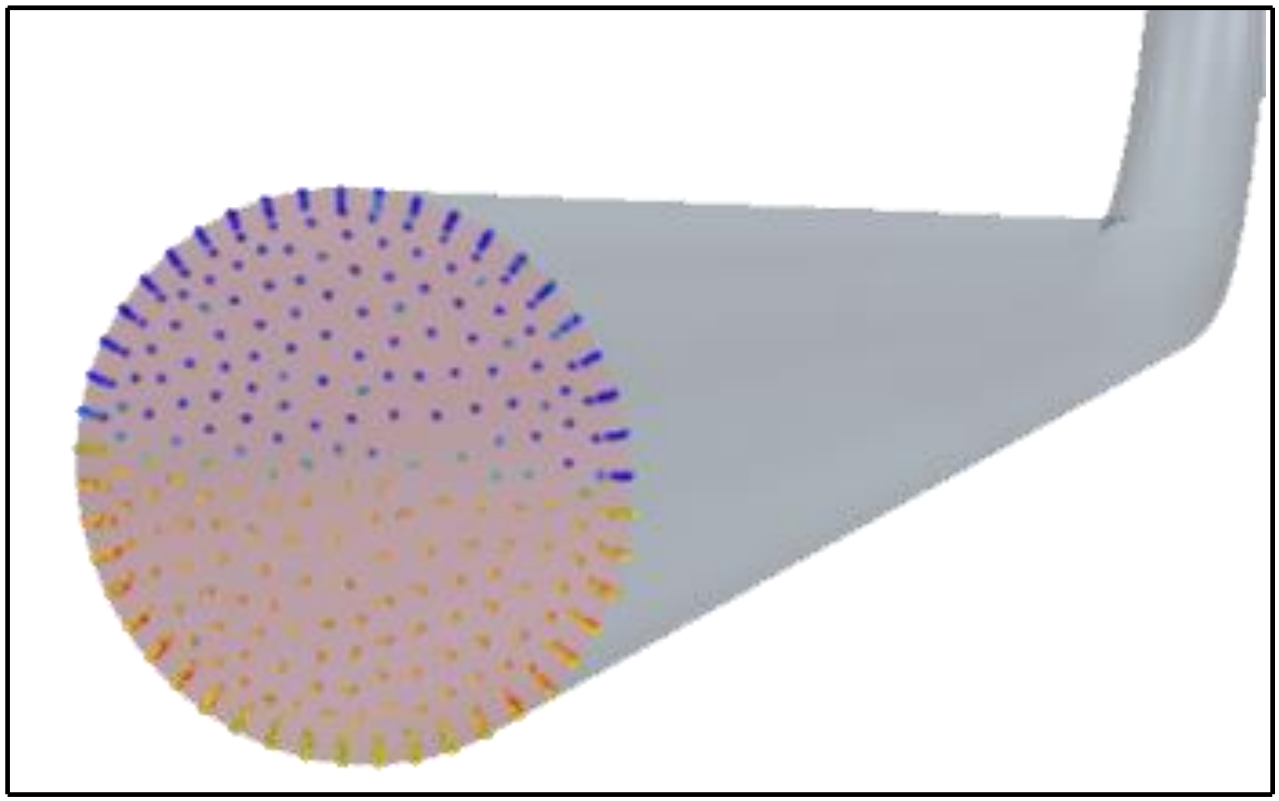

Figure 5.12 Contour of Sand Particles Traveling Along Short Sections of a Horizontal Pipeline with Bends.

Table 5.4 CFD Simulation Cases for Four-Phase (Gas-Oil-Water-Sand) Flow Through a Horizontal Pipeline

Case	Inlet Velocity (m/s)	Volume Fraction of Gas	Volume Fraction of Oil	Volume Fraction of Water	Sand Particles per second
9	1	0.50	0.40	0.10	150
10	2	0.50	0.40	0.10	300

5.6.4 Volume Fraction, Velocity, and Tracking of Sand Particles

It was assumed that as their initial condition, the particles were stationary. Hence, the motion of these solids was generated due to the drag from the continuous oil-gas-water-sand flow. The presence of sand might modify the flow patterns, in particular the short sections of horizontal pipelines with bends, as it is in these locations where solids might accumulate in significant amounts because of the flow's decreasing velocity, as shown in Figure 5.13. The main flow patterns that were developed with four-phases dominate the flow. At the short of sections of the horizontal pipeline with jumpers and bends, the flow is stratified and flow drags the particles along the pipe, with some of them being suspended due to wall-induced friction.

Large fractions of sand and low inlet velocity might induce particles to start accumulating in the bends and Jumpers due to the friction. If this occurs, sand will be deposited at the bottom of the pipeline and the pressure will build up due to the blockage. If build-up occurs, the cross-sectional area for the continuous flow will be reduced, leading to an increase in the velocity. Some of the sand particles will then be flushed forward due to the flow drag.

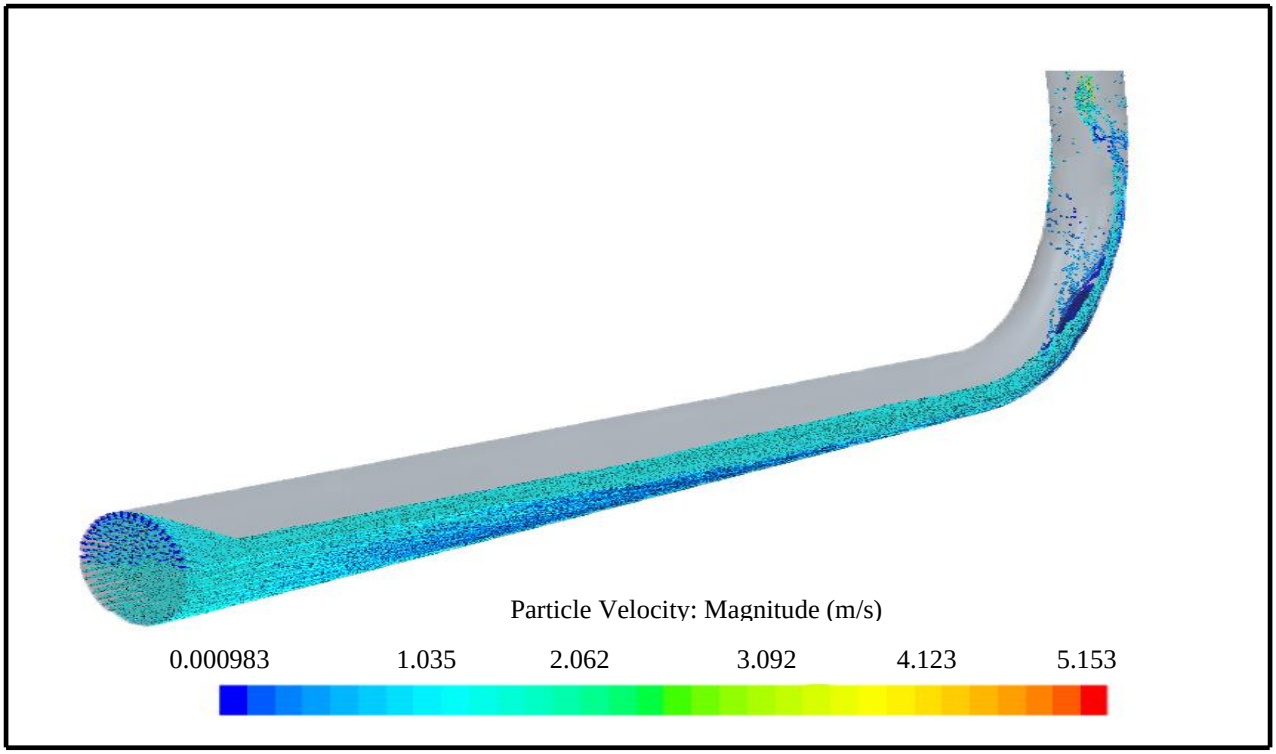

Figure 5.13 Initial Accumulation of Sand Particles at Short Sections of a Horizontal Pipeline with Bends.

5.7 Summary of Computational Fluid Dynamics Results

Table 5.5 Results Summary for Different Multi-Phase Flow Configurations of Gas-Oil-Water with Sand Particles Through a Horizontal Pipeline.

Parameter	**Two-Phases**	**Three-Phases**	**Four-Phases**
	Horizontal Pipeline		
Volume Fraction (Flow Patterns)	Stratified or Wavy Flow	Stratified or Wavy Flow	Stratified or Wavy Flow
Pressure or Forces	Low	High	Significant but not as high as three-phase flow
Pressure vs. Volume Fraction of Oil	Pressure increases as the volume fraction of oil increases	Not Applicable	Not Applicable
Force vs. Velocity	Force increases with an increase in inlet velocity	Force increases with an increase in inlet velocity	Not Applicable

A flow pattern map was calculated based on the Taitel and Duckler theoretical model and according to Equations:

$$\upsilon_{SG} = \frac{Q_G}{A} \tag{5.29}$$

$$\upsilon_{SL} = \frac{Q_L}{A} \tag{5.30}$$

where υ_{SG} (m/s) and υ_{SL} (m/s) are the superficial velocity of the gas and liquid, respectively, Q_G and Q_L are the volumetric flow rate of the gas and liquid in cubic meters per second, respectively, and A is the area of cross section in meters sq.

Table 5.6 Comparison Between Theoretical Solution by Taitel and Duckler and CFD Numerical Results.

No	υ_{SG} **(m/s)**	υ_{SL} **(m/s)**	**Flow Patterns**	
			Taitel and Duckler	**CFD**
1	0.1	0.05	Stratified smooth	Stratified smooth
2	5.0	0.15	Stratified wavy	Stratified wavy
3	1.5	1.0	Slug flow	Slug flow
4	10	0.1	Annular flow	Annular flow

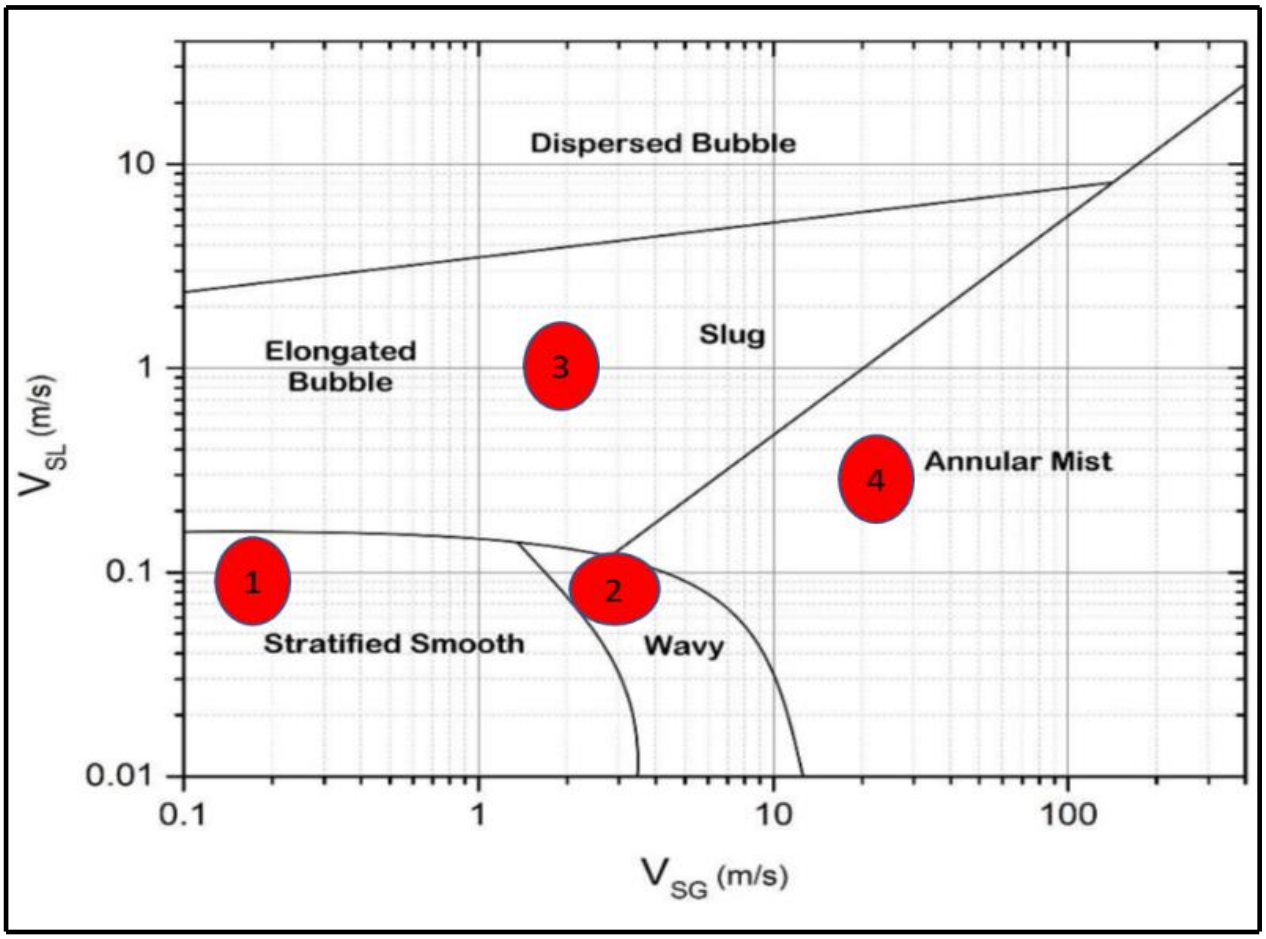

Figure 5.14 Flow Pattern Map of Liquid and Gas in a Horizontal Pipeline [30].

Figure 5.14 indicates the different flow patterns developed depending on the superficial velocity of the gas (υ_{SG}) and superficial velocity of the liquid (υ_{SL}). The red dots represent the selected points to benchmark the flow regimes in short sections of horizontal pipelines.

A numerical model was used to validate the flow patterns identified on the map. Table 5.3 presents flow patterns with corresponding superficial velocity points taken from the map and analyzed using CFD simulations.

As shown in the contour of the numerical analysis in Figure 5.7, the results have a good agreement according to the theoretical flow pattern map of Taitel and Duckler. It is expected to have a smooth stratified flow at very

low flow rates (see Figure 5.7 (a)). As the velocity of the gas starts increasing, a disruption between the liquid and gas phases occurs such that waves are developed on the surface (see Figure 5.7 (b)). Similarly, a blockage of the pipe happens at the beginning of the pipeline, which represents the condition where a slug was developed as illustrated in Figure 5.7 (c). If the velocity of the gas keeps increasing such that the ratio of the velocity of the gas to the velocity of the liquid is very large, annular flow can develop as illustrated in Figure 5.7 (d).

In general, there is a good agreement between the theoretical solution by Taitel and Duckler and the numerical results.

5.8 Conclusions and Recommendations

This section presented the results obtained from a multi-phase flow model applied through short sections of a horizontal pipeline with multiple bends and jumpers. As shown, it is recommended to perform CFD simulations and analysis for the entire jumper by coupling the stress solver with the fluid solver so that maximum principal stresses and displacements are obtained. The U-shaped horizontal pipeline can then be specified based on the environmental conditions and material of the steel pipe to finally determine the fatigue life of the jumper.

It is also recommended to model and analyze the three-phase flow in a jumper independently of a two-phase flow, since both generate a different response on the structure of pipelines. Further, given the actual results of the screening methodology, it is suggested to modify the flow rate of the production fluid to prevent the fluid frequency from falling within 10% of the natural frequencies.

There is, as yet limited research and work on four-phase flow through horizontal pipelines. A small-scale prototype of the jumper could manufactured to validate and compare the numerical results for the two/three/four-phase flow configurations.

Additionally, there are several different parameters that can be studied with regard to fluid and geometry. It is therefore, recommended that experiments be performed to identify the parameters or interactions of parameters that have an impact on the life of the pipe. As well, CFD simulations are recommended to study the effect of varying the following:

- the volume fraction of each phase within the three-phase flow.
- the particle diameter for gas-oil-water flow with sand particles.
- the initial velocity of the gas-oil-water flow with sand production using the same particle flow rate and volume fraction of the phases.
- Moreover, the test results showed good agreement between the numerical results and the theoretical flow pattern map of liquid and gas in of Taitel and Ducker's horizontal pipeline, as shown in the contour of the numerical analysis in Figure 5.7 and Figure 5.14.

Finally, it is worth noting that the internal flow dose not appear to be the only source of pressure gradient. External flow caused by the current or waves can induce a significant pressure drop on the pipeline phenomenon that is known as Induced pressure fluctuation and pipe blockage. This phenomenon could be considered for future work to simulate a more realistic interaction scenario.

Chapter 6

Summary, Conclusions and Recommendations

6.1 Summary

The present work applied four-phase flow techniques in unison to investigate of particle behaviors of simulated four-phase (sand, water, gas and oil) flow through short sections of a horizontal pipelines with multiple bends and jumpers.

The behaviors were observed in an experimental study as well as through computational fluid dynamics (CFD) simulations. As well, this research examined a four-phase (sand, water, gas and oil) flow problem that occurred in a complex horizontal pipeline and considered experimental and numerical approaches to study the problem in the context of the O&G industry.

In general, the experimental investigation of multi-phase fluid flow, is limited by the availability of experimental techniques and apparatuses. The present work utilized existing apparatuses to conduct experimental procedures as well as CFD simulations in order to extend the experimental results. Establishing a pathway to address some of the challenges of multi-phase flows is at the core of the overall contribution of this thesis.

The novel aspects of the study have been published in seven articles in the proceedings of seven international conferences.

6.2 Conclusions

A four-phase four-fluid pipeline unsteady-state model was developed in this work to study four-phase flows (CO_2, oil, water, sand) used in O&G industry pipelines. The experiments applied and validated the proposed model, with the main pipeline flow properties summarized as follows:

- In each experiment of four-phase (CO_2, oil, water, sand) flow, intervals were used to modify the gas, water, and oil flow rates and solid concentrations from the minimum to the maximum. To detect data trends, the pressure drops were plotted over the flow rates and pipeline distance. It was concluded that the empirical results are reliable, because the validation of the experimental results provided good predictions and a reasonable approximation.
- The results including pressure drops and temperature distribution, were found to show good agreement.
- The results also reveal that for the given conditions, the gas volume fraction increases along the pipeline causing the liquid volume fraction to decrease.
- Additionally, it was found that the four-phase flow pressure drop increases along with increase in flow rates in four-phase (CO_2, oil, water, sand) flow tests. We also noticed that the four-phase pressure drops rise with the rise in the gas flow rate (gas superficial velocity) for (CO_2, oil, water, sand) four-phase flow. This occurs because the gas phase disturbs the flow and extra pressure loss occurs in the mixture of four-phase (CO_2, oil, water, sand) flow. Moreover, the experiment explained the impact of rising solid particle concentrations and flow rates on pressure drops of four-phase (CO_2, oil, water, sand) flow. It was generally observed that the four-phase (CO_2, oil, water, sand) flow pressure drops increase in solid particle concentrations increase. As well, it was noted that higher viscosity liquid establishes extra frictional shear forces along the pipeline, leading to even more substantial pressure drops.
- The model used in this work was validated in relation to experimental data on a typical four-phase (CO_2, oil, water, sand) flow in short sections of a horizontal pipeline.
- A multi-phase flow in a horizontal pipeline was devised in order to carry out tests on four-phase flows. This also included careful calibration of sensors for both temperature and pressure.
- To effectively gauge how pressure impacts transient flow behavior, it was necessary to first analyze temperature, pressure, and gas velocity profiles in short sections of horizontal pipeline systems.
- The research findings may also help regulatory agencies to improve guidelines for the design and operation of four-phase (gas-oil-water-sand) flow in short sections of horizontal pipeline systems that

include multiple bends and jumpers.

The CFD simulation approach to multi-phase flow through a horizontal pipeline demonstrates some good agreements and outcomes with regard to experimental works. With the aim of building a model that can be applied in practical problems with fewer parameter boundary limitations, some analysis was performed under various conditions, after validating the developed model. A few of the approaches are listed below:

- Building a CFD model with a Eulerian multi-phase to simulate multi-phase flow through short sections of a horizontal pipeline.
- Demonstrating, with diagram, an experimental flow loop horizontal pipeline sited in our laboratory.
- Simulating two/three/four-phase (gas-oil-water-sand) flows to compare with our own experimental results.
- Validating two/three/four-phase (gas-oil-water-sand) flows with reference to the experimental data.
- Mesh size and inflation layers near the wall were finalized after checking of mesh independency in the simulation results and in consideration of the convergence requirement of the dimensionless wall distance ($y+ > 30$). The minimum number of nodes required for the pipeline geometries were 140,000 Furthermore, 10 inflation layers with a growth rate of 20% were used near the boundaries.
- Length-independent results were ensured through the analysis of the output parameter, i.e., pressure gradient at different cross sections of the pipeline. This was performed to verify the minimum flow development section or entrance length (50Dh) and to analyze the variations in pressure gradients along the length. It was found that sand concentrations are proportionally related to pressure gradients.

6.3 Recommendations for Future Work

Multi-phase flow represents a wide research area. The experimental setup of four-phase flow used in this thesis has the capacity to conduct different types of multi-phase flow analysis. The following recommendations concern how this research could be continued in the future using the developed this set-up.

From previous studies, it was seen that pipe diameter influences the flow structure of pipelines. This

experiment on flow loop horizontal pipeline was done with 20 mm clear PVC piping. Therefore, future experiments on flow loop horizontal pipelines should be done using pipes of different diameters to see the ramification of pipe diameter on flow characteristics.

A potential future study could use high resolution and high-frequency pressure and temperature sensors to detect the changes of flow structures. The sensors should be utilized around the pipeline cross-section area, so that they can capture every change in multi-phase flow. Wavelet packet transformation can identify different pressure fluctuations and it is possible to determine the flow pattern only by seeing the pressure signal.

There are many interesting directions for continued research in this field of study. A few of the more promising directions, organized by topic, are listed in the following points:

- An investigation on the entrainment behaviour of a sand bed subjected to gas-water-oil multi-phase steady and unsteady flows in offshore pipeline systems that include multiple bends and jumpers.
- An investigation on the impact of high pressure and/or high temperature on bubble and particle transport characteristics in a large-scale four-phase gas-oil-water-sand flow test facility.
- Numerical analysis could also be used to predict critical and optimal transport velocities during four-phase production pipeline systems and sand unloading operations.

The results of this thesis are recommended to for application in O&G industry pipelines. The findings will help develop guidelines for specifications based on environmental conditions and pipe material in order to determine the fatigue life of pipelines with multiple bends and jumpers.

Furthermore, because there is yet limited research and work on gas-oil-water-sand of multi-phase flow in horizontal pipelines with multiple bends, several different parameters could be studied with regard to fluid and geometry.

Therefore, we recommend that experiments to be designed that can identify the parameters or interactions of parameters that have the greatest impact on the life of pipelines. We also recommend using CFD simulations to study the effect of the following:

- The volume fraction of each phase within a three-phase flow.
- The particle diameter of oil-gas-water flow with sand particles.
- The initial velocity for the oil-gas-water flow with sand production using the same particle flow rate and volume fraction of the phases.
- How external flow, caused by currents or waves, can induce significant pressure gradients on the structure of pipelines.

Future research on the effect of these parameters on four-phase flow in short sections of horizontal pipelines will allow for greater accuracy, efficiency, and economic and financial benefits.

REFERENCES

1- Swindell, R. (2011, September 01). Hidden integrity threat looms in subsea pipework vibrations. (Xodus Group) Retrieved October 15, 2012, from Offshore: http://www.offshore mag.com/articles/print/volume-71/issue-9/production-operations/hidden-integrity-threat-looms-in-subsea.html.

2- Pontaza, J., & Menon, R. (2011). Flow-Induced Vibrations of Subsea Jumpers due to Internal Multi-phase flow. 30th International Conference on Offshore Mechanics and Artic Engineering. Rotterdam.

3- Riverin, J., de Langre, E., & Pettigrew, M. (2006). Fluctuating forces caused by internal two-phase flow on bends and tees. Journal of Sound and Vibration, 1088-1098.

4- Pontaza, J., & al, e. (2013). Flow-induced Vibrations of High gas rate Well Jumpers: Tees vs. Bends. Proceedings of the ASME 2013 32nd International Conference on Ocean, Offshore and Artic Engineering. Nantes.

5- Riverin, J., & Pettigrew, M. (2007). Vibration Excitation Forces due to Two-phase Flow in Piping Elements. Journal of Pressure Vessel Technology, 7-13.

6- Ramdin, M., & Henkes, R. (2011). CFD for Multi-phase Flow Transport in Pipelines. Proceedings of the ASME 2011 30th International Conference on Ocean, Offshore and Artic Engineering.

7- Energy Institute. (2008). Guidelines for the avoidance of vibration induced fatigue failure in process pipework. London: Energy Institute.

8- Keskin, C., Zhang, H.-Q., & Sarica, C. (2007). Identification and Classification of New Three-Phase Gas/Oil/Water Flow Patterns. SPE Annual Technical Conference and Exhibition. Anaheim, California.

9- Ersoy, G., Sarica, C., Al-Safran, E., & Zhang, H. (2011). Experimental Investigation of Three-Phase Gas-Oil-Water Slug Flow Evolution in Hilly-terrain Pipelines. SPE Annual Technical Conference. Denver.

10- Al-lababidi, S., Yan, W., & Yeung, H. (2012). Sand Transportations and Deposition Characteristics in Multi-phase Flows in Pipelines. Journal of Energy Resources Technology, 134.

11- Bello, O., Reinicke, K., & Teodoriu, C. (2005). Particle Holdup Profiles in Horizontal Gas-liquid-solid Multi-phase Flow Pipeline. Chemical Engineering & Technology, 1546-1553.

12- Been, J. (2011). Comparison of the Corrosivity of Dilbit and Conventional Crude. Alberta Innovates Technology Futures.

13- National Aeronautics and Space Administration. (2008). Navier-Stokes Equations: 3-dimensional-unsteady.

14- Bratland, O. (2010). Pipe Flow 2: Multi-phase Flow Assurance.

15- Kwon, O., Ryou, S. and Sung, W., “Numerical Modeling Study for the Analysis of Transient Flow Characteristics of Gas, Oil, Water, and Hydrate Flow through a Pipeline”, Korean Journal of Chemical Engineering, 18(1), 88-93(2001).

16- Bergman, T. L., Lavine, A. S., Incropera, F. P. and Dewitt, D. P., “Fundamentals of Heat and Mass Transfer”, 7th edition, John Wiley & Sons (2011).

17- Gnielinski, V., “New Equations for Heat and Mass Transfer in Turbulent Pipe and Channel Flow”, International Journal of Chemical Engineering,16, 10 (1976).

18- Whitaker, S., “Forced Convection Heat Transfer Correlations for Flow in Pipes”, AIChE Journal,18(2), 361–371 (1972).

19- Timoshenko, S., & Goodie, J. (1970). Theory of Elasticity (3rd ed.). New York: McGraw-Hill.

20- http://www.rheosense.com/applications/viscosity/newtonian-non-newtonian. Retrieved October 20, 2016.

21- Cooper, P., Burnett, C., & Nash, I. (2009). Fatigue Design of Flow line Systems with Slug Flow. Proceedings of the ASME 2009 28th International Conference on Ocean, Offshore and Arctic Engineering. Honolulu.

22- Encyclopedia, T. G. (1979). The Free Dictionary by Farlex. Retrieved August 3, 2013, from http://encyclopedia2.thefreedictionary.com/Gas-Oil+Ratio.

23- Bello, O. (2008). Modelling Particle Transport in Gas-oil-sand multi-phase flows and its applications to production operations. Clausthal University of Technology.

24- Aquatrol Valve Company, Inc., "www.aquatrol.com," [Online]. Available: http://www.aquatrol.com/69--Relief-Valves.htm.

25- Emerson, "www.emersonprocess.com," [Online]. Available: http://www2.emersonprocess.com/enus/brands/rosemount/flow/magneticflowmeters/8711-wafer-sensor/pages/index.aspx.

26- Omega Engineering inc, [Online]. Available: www.omega.ca.

27- JJ Downs Industrial Plastics, "https://www.jjdowns.com/," [Online].

28- K. M. Boone, A Study of Axial and Radial Flows for Annular Channels with Roughened Walls, M.Eng. thesis St. John's: Memorial University of Newfoundland, 2005.

29- FESTO AG & Co. KG, "https://www.festo.com," [Online].

30- Taitel, Y., Dukler, A. E., A model for prediction flow regime transitions in horizontal and near horizontal gas-liquid flow, AIChE journal, vol. 22, pp. 47-55, 1976.

31- Volcado, J. J. & Charles, M. E., Prediction of pressure gradient for the horizontal turbulent flow of slurries, proceeding of the 2nd international conference on the hydraulic transport of solids in pipes, Coventry, UK, paper C1, pp. 1-12, 1972.

32- Parazonka, W., Kenchington, J. M. & Charles, M. E., Hydro transport of solids in horizontal pipes: effects of solids concentration and particle size on the deposit velocity, Canadian journal of chemical engineering, vol. 59, no. 3, pp. 291-296, 1981.

33- Oroskar, A. R., Turian, R. M., The critical velocity in pipelines of slurries, AIChE journal, vol. 26, no. 4, pp. 550-558, 1980.

34- Salama, M. M., Sand production management, journal of energy resources technology, vol. 122, no. 1, pp. 29-33, 2000.

35- Wilson, K. C., A unified physically based analysis of solid-liquid pipeline flow, proceeding of 4th int. conference on the hydraulic transport of solid in pipes, Banff, Alberta, Canada, paper A1, pp. 1-16, 1976.

36- Televantos, Y., Shook, C., Carleton, A. & Streat, M., Flow of slurries of coarse particles at high solids concentrations, Canadian journal of chemical engineering, vol. 57, pp. 255-262, 1979.

37- Hsu, F. L., Turian, R. M. & Ma, T. W., Flow of noncolloidal slurries in pipelines, AIChE journal, vol. 35, pp. 429-442, 1989.

38- Doron, P., Granica, D. & Barnea, D., Slurry flow in horizontal pipes experimental and modeling, int. journal multi-phase flow, vol. 13, pp. 535- 547, 1987.

39- B. Moradi, M. Hossain & G. Oluyemi, Stratified three phase flow in pipes, Int., WIT Transactions on Engineering Sciences, Vol 89, © 2015 WIT Press www.witpress.com, ISSN 1743-3533 (on-line), doi:10.2495/MPF150291.

40- Doron, P., Barnea, D., A three-layer model for solid-liquid flow in horizontal pipes, int. journal multi-phase flow, vol. 19, no. 6, pp. 1029-1043,1993.

41- Taitel, Y., Barnea, D. & Brill, J. P., Stratified three-phase flow in pipes, Int. journal multi-phase flow, vol. 21, no. 1, pp. 53-60, 1995.

42- Yang, Z. L., Ladam, Y., Laux, H., Danielson, T., Goldszal, A., Martins, A. L., Simulation of sand transport in a stratified gas-liquid two-phase pipe flow, BHR multi-phase production technology 13, pp. 327-342, 2007.

43- Almedeij J. H. and Algharaib, M. K., (2005). 'Influence of sand production on pressure drawdown in horizontal wells: theoretical evidence', Journal of Petroleum Science and Engineering, 47(3-4), pp. 137-145.

44- Doron, P., Simkhis, M. & Barnea, D., Flow of solid-liquid mixtures in inclined pipes, int. journal multi-phase flow, vol. 23, no. 2, pp. 313-323, 1997.

45- Bird, R. B., Stewart, W. E. & Lightfoot, E. N., Transport phenomena, chapter 6, Wiley, New York, 1960.

46- Paras, S. V., Karabelas, A. J., Droplet entrainment and deposition in horizontal annular flow, int. journal multi-phase flow, vol. 17, pp. 455-468, 1991.

47- Xiao, J. J., Shoham, O., & Brill, J. P., A comprehensive mechanistic model for two-phase flow in pipelines, society of petroleum engineers inc., New Orleans, Louisiana, 1990.

48- Lee, A.-H., Sun, J.-Y., Jepson, W. P. (1993). Study of flow regime transitions of oil-water-gas mixtures in horizontal pipelines. In Proceedings of the Third (1993) International Offshore and Polar Engineering Conference (pp. 159–164). Singapore: The International Society of Offshore and Polar Engineers.

49- Kwon, O., "Numerical Modeling Study for the Analysis of Multi-phase Transient Flow of Natural Gas-Oil-Water-Hydrate through Seabed Pipeline:' Ph.D. Disser," The Hanyang Univ., Seoul, Korea (1999).

50- Chica, L. (2011). Jumper Analysis with Interacting Internal Two-Phase Flow. Houston: College of Technology.

51- Clough, R. W., & Penzien, J. (1993). Dynamics of Structures (2nd ed.). New York: McGraw-Hill Publishing Company.

52- Cooper, P., Burnett, C., & Nash, I. (2009). Fatigue Design of Flowline Systems with Slug Flow. Proceedings of the ASME 2009 28th International Conference on Ocean, Offshore and Arctic Engineering. Honolulu.

53- Encyclopedia, T. G. (1979). The Free Dictionary by Farlex. Retrieved August 3, 2013, from http://encyclopedia2.thefreedictionary.com/Gas-Oil+Ratio.

54- Energy Institute. (2008). Guidelines for the avoidance of vibration induced fatigue failure in pipework. London: Energy Institute.

55- Ersoy, G., Sarica, C., Al-Safran, E., & Zhang, H. (2011). Experimental Investigation of Three-phase Gas-Oil-Water Slug Flow Evolution in Hilly-terrain Pipelines. SPE Annual Technical Conference. Denver.

56- Hirt, C., & D., N. B. (1981). Volume of Fluid (VOF) Method for the Dynamocs of Free Boundaries. Journal of Computational Physics, 201-225.

57- Izarra, R. (2009). Second Moment Modelling for the Numerical Simulation of Passive Scalar Dispersion of Air Pollutants in Urban Environments. Siegen.

58- Jia, D. (2012). Slug Flow Induced Vibration in a Pipeline Span, a Jumper, and a Riser Section. Offshore Technology Conference. Houston.

59- Keskin, C., Zhang, H.-Q., & Sarica, C. (2007). Identification and Classification of New Three-phase Gas/Oil/Water Flow Patterns. SPE Annual Technical Conference and Exhibition. Anaheim, California.

60- McMurtry, P. (n.d.). Length and Time Scales in Turbulent Flows. Salt Lake City, Utah, United States. Retrieved fromwww.eng.utah.edu/~McMurtry/Turbulence/turblt.pdf.

61- National Aeronautics and Space Administration. (2008). Navier-Stokes Equations: 3-dimensional-unsteady.

62- Pontaza, J., & Menon, R. (2011). Flow-Induced Vibrations of Subsea Jumpers due to Internal Multi-phase flow. 30th International Conference on Offshore Mechanics and Artic Engineering. Rotterdam.

63- Pontaza, J., & al, e. (2013). Flow-induced Vibrations of High gas rate Well Jumpers: Tees vs. Bends. Proceedings of the ASME 2013 32nd International Conference on Ocean, Offshore and Artic Engineering. Nantes.

64- Ramdin, M., & Henkes, R. (2011). CFD for Multi-phase Flow Transport in Pipelines. Proceedings of the ASME 2011 30th International Conference on Ocean, Offshore and Artic Engineering.

65- Riverin, J., de Langre, E., & Pettigrew, M. (2006). Fluctuating forces caused by internal two-phase flow on bends and tees. Journal of Sound and Vibration, 1088 1098.

66- Riverin, J., & Pettigrew, M. (2007). Vibration Excitation Forces due to Two-phase Flow in Piping Elements. Journal of Pressure Vessel Technology, 7-13.

67- Science Flow. (2013). Flow-3D. Retrieved October 20, 2013, from Flow Science: http://www.flow3d.com/cfd-101/cfd-101-implicit-explicit-schemes.html.

68- [Soviet State. (1979). The Free Dictionary. Retrieved August 25, 2013, from The Great Soviet Encyclopedia: http://encyclopedia2.thefreedictionary.com/Gas-Oil+Ratio.

69- STAR CCM+. (2013). CD-adapco Star-CCM+. Retrieved October 10, 2013, from C:\Program Files\CDadapco\STARCCM+8.04.007\doc\online\wwhelp\wwhimpl\js\html\wwhelp.htm.

70- [Stour, P. (1988, October). Rhode Island Sea Grant Fact Sheet. Retrieved August 14, 2013, from http://seagrant.gso.uri.edu/factsheets/sand.html.

71- Swindell, R. (2011, September 01). Hidden integrity threat looms in subsea pipework vibrations. (Xodus Group) Retrieved October 15, 2012, from Offshore: http://www.offshoremag.com/articles/print/volume-71/issue-9/production-operations/hidden-integrity-threatlooms-in-subsea.html.

72- Timoshenko, S., & Goodie, J. (1970). Theory of Elasticity (3rd ed. ed.). New York: Mc Graw Hill.

73- AT Petkova, RD Leapman, Z Guo, and WM Ya. Science, 2005.

74- AL Sam ways, LJS Bradbury, HH Bruun-International journal of multi-phase flow, 1997.

75- O. Bratland, Pipe Flow 1 - Single-phase Flow Assurance, Ove Bratland, 2013.

76- P. Prickaerts, "Controlling the split of a two-phase gas- Liquid flow from a single flow line to a dual riser," Master's thesis, Delft University of Technology, 2011.

77- S. W. Churchill, "Friction-factor equation spans all fluid-flow regimes," Chemical Engineering, vol. 84, pp. 91–92, 1977.

78- V. H. Halvorsen, J. K. Lervik and G. Klevjer, Hydrate and Wax Prevention of Risers by Electrical Heating, The Tenth International Offshore and Polar Engineering Conference, 28 May-2 June, Seattle, Washington, USA, 2000.

79- R. IJzermans and R. Lacy, "Technical description Shell Flow Correlations," Tech. Rep. GS. 09. 51663, Shell Global Solutions, 2009.

80- Rahman, M.A., Gomez, J., Heidrick, T., Fleck, B.A., and McMillan, J. Correlations of the Droplet Size-Velocity of the Two-Phase, Air/Liquid Spray Using a Particle-Dynamic-Analyzer. in ASME 2008 Fluids Engineering Division Summer Meeting collocated with the Heat Transfer, Energy Sustainability, and 3rd Energy Nanotechnology Conferences. 2008.

81- Rahman, M.A., Adane, K.F., and Sanders, R.S., An improved method for applying the Lockhart Martinelli correlation to three-phase gas-liquid-solid horizontal pipeline flows. Canadian Journal of Chemical Engineering, 2013. 91(8): p. 1372-1382.

82- Rehman, S.R., Zahid, A.A., Hasan, A., Hassan, I., Rahman, M.A., and Rushd, S., Experimental Investigation of Volume Fraction in an Annulus Using Electrical Resistance Tomography. SPE Journal, 2019(March 2018): p. 1-10.